FAULT LOCATION IN DISTRIBUTION SYSTEMS USING MATHEMATICAL ANALYSIS AND SUPPORT VECTOR MACHINE

SOPHI SHILPA GURURAJAPATHY

FACULTY OF ENGINEERING
UNIVERSITY OF MALAYA
KUALA LUMPUR

2017

FAULT LOCATION IN DISTRIBUTION SYSTEMS USING MATHEMATICAL ANALYSIS AND SUPPORT VECTOR MACHINE

SOPHI SHILPA GURURAJAPATHY

THESIS SUBMITTED IN FULFILMENT OF THE REQUIREMENTS FOR THE DEGREE OF DOCTOR OF PHILOSOPHY

FACULTY OF ENGINEERING
UNIVERSITY OF MALAYA
KUALA LUMPUR

2017

UNIVERSITY OF MALAYA
ORIGINAL LITERARY WORK DECLARATION

Name of Candidate: **Sophi Shilpa Gururajapathy**

Matric No: **KHA 130083**

Name of Degree: **Doctor of Philosophy**

Title of Thesis ("this Work"): **FAULT LOCATION IN DISTRIBUTION SYSTEMS USING MATHEMATICAL ANALYSIS AND SUPPORT VECTOR MACHINE**

Field of Study: **Power System**

I do solemnly and sincerely declare that:

(1) I am the sole author/writer of this Work;
(2) This Work is original;
(3) Any use of any work in which copyright exists was done by way of fair dealing and for permitted purposes and any excerpt or extract from, or reference to or reproduction of any copyright work has been disclosed expressly and sufficiently and the title of the Work and its authorship have been acknowledged in this Work;
(4) I do not have any actual knowledge nor do I ought reasonably to know that the making of this work constitutes an infringement of any copyright work;
(5) I hereby assign all and every rights in the copyright to this Work to the University of Malaya ("UM"), who henceforth shall be owner of the copyright in this Work and that any reproduction or use in any form or by any means whatsoever is prohibited without the written consent of UM having been first had and obtained;
(6) I am fully aware that if in the course of making this Work I have infringed any copyright whether intentionally or otherwise, I may be subject to legal action or any other action as may be determined by UM.

Candidate's Signature Date:

Subscribed and solemnly declared before,

Witness's Signature Date:

Name:

Designation:

ABSTRACT

Distribution systems are continuously exposed to fault occurrences due to various reasons, such as lightning strike, failure of power system components due to aging of equipment and human error. These phenomena affect the system reliability and results in expensive repairs, damaged work in process, lost productivity and power loss to customers. Due to this, various intelligent methods have been developed to locate fault in distribution system. However, fault location using intelligent methods is challenging since it requires training data for processing. The training data is commonly created by simulation, which is time consuming. Therefore, in this work, a fault location method based on previous work is proposed using limited simulation data. The existing method was improved by estimating voltage sag data using support vector machine, thus limiting the simulated data. Faulty section is identified by comparing the actual voltage sag data with the simulated and estimated voltage sag data. An improved ranking and Euclidean distance approach for fault distance is also presented. A method using SVM is also proposed to identify the faulty phase, fault type, faulty section and fault distance. By having these features, a more accurate and effective fault location can be obtained. The method identifies faulty phase and fault type using support vector classification analysis. Meanwhile, the faulty section and the fault distance are identified using support vector regression analysis. The effectiveness of the proposed method was tested on an actual TNB distribution network from Malaysia and SaskPower distribution network from Canada. The test cases were conducted for all types of fault and for various fault resistances. The test results have proven the effectiveness of the proposed method in locating fault under various conditions. It has shown improvement over the existing trigonometric methods in locating different types of faults and may serve as an alternative technique for estimating fault location in distribution networks.

ABSTRAK

Sistem pengagihan akan terus menghadapi kejadian kesalahan kerana pelbagai sebab, seperti kilat, kegagalan komponen sistem kuasa kerana penuaan peralatan dan kesilapan manusia. Fenomena ini memberi kesan kepada kebolehpercayaan sistem dan keputusan dalam pembaikan mahal, bekerja rosak dalam proses, kehilangan produktiviti dan kehilangan kuasa kepada pelanggan. Oleh yang demikian, pelbagai kaedah pintar telah dibangunkan untuk mencari kesalahan dalam sistem pengedaran. Walau bagaimanapun, lokasi bersalah menggunakan kaedah bijak mencabar kerana ia memerlukan data latihan untuk pemprosesan. Data latihan dicipta oleh simulasi, yang memakan masa. Oleh itu, dalam kerja-kerja ini, satu kaedah lokasi bersalah lebih baik adalah dicadangkan menggunakan data simulasi terhad. Kaedah yang sedia ada telah dipertingkatkan dengan menganggarkan data sag voltan menggunakan sokongan mesin vektor, dengan itu menghadkan data simulasi. Satu kedudukan yang lebih baik dan pendekatan jarak Euclidean untuk jarak kesalahan juga dibentangkan. Kaedah menggunakan pada SVM juga dicadangkan untuk mengenal pasti fasa rosak, jenis kesalahan, bahagian yang rosak dan jarak bersalah. Dengan adanya ciri-ciri ini, lokasi kesalahan yang lebih tepat dan berkesan boleh diperolehi. Kaedah ini mengenal pasti fasa rosak dan jenis kesalahan menggunakan analisis sokongan klasifikasi vektor. Sementara itu, bahagian yang rosak dan jarak kesalahan dikenal pasti dengan menggunakan analisis sokongan vektor regresi. Keberkesanan kaedah yang dicadangkan telah diuji pada rangkaian pembahagian TNB yang sebenar dalam rangkaian pengedaran Malaysia dan SaskPower dari Kanada. Kes-kes ujian telah dijalankan untuk semua jenis kesalahan dan untuk pelbagai rintangan bersalah. Keputusan ujian telah menunjukkan peningkatan berbanding kaedah trigonometri yang sedia ada dalam mencari jenis kesalahan dan boleh berkhidmat sebagai teknik alternatif untuk menganggarkan lokasi bersalah dalam rangkaian pengedaran.

ACKNOWLEDGEMENTS

I would like to express my sincere thanks to my supervisors, Associate Professor Dr. Hazlie Bin Mokhlis and Dr. Hazlee Azil Illias for their continuous supervision and motivation. I would also like to thank the Ministry of Education and University of Malaya for supporting the work through research grant of HIR (H-16001-D00048), UMRG (RG135/11AET) and FRGS (FP026-2012A).

I would also like to express my greatest thanks to my family and friends for their support and encouragement.

TABLE OF CONTENTS

LIST OF FIGURES

LIST OF TABLES

LIST OF SYMBOLS AND ABBREVIATIONS

ANN	:	Artificial Neural Network
CT	:	Current Transformer
DG	:	Distributed Generation
DLGF	:	Double Line to Ground Fault
DNN	:	Deep Neural Network
ERM	:	Empirical Risk Minimization
ELM	:	Extreme Learning Machine
FFT	:	Fast Fourier Transform
GA	:	Genetic Algorithm
GPS	:	Global Positioning System
IEC	:	International Electro technical Commission
IEEE	:	Institute of Electrical and Electronics Engineers
LLF	:	Line to Line Fault
LLLGF	:	Three Phase to Ground Fault
MAE	:	Mean Absolute Error
MLP	:	Multi-Layer Perceptron
PSCAD	:	Power System Computer Aided Design
PT	:	Potential Transformer
p.u	:	Per unit
R	:	Regression
RBF	:	Radial Basis Function
RMSE	:	Root Mean Square Error
SLGF	:	Single Line to Ground Fault
SRM	:	Structural Risk Minimization

SVC	:	Support Vector Classification
SVM	:	Support Vector Machine
SVR	:	Support Vector Regression
TNB	:	Tenaga Nasional Berhad
2D data	:	Two Dimensional data
3D data	:	Three Dimensional data
d_{sn}	:	Shortest distance from fault to the linear line joining voltage sag data from database
f_d	:	Fault Distance
i , j	:	Nodes
L	:	Equivalent Inductance
m	:	Slope of line $y = mx + c$
n	:	Total number of possible faulty sections
R_f	:	Fault Resistance
$R_f(x)$, $R_f(x+1)$	:	Fault Resistance from database nearer to the estimated fault resistance
s	:	Faulty section
t_1	:	Time taken for the travelling wave from measurement node to fault location
t_2	:	Time taken for the reflected wave from fault location to measurement node
V	:	Voltage magnitude
V_f	:	Voltage magnitude during fault
V_s	:	Source Voltage
$V_{a,i}^{R_f(x)}, V_{b,i}^{R_f(x)}, V_{c,i}^{R_f(x)}$	:	Voltage sag at phase a, b and c at node *i* and fault

		resistance $R_f(x)$
$V_{a,i}^{R_f(x+1)}, V_{b,i}^{R_f(x+1)}, V_{c,i}^{R_f(x+1)}$	:	Voltage sag at phase a, b and c at node *i* and fault resistance $R_f(x+1)$
$V_{a,j}^{R_f(x)}, V_{b,j}^{R_f(x)}, V_{c,j}^{R_f(x)}$	:	Voltage sag at phase a, b and c at node *j* and fault resistance $R_f(x)$
$V_{a,j}^{R_f(x+1)}, V_{b,j}^{R_f(x+1)}, V_{c,j}^{R_f(x+1)}$	:	Voltage sag at phase a, b and c at node *j* and fault resistance $R_f(x+1)$
$V_{c,i}^{R_f(x)}$	:	Voltage sag at phase c, node *i* and fault resistance $R_f(x)$
V_{af}, V_{bf}, V_{cf}	:	Voltage sag magnitude at phase a, b and c
$V_{i,\min}^{R_f(x)}, \phi_{i,\min}^{R_f(x)}$	:	Minimum value of phase voltage and angle at node *i* and fault resistance $R_f(x)$
$V_{i,\max}^{R_f(x+1)}, \phi_{i,\max}^{R_f(x+1)}$	:	Maximum value of phase voltage and angle at node *i* and fault resistance $R_f(x+1)$
$V_{j,\min}^{R_f(x)}, \phi_{j,\min}^{R_f(x)}$		Minimum value of phase voltage and angle at node *j* and fault resistance $R_f(x)$
$V_{j,\max}^{R_f(x+1)}, \phi_{j,\max}^{R_f(x+1)}$		Maximum value of phase voltage and angle at node *j* and fault resistance $R_f(x+1)$
Z_l	:	Line impedance per unit length
Z_s	:	Source Impedance
Z_f	:	Fault Impedance
ϕ	:	Phase angle
ϕ_f	:	Phase angle during fault

LIST OF APPENDICES

CHAPTER 1: INTRODUCTION

1.1 Introduction

In general, electrical power systems undergo three processes before reaching customers namely; generation, transmission and distribution. Power is generated in a power plant and then transmitted to the transmission station via step-up transformer. The transmitted power is then distributed through distribution system, in which the power is supplied to various customers including industries, offices and houses. The primary objective of distribution systems is to ensure customers having reliable power supply. However, power supply could be interrupted and such interruption cannot be totally avoided due to environmental factors such as storms, lightning strikes, snow and freezing rain. Interruption could also be caused by technical problems due to aging or improper maintenance of power system components. For example, in transformers, the winding insulation breakdown may lead to short circuits. These factors could lead to a system fault that degrades the reliability of power supply.

When a fault occurs in a distribution system, it causes voltage sag, voltage swell, temporary losses of supply, or system blackout. Voltage sag causes sensitive equipment such as a power drive, process control and automated machines in semi-conductor factories to trip and leads to shutdown (Melhorn, Davis, & Beam, 1998). This event damages equipment in power utilities and affects the industrial production. From a survey in (Force, 2004), it was found that more than 80% of the interruption in distribution systems was caused by faults, which caused power outage to every customer on the system. The average cost for an outage duration of 1 hour was USD3 for residential customers, USD1200 for commercial and USD82000 for large industrial customers (Leora, Michael, Kent Van, Aaron, & Joseph, 2003). Hence, it is very important for the utility to identify the fault as quickly as possible to minimize the impact of fault, power outage and interruption time. Furthermore, a fast fault location

will also improve reliability indexes, such as System Average Interruption Duration Index (SAIDI), Customer Average Interruption Duration Index (CAIDI), and System Average Interruption Frequency Index (SAIFI). These indices are very important for utility to gain trust from the customers, mainly in deregulated business environments.

Faults can be classified as temporary faults and permanent faults. Temporary faults are caused due to various reasons such as unfavorable environmental condition, physical contact between lines, momentary contact of animals or birds, or contact due to wind and trees which create a short circuit path. If temporary faults are not cleared, eventually they change into permanent faults sooner or later. Permanent fault will remain until the short circuit is identified and removed. Some of the causes for permanent faults are cable insulation failure due to improper maintenance, objects falling on overhead lines and lines falling on earth. When this happens, the protective devices trips off and stop the power from being supplied to the faulted areas. Commonly, the maintenance crews are deployed to identify the faulted area and repair the damage. This approach requires long inspection time. Hence, there is a necessity to identify fault quickly in order to restore power to the faulted area. It also helps to maintain network reliability and provide better service to customers.

1.2 Problem Statement

Due to the importance of locating fault, automated fault location is essential to identify fault and expediting the restoration process. Various methods such as travelling wave based, impedance based and knowledge based methods have been developed to locate fault in distribution systems. All of the methods aimed at detecting fault location as accurately as possible. However, travelling wave method was developed for transmission systems, which is different from distribution system characteristic having multiple laterals. Impedance-based method uses the voltage and current from

measurement node to calculate the fault distance. These methods such as in (Jun, Lubkeman, & Girgis, 1997; Salim, Resener, Filomena, Rezende Caino de Oliveira, & Bretas, 2009; Seung-Jae et al., 2004), determined the fault distance from a particular bus. For a distribution network with multiple branches, it may result in multiple possibilities of fault locations. Due to the limitations, knowledge-based method can be an alternative solution for fault location. In general, this type of method analyzes a set of voltage sag data or current data obtained during fault for locating fault. This voltage sag or the current data can be from actual fault events or from simulation. The methods in (Lilik Jamilatul Awalin, Mokhlis, Abu Bakar, Mohamad, & Illias, 2013; Hazlie Mokhlis & Li, 2011; H. Mokhlis & Li, 2007) depend on the simulated data stored in database for matching the data with actual fault data. The database was created through simulation, which is time consuming. Also, huge data needs to be stored to ensure accurate fault location. A limited stored data will cause inaccurate fault location for a method that depends on huge data such as proposed by (Lilik Jamilatul Awalin et al., 2013).

Ferrero (Ferrero, Sangiovanni, & Zappitelli, 1995) explained the difficulty to determine fault type using traditional methods (ie. deterministic methods). The method using voltage sag characteristic (Namrata B. Pawar, 2014; Suresh Kamble, 2014) identifies the fault type by comparing the pattern of pre-fault voltage with the voltage during fault. However, for fault far from the measurement location, the difference is not noticeable and may lead to wrong identification of fault type. The methods such as (Dash, Samantaray, & Panda, 2007; Parikh, Das, & Maheshwari, 2010) identify fault type for transmission systems. In (Ravikumar, Thukaram, & Khincha, 2008), the fault type, faulty section and distance together of faulted lines in a transmission system is identified. Most of the methods have been proposed for transmission systems and not on distribution systems since lateral branches have to be considered in distribution systems.

This required some modifications in the existing methods. Also, accurate fault location is quite difficult to pinpoint due to the complexity of power distribution systems, such as non-homogeneity of lines, unbalanced network and lateral branches.

An effective fault location in distribution systems should be able to identify the following: faulty phase, fault type, faulty section and fault distance. Hence, automated fault location research is very important to overcome these drawbacks and to detect accurate fault location in order to expedite the restoration process.

1.3 Objective

The objectives of this research are:

1. To establish a method to identify the fault type in distribution system using support vector classification analysis considering the faulty phase.
2. To propose a method to estimate voltage sag data using support vector regression based on limited simulated data.
3. To estimate the fault distance using Euclidean approach and support vector regression analysis.

1.4 Methodology and Scope of Research

To achieve the objectives of the research, the following tasks have been carried out:

a. The background of distribution system and the fault location problems are studied. Recent developments of technology, influencing the fault location are also studied.

b. Various fault location methods for transmission and distribution systems have been studied. The importance of accurate fault identification and the advantages and disadvantage for each of the existing method are reviewed. Since the

proposed method is based on voltage sags information, related methods using voltage sags to locate faults are studied thoroughly.

c. Considering the simulation time for creating database and the advantage and disadvantages of the existing methods, the proposed method is developed. It will also account for possible improvements to the existing methods.

d. Simulations are carried out using PSCAD software and the algorithm of proposed method is developed using MATLAB programming.

e. In order to evaluate the proposed method, two different networks, namely from Tenaga Nasional Berhad (TNB) the distribution network from Malaysia and SaskPower distribution network from Canada are modelled and simulated using PSCAD software. A fault simulation is conducted to generate voltage sag waveform data for testing purpose.

f. Finally, for test cases, fault was simulated at the mid-point of all sections of the distribution network for various fault resistance and the proposed method identifies the faulty phase, fault type, faulty section and fault distance.

1.5 Thesis Outline

The thesis consists of seven chapters. The present introductory chapter covers the introduction, objectives of research and the main tasks carried out in this study.

Chapter 2 presents literature survey on existing fault location techniques. The methods discussed include conventional based, travelling wave-based, impedance-based and knowledge-based techniques. A review of the methods and its basic theory, associated assumptions are explained. The working principle of each method along with its requirements, advantages and limitations are discussed. From this review, a fault location method able to address the limitations of existing methods is proposed.

Chapter 3 describes the fundamental theory and characteristics related to fault in distribution systems. It explains the basics of voltage sag profile, characteristics of voltage sag and the impact of voltage sag in distribution systems. Also, the influence of faults in the context of voltage sag profile is discussed since the proposed method utilizes voltage sag to locate fault. The fault types in distribution network are also discussed. It also discusses the economic losses to customers and industries due to the voltage sag in distribution system.

Chapter 4 describes the proposed fault location method and the difference between the previous methods and the proposed method. It explains the proposed estimation of voltage sag using Support vector regression analysis. Fault type classification using two-dimensional and three-dimensional analysis of Support vector machine is discussed. The identification of faulty section using matching approach is explained. Also, fault distance using Euclidean distance and Support vector regression is discussed in detail.

Chapter 5 presents the implementation and validation of the proposed method. The algorithm of the proposed fault distance considering faulty phase, fault type, faulty section and fault distance are explained. Two different types of radial distribution network are considered for validation of the method, namely TNB and SaskPower distribution networks. The networks are simulated using PSCAD software to generate voltage sag data tests.

Chapter 6 reports on the test results of the proposed method. The performance of the proposed method considering the effects of voltage sag, fault resistance, fault type, length of line section and fault location are discussed. The results of faulty phase, fault type, faulty section and fault distance are discussed in detail.

Chapter 7 briefs the conclusions of the work. The main findings of the research and the future work to improve the proposed method are discussed.

CHAPTER 2: LITERATURE REVIEW

2.1 Introduction

Distribution systems supply electric power to customers and occupy a significant position in power systems. Effective planning of distribution systems is required to meet day by day growth in domestic and industrial loads. However, fault may occur in distribution systems, which are unavoidable due to natural causes of wind or any other incidents. The fault causes current to pass through improper path, which will damage the equipment and lead to power interruption (Anderson, 1995). Hence, in order to maintain continuous power supply to customers, faulty line has to be identified and isolated from the system. The severity of the fault depends on the short-circuit location, the path taken by fault current and its voltage level.

The information about fault in a distribution system can be obtained at the operation center using protective device operation or using end user information. Then, fault location is identified using visual inspection or by a manual process of setting the relay to on/off condition until the circuit breaker trips. However, this process is time consuming and on long run will damage the performance of cables. Also visual inspection is difficult for underground cables. Hence, various fault location methods have been proposed by researches over years to locate fault.

This chapter discusses various methods in identifying the fault location. Faults in distribution system can be identified using methods such as conventional technique, travelling wave based, impedance based method and artificial intelligent methods. A review of the methods is presented in the following section and its basic theory, associated assumptions, advantages and disadvantages are discussed. From this review, a fault location method able to address the limitation of existing methods is proposed.

2.2 Conventional Technique

Before the introduction of automated fault location techniques, utility companies used conventional techniques to locate faults. Commonly, fault in distribution systems is identified based on the customers' complaint area. The location of the fault is then identified by visual inspection. For a small area, foot patrol is practiced to search the possible fault location while for a larger scale area, automobile or helicopter is commonly used. This approach of fault location is suitable for overhead lines. However, for underground cables, the fault line is not noticeable through visual inspection.

In case of underground cables sectionalizing method is used as an inspection aid, the older sectionalizing method has been called as "Cut and Try Method" or the "Divide and Conquer Method." The method is used for locating fault on underground cable. In this method, both ends of cable section are cut or separated and cut sections are individually tested using dc hipot or other tests ("IEEE Guide for Fault Locating Techniques on Shielded Power Cable Systems," 2007). The illustration of "Cut and Try method" is shown in Figure 2.1.

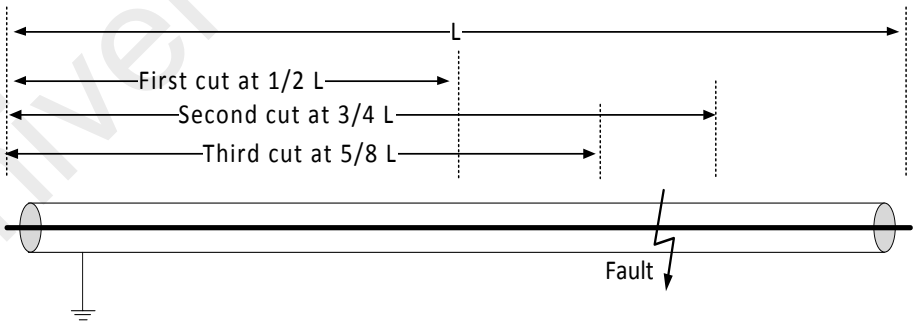

Figure 2.1 Cut and Try Method

A faulted cable will have a lower insulation resistance than a cable with no fault. The fault resistance is measured and a hole is dug half way down the length of the cable section. The cable is cut at half and the resistance measurement is made on each half. The faulted half of the cable will have a lower resistance than the un-faulted half. Also, the faulted half resistance is the same as the fault resistance measured on the complete

length of cable. A second dig is made half the distance down the faulted half. The cable is cut again and the process is repeated until a short section is identified. Eventually, the remaining short faulted section can be replaced. The disadvantages of the method are it is very crude and costly.

Later, "sectionalizing by re-fusing" is followed, where a sectionalizing switch isolates the faulty section from the rest of the system so that the healthy part can supply power to customer. This minimizes interruption duration and the interruption cost. The investment cost of a sectionalizing switch is $20,337 and breaker type switch is $4,700 respectively. The annual maintenance cost is 2% of the annual investment cost and life period of the switches is assumed to be 20 years with an interest rate of 8% (Billinton & Jonnavithula, 1996). Therefore, optimal placement of sectionalizing switches plays a vital role in distribution systems. This method typically results in damage to customer and utility equipment due to switching surges and fault currents. Therefore, this is not a recommended method for fault location ("IEEE Guide for Fault Locating Techniques on Shielded Power Cable Systems," 2007).

For systems where neutrals are not solidly grounded or transformers that cannot be disconnected, tracing method was used to identify fault location (Bastard, Garcia-Santander, Pivert, Gal, & Parra, 2002). The tracer method uses the measurements taken by a trained person walking the cable route or by distributing electromagnetic signal. The most popular tracer methods are Impulse method and Earth gradient methods. The method requires more man power and is time consuming. This method is widely used for pinpointing the fault location after determining the approximate location (A. A. Bhole, 2014).

Not every fault can be found and recognized, especially if the faults are momentary or non-permanent fault, and the damage is small. It means that these traditional methods

do not satisfy the requirements imposed on the fault location. The locating process is time consuming and might expose additional stress to the equipment during the switching on/off of a section. Due to these problems, many automated fault location methods have been introduced for the purpose of expediting the process of locating faults.

2.3 Travelling Wave Method

Travelling wave method is based on the principle of reflection and transmission of the travelling waves between the line terminal and the fault location. The illustration of the method is shown in Figure 2.2.

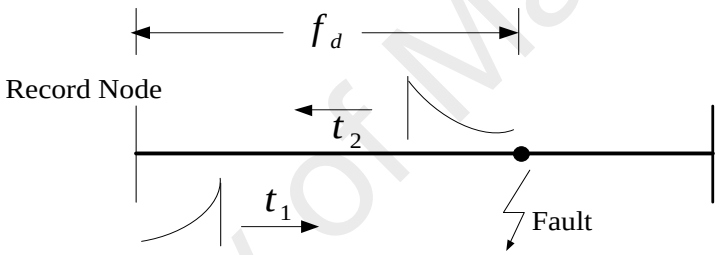

Figure 2.2 Travelling wave method

The fault distance is identified using

$$f_d = \frac{v*(t_2 - t_1)}{2} \tag{2.1}$$

where *v* is the velocity of the traveling wave, t_1 is the time taken for the travelling wave from the measurement node to the fault location and t_2 is the time taken for the reflected wave from the fault location to the measurement node and f_d is the fault distance which needs to be identified.

Travelling wave method requires sensors, Global Positioning System (GPS), fault transient detectors and high speed data acquisition devices to capture the transient

waveform for fault location. A method using maximum likelihood estimation is presented in (Ancell & Pahalawaththa, 1994). The accuracy of the method is determined as a function of fault initiation angle and fault distance. However, the accuracy of the method depends on the selection of basic set of parameters from data signals. In (Lee & Mousa, 1996), an investigation on the lightening related fault is analyzed. The time of arrival of generated travelling wave by fault is identified using GPS. The advantage is that the method is not affected by the load variance, high grounding resistance and series capacitor bank.

In (Bao & Mao, 2011), single terminal and two terminal travelling wave methods are analyzed and compared, which give the merits and demerits of each method. It shows that two-terminal location method has broad prospects than single terminal method. The proposed traveling wave fault location method is fast and gives accurate fault location and can reduce the power loss. A single terminal fault location method using the time and frequency domain characteristics of the fault is proposed in (Lin, He, Li, & Qian, 2012) for transmission lines. The method calculates fault distance based on the determined time and velocity. It shows that the method is not affected by fault type, resistance, distances and inception angles. Also, the fault location method can be used in both transposed and un-transposed circuits.

In (Mosavi & Tabatabaei, 2014), a travelling wave method without using GPS timing is suggested. The method records the transient wave at the bus bars using wavelet de-noising. The transient wave has information about the fault and its statistic parameters are trained using Artificial Neural Network (ANN) to locate fault. However, this method gives higher error compared to the fault location using GPS although the cost is reduced by omitting GPS receiver.

A real time travelling wave based fault location method is proposed in (Lopes, Silva, Costa, Neves, & Fernandes, 2015). The method is based on two terminal travelling wave and links both the ends of a transmission line by a communication system. The method is proposed with two possible situations of negligible and large data transmission latency. The advantage of the method is that it can be used in either synchronized or unsynchronized two terminal data.

From the review papers, it is noticed that travelling wave method is more widely used in overhead transmission lines and not in distribution lines. The reason is due to the presence of lateral branches and sub-branches in distribution systems. The disadvantage of this method is that it requires devices such as GPS and sensors to capture transient waveform (Lee & Mousa, 1996), which makes the method costly to implement.

Another category is using travelling wave based on the high frequency components of voltage and current caused by the inceptions of faults. In high frequency method, the high frequency voltage and current transient signals are injected to determine the fault location. The approach makes use of a stack-tuner circuit to act as a high frequency switch (Johns & Agrawal, 1990). In (Han, Yu, Al-Dabbagh, & Wang, 2007), high frequency components are used to detect fault location by injecting sinusoidal signals. It creates a feedback by further analyzing each branch, starting from the first sequence until the last by separating each layer onto a different branch. The actual fault is obtained by repeated searching process. Two sinusoidal signals with different frequencies are injected into faulted lines and calculated with feature extraction schemes. Accurate result was obtained using simulation program in the tested line with seven branches. High frequency components have also been utilized in (H. K. K. Abolfazl Jalilvand, 2010) to detect arching faults in distribution networks. The method

is based on the frequency spectrum analysis to automatically identify the state transformation of a duffing oscillator. By utilizing the applications of FIR filter bank and duffing oscillator, the location of faults is identified. The methods are complex and expensive because they require the use of specially tuned filters for measuring high frequency components.

2.4 Impedance Based Method

Impedance based methods are popular among electric power utilities because they are simple and economical compared to traveling wave and high frequency component techniques. The basic principle of the impedance based method is using the impedance value as seen from the measurement node for fault location. It uses the voltage and current data for impedance calculation. This method is further classified as one-end method and two-end method. The one end method uses the substation voltage and current for fault location. The two-end method uses the voltage and current at both the ends of the distribution system for fault location identification.

2.4.1 One-Ended Measurement Approach

The process of impedance based fault location using one-ended measurement is described in Figure 2.3 using a simple circuit model.

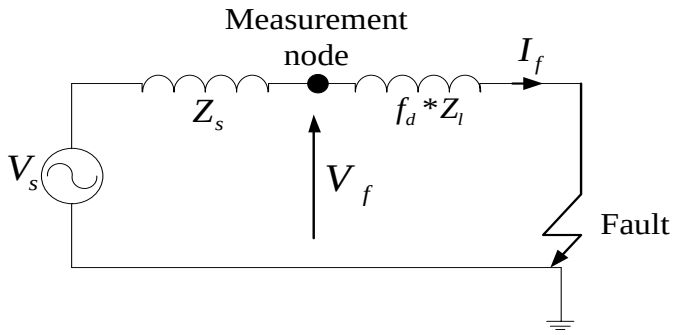

Figure 2.3 Impedance based method

The measurement node records the fundamental component of voltage and current values during fault condition. V_f and I_f correspond to the voltage and current during fault, Z_l is the line impedance per unit length, f_d is the fault distance from the measured node, V_s is the source voltage and Z_s is the source impedance. Based on Ohms Law, voltage and current from the measurement node can be used to find fault distance using

$$f_d = \frac{V_f}{I_f \times Z_l} \tag{2.2}$$

Different approaches are followed for finding the fault distance considering all types of fault such as Single line to ground fault (SLGF), Line to line fault (LLF), Double line to ground fault (DLGF) and Three phase to ground fault (LLLGF) and for different fault resistances. Methods such as Reactive component method (Sant & Paithankar, 1979, 1983), Takagi algorithm (Takagi, Yamakoshi, Yamaura, Kondow, & Matsushima, 1982), Girgis method (Adly A. Girgis, 1993) and various other approaches have been discussed in detail. The objective of these methods is to estimate the locations of fault on radial distribution systems.

Reactive component method estimates the apparent reactance of the line from the measurement node to the fault and then converts the calculated reactance to distance. (Sant & Paithankar, 1979) calculated the ratio of the reactive component of the apparent impedance to the reactance of the line for fault location. They also studied the effect of line capacitances on the fault location (Sant & Paithankar, 1983). However, the limitation of the method is that the fault resistance is not considered. Hence, the method is not valid for practical cases and is likely to have substantial errors.

Takagi algorithm uses fundamental frequency of voltage and current during fault and before fault (Takagi et al., 1982). The method uses Thevenin equivalent using voltage and current of a faulty line to locate the fault. However, the fault distance is identified using the assumption that the phase angle and fault current are equal. Hence the equation works for homogenous systems. The method was tested in practical transmission line systems and reported to operate satisfactorily.

Girgis et.al (Adly A. Girgis, 1993) derived a fault location equation more suitable for distribution systems. In this method, the fault distance and fault resistance are solved by identifying the real and imaginary parts of apparent impedance equation. The method also proposed an iterative procedure to calculate the voltage and load current at each bus. The updated voltage and current determine the fault distance for each section. The limitations of this method were discussed in (R. Das, Sachdev, & Sidhu, 1997) which are as follows:

1. The accuracy of the algorithm is affected by the dynamic nature of the loads not considered by this technique.
2. Distribution systems usually have multiphase and multiple laterals, which are not considered.
3. The technique was tested for a simple system with one single-phase lateral. For a fault on the lateral, the technique provided two estimates. Reduction of multiple estimated to a single estimate has not been discussed.
4. The technique provides inaccurate estimates for lines that have many sections.

In (Jun et al., 1997), the load modeling is accounted for fault distance calculation. The mutual coupling among different phases was regarded as the boundary condition of the proposed method. The boundary condition of the proposed method was described in the following equation,

$$V_a = f_d\left(Z_{aa}I_a + Z_{ab}I_b + Z_{ac}I_c\right) + I_f R_f \quad (2.3)$$

where Z_{aa} is the voltage measured in monitoring node in phase A,

f_d : Fault distance

I_f : Fault current

I_a, I_b, I_c : Fault current in the line phase

R_f : Fault resistance

Z_{aa} : Self-impedance of line

Z_{ab} and Z_{ac} : Mutual impedance of line

A direct approach is presented in (Choi, Lee, Lee, & Bo-Gun Jin, 2004), which can be used for both balanced and unbalanced systems. The fault-location equations use line impedance matrix, load impedance matrix and fault admittance matrix. The method utilizes matrix inverse lemma for directly solving complicated three-phase circuit equations. However, this method is used only for phase-to-ground fault. An extended method using direct circuit analysis for line to line fault was proposed in (Yang;, 2007) for unbalanced operation of distribution feeders. Since distribution loads vary over time, a technique for compensation of load variation by introducing load impedance compensation was also presented.

The work in (Bretas, 2011; Filomena, 2008; Seung-Jae et al., 2004) utilizes an iterative approach for fault current calculation which in turn used for calculating fault distance. Due to repetitive iteration, there is a possibility of getting computational error

due to truncation or round-off. The method in (Seung-Jae et al., 2004) was proposed only for SLGF. The method first identifies fault current and load current using an iterative procedure and then the fault distance using current pattern matching rules.

A comparison on the performance of some of the most cited impedance based methods (Adly A. Girgis, 1993; Choi et al., 2004; D. Novosel, 1998; R. Das, 1998; Jun et al., 1997; M. Saha, 2002; Sachdev & Agarwal, 1988; Springs, 1998; Srinivasan & St-Jacques, 1989; Warrington, 1968) is presented in (Mora-Flòrez, Meléndez, & Carrillo-Caicedo, 2008). Each method has been tested and compared in a simulated network. Additionally, (Mora-Flòrez et al., 2008) compares the fundamental working principle of each method, such as fault distance equation, modeling of lines, and the used-load models. From the test results, the method with the best global performance was proposed in (R. Das, 1998). The lowest error of fault distance for single-phase fault is obtained by Choi (Choi et al., 2004). On the other hands, the methods proposed by (Warrington, 1968), (D. Novosel, 1998) and (Srinivasan & St-Jacques, 1989) exhibited excellent results for different fault resistance values. The common results from all of the proposed methods show good performance in locating single phase faults. However, the comparison result in (Mora-Flòrez et al., 2008) focuses more on the accuracy of the fault distance and avoided discussing the multiple possible fault locations.

The main advantage of impedance based method is that it is more economical to be implemented since it requires only the measurement data at one end of the line. The accuracy of impedance-based method is dependent on the accuracy of line parameters, line characteristic and the accuracy of load value. However, the accuracy can be affected by several conditions such as system non-homogeneity, multiple laterals, measurement error in line parameters, inaccurate relay measurements and effect of fault

resistance as described in ("IEEE Guide for Determining Fault Location on AC Transmission and Distribution Lines," 2005).

2.4.2 Two-Ended Measurement Approach

A technique using two-terminal data for fault location is presented in (Novosel, Hart, Udren, & Garitty, 1996). The method estimates fault location using unsynchronized post fault phasors. The method utilizes the advantage of digital technology and numerical relaying for off-line fault location. The short line is represented by lump model and compared with long lines. The accuracy of the method is not affected by fault type, fault resistance, load current and source impedance. Also, this method does not require real time communications since the fault location analysis is done offline.

A fault location method using two-terminal synchronized voltage and current was described in (Ying-Hong, Chih-Wen, & Chi-Shan, 2002). The proposed algorithm is divided into two steps. The first test is to identify the faulted leg. The superimposed positive-sequence quantities are used as the input to the subroutine for identifying the faulted leg. The second step is to locate fault on the faulted leg. In the second step, superimposed positive-sequence quantities and post fault positive- sequence quantities are adopted for locating the fault. The test results show that the accuracy of the fault location is very high under various fault resistance, fault location, pre-fault loading conditions, source impedance and fault types.

Although the two-ended approach has shown to produce accurate results, its main drawback is the implementation cost. It is more expensive than one-ended approach as measurements are taken at both ends of the line. In addition to the cost, communication links may be required to transmit the measurement value to a control centre.

2.5 Knowledge Based Method

Due to the complexity of distribution systems and various uncertainty factors such as unknown fault resistance that are difficult to address using impedance-based techniques and travelling wave techniques, a knowledge-based technique can be a good option. The knowledge-based technique is based on various methods such as:

- Artificial Neural Network (ANN)
- Support Vector Machine (SVM)
- Fuzzy Logic
- Genetic Algorithm (GA)
- Matching approach
- Hybrid method

2.5.1 Artificial Neural Network

Artificial Neural Network (ANN) is one of the intelligent techniques that is used for locating faults in distribution systems. ANN recognizes difficult patterns of information, which made it possible to locate faults. However, they need a training process to locate the fault with a set of data input and the expected outcome. A general concept of ANN is shown in Figure 2.4, where voltage phase (V) and angle (ϕ) are the training input noted from measurement node and the target output is the fault location.

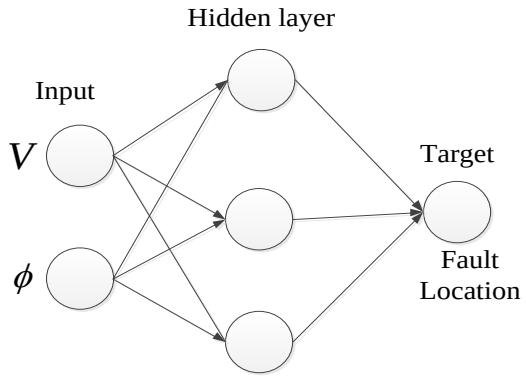

Figure 2.4 Artificial neural network

In (Purushothama, Narendranath, Thukaram, & Parthasarathy, 2001), ANN uses two approach of finding fault distance in transmission lines using one end measurement and two end measurement. It uses cascade correlation for fault detection and is concluded that both approaches (one end and two end measurement) perform equally good in identifying fault location. Also, it is noted that cascade correlation uses less amount of epochs and less number of hidden layers compared to Multilayer perceptron (MLP).

A method to detect high impedance fault for nonlinear arcing is proposed in (Khorashadi-Zadeh, 2004). The method evaluates lower order harmonics of voltage and current. An application of ANN to classify and locate fault in transmission system is proposed in (Hagh, Razi, & Taghizadeh, 2007). The method considers fault resistance and is independent of the fault inception angle. It utilizes the fundamental component of pre-fault and post-fault positive sequence components of voltage and current as input for estimating the fault location. The method considers MLP with back propagation training algorithm and Levenberg-Marquardt optimization method.

Javadian (Javadian, Nasrabadi, Haghifam, & Rezvantalab, 2009) proposed a method using MLP neural network for identifying fault type and location. The method was implemented on a distribution system considering Distributed Generator (DG). The fault current at three phases was used as input to neural network. MLP nets with back propagation as a learning algorithm which is most commonly used. However, due to more calculations in MLP network and low convergence speed of the back propagation algorithm, various other algorithms proposed to increase the convergence speed and are shown as follows:

- Gradient decent
- Gradient decent with momentum
- Gradient descent with momentum & adaptive learning rate

- Gradient descent with adaptive learning rate
- Levenberg-Marquardt
- Quasi-Newton
- Conjugate gradient

An approach using MLP neural network was reported in (Seyed & Maryam, 2011), which includes distribution generators in the distribution system for fault type and location identification. (Prarthana Warlyani, 2011) proposed a fault classification algorithm for transmission network using ANN. The method uses voltage and current to classify double line to ground fault at various fault location, fault resistance and inception angle. The method is tested for double line to ground fault and not on all fault types.

In the work of (Aslan, 2012), a method using feed-forward ANN is used to classify and locate faults in distribution network. The method uses fault voltage and current samples to locate fault. The proposed method was tested for various fault type, fault location, fault resistance and fault inception angle and a maximum percentage error of 3% is obtained in the analyzed test cases. The advantage of the method is that the ANNs can be trained off-line with the data reflecting modifications on the existing system such as demographic data of the area and seasonal or daily energy demand and generation levels. After training, on-line fast and accurate fault location can be identified.

The main advantage of ANN is its simplicity in implementation. The disadvantage of the method is that it is highly dependent on the amount and quality of the trained data in producing a well-trained ANN algorithm. A limited amount of information will therefore affect the performance of the method. This problem happens for distribution systems with limited information resulting from an insufficient number of monitoring devices. Other disadvantage of ANN is that the training process has slow convergence.

Also, the parameters such as hidden layers, neurons and learning rate are identified using trial and error case. In addition, the ANN algorithm needs to be re-trained whenever the system undergoes changes.

2.5.2 Support Vector Machine

Another recent type using knowledge based method is Support Vector Machine (SVM). SVM is widely used in classification and regression technique (Bouboulis, Theodoridis, Mavroforakis, & Evaggelatou-Dalla, 2015) gaining popularity among various intelligent techniques, due to its performance. The number of support vectors for SVM is determined by SVM algorithm whereas in neural network the numbers of hidden nodes are determined by trial and error method. This facility makes SVM a better classification algorithm than ANN. Also, SVM does not require any training effort as like neural network for good performance.

SVM was presented by Vapnik and Cortes, which became a novel machine for data analysis (Cortes & Vapnik, 1995; Vapnik, 1982, 1995). It uses a technique called the kernel trick to do extremely complex data transformation of mapping the original data into high-dimensional feature space. SVM identifies hyper plane to separate the data based on the defined outputs. Nowadays, SVM applications are common is several tasks such as face recognition (Guo, Li, & Chan, 2001; Yanhun & Chongqing, 2003), time series prediction (Cao & Tay, 2003; Sapankevych & Sankar, 2009), signal processing (Parsaei & Stashuk, 2012; Rojo-Álvarez et al., 2005) image processing (Kui & Kim-Hui, 2006; Shutao, Kwok, Tsang, & Yaonan, 2004) and fault diagnosis. SVM is found to be effective for power system applications due to its ability to work with existing pattern of data and its ability to solve small quantity of nonlinear samples even in high dimensions. The classification and regression analysis using SVM is discussed in detail.

2.5.2.1 Support Vector Classification (SVC)

The concept of SVM classification is shown in Figure 2.5 for classification between two classes (Class 1 and Class 0). The points are marked using training set voltage phase and angle data for fault classification. Support vectors are the elements of the training set which identify the dividing hyper plane. The black circles represent Class 1 and the empty circles represent Class 0. The input for Class 1 and 0 are from measurement node (V and ϕ) and the target output is the type of fault by identifying the optimal hyper plane. The objective is to identify the hyper plane for classification of 1 and 0 classes. The hyper plane separates all the samples and also maximizes the margin between two types. The margin is defined as the sum of the minimum distance between training data set and the separating hyper plane.

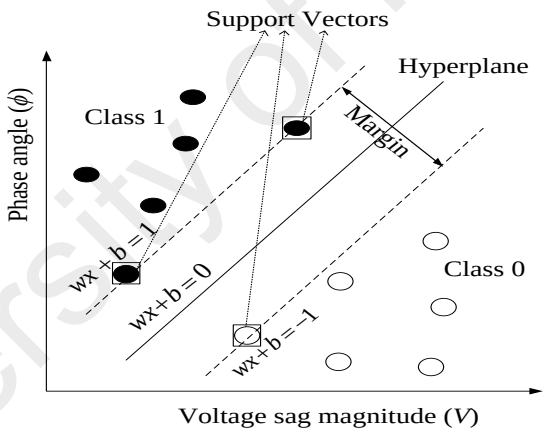

Figure 2.5 Linear classification using SVM

Suppose the training samples are $\{x_i, y_i\}$ where i=1 to l, $x_i \in R^n$ represents independent variables and $y_i \in (-1,+1)$. Hyper plane can be expressed as

$$f(x) \Rightarrow wx + b = 0 \tag{2.4}$$

where w is vector of coefficients and b is a constant. The perpendicular distance from hyperplane to origin is $|b|/\|w\|$. If the output is $y_i = +1$ then the training samples satisfy the following constraint

$$x_i.w + b \geq +1 \tag{2.5}$$

If $y_i = -1$ then the constraint is given as

$$x_i.w + b \leq -1 \tag{2.6}$$

The margin is the distance between the two equations and is given as $2/\|w\| = 2/\sqrt{w^T w}$ where $\|w\|$ is the Euclidean norm of w.

The equations (2.5) and (2.6) are combined into one set of inequality where w and b are maximum. The generalized classifier which can distinguish between Class 1 and Class 0 can be expressed as

$$\min_{w,b} \frac{1}{2} w^T w \quad \text{subject to} \quad y_i(x_i.w + b) - 1 \geq 0 \tag{2.7}$$

$$y_i(x_i.w + b) \geq 1 \tag{2.8}$$

This type of problem is Quadratic optimization problem. The training data appears in the dot product of vectors. This is crucial property which allows generalizing the procedure to non-linear case. This can be solved using Lagrangian formulation. The Lagrangian multiplier $\alpha_i = 1,....l$ is introduced to the inequality constraint (2.7). The inequality constraint is multiplied by Lagrangian multiplier and subtracted from objective function to form Primal Lagrangian as shown by

$$L_p = \frac{1}{2}\|w\|^2 - \sum_{i=1}^{l} \alpha_i y_i (x_i.w + b) \tag{2.9}$$

The Lagrangian has to be minimized with respect to the primal variables *w* and *b* and maximized with respect to Lagrangian multiplier α_i. At the optimal point the equations are $\frac{\partial L}{\partial b} = 0$ and $\frac{\partial L}{\partial w} = 0$ which translates into $w = \sum_{i=1}^{l} \alpha_i x_i y_i$ for $\alpha_i \geq 0$ and $\sum_{i=1}^{l} \alpha_i y_i = 0$. Support vector training therefore amounts to maximizing L_D with respect to α_i. Every training point has a Lagrangian multiplier α_i. The points which $\alpha_i \neq 0$ are called 'support vectors' and lie on the hyperplane. The hyper plane that optimally separates the data is the one that minimizes $\frac{1}{2}\|w\|^2$

Substituting $w = \sum_{i=1}^{l} \alpha_i x_i y_i$ in Equation (2.9) gives Dual Lagrangian, L_D

$$L_D = \sum_{i=1}^{l} \alpha_i - \frac{1}{2} \sum_{i=1}^{l} \sum_{j=1}^{l} \alpha_i \alpha_j y_i y_j (\phi(x_i)\phi(x_j)) \tag{2.10}$$

subject to $\sum_{i=1}^{l} \alpha_i y_i = 0$ for i=1,2,…..l

where $\phi(x_i)\phi(x_j)$ is the kernel function and is represented as $K(x_i x_j)$. The value of kernel function is equivalent to the inner product of two vectors x_i and x_j in the feature space $\phi(x_i)$ and $\phi(x_j)$. Kernel function transforms non-linear separable dataset into a new high dimension space where the dataset is made linearly separable. Different types of kernel used for training the SVM are

- Linear Kernel $K(x, y) = x.y$

- Polynomial Kernel $K(x, y) = (\gamma(x.y) + \gamma)^{\deg ree}$ with $\gamma > 0$
- Radial basis kernel $K(x, y) = \exp(-\gamma \|x.y\|^2)$ with $\gamma > 0$
- Sigmoid kernel $K(x, y) = \tanh(\gamma(x.y) + \gamma)$

Where γ is the kernel parameter. By solving the dual lagrangian, the nonlinear decision function is obtained as $f(x) = \text{sgn}(\sum_{i=1}^{l} \alpha_i y_i k(x, x_i) + b)$ where *x* is the test vector, *b* is the constant found from the primal constraints and is computed by $\alpha(y_i(w.x_i + b) - 1) = 0, i = 1,.....,l$ such that α_i is not zero and sgn is a signal function.

2.5.2.2 Multiclass SVM

SVMs are inherently two-class classifiers. If the classes are more than two then multiclass SVM is used. Multiclass SVM is of two types one-versus-all (OVA) and one-versus-one (OVO).

a) One-versus-all (OVA): OVA concept is the simplest multiclass SVM method. For analysis, consider *k* multiclass problem. OVA finds SVM classifier $f(x) = wx_i + b$ for each Class 1 and remaining all others as Class 0. The OVA reduces *k*-multiclass problem into *k* binary problems.

b) One-versus-one (OVO): OVO concept is more complex than OVA concept. This method involves the construction of SVM classifiers for all pairs of classes; in total there are *k*(*k*-1)/2 pairs. In other words, for every pair of classes, a binary SVM problem is solved. The decision function assigns an instance to a class that has the largest number of votes, so-called Max wins strategy. If ties still occur, each sample will be assigned a label based on the classification provided by the furthest hyper plane. One of the benefits of this approach is that for every pair of

classes deal with a much smaller optimization problem and a total of $k(k\text{-}1)/2$ problems to be solved.

An investigation using SVC for fault type in transmission line is proposed in (Dash et al., 2007). The method uses post fault current samples and firing angle as input to SVM. SVMs are trained with polynomial kernel and Gaussian kernel to obtain the optimized classifier. The method identifies the fault classification, ground detection and section identification. In (Parikh et al., 2010), SVM based fault classification scheme using zero sequence current and three phase current was proposed. This method was proposed for a series compensated transmission lines with fixed series capacitor at transmission lines. (Dash et al., 2007; Parikh et al., 2010) proposed fault type identification in transmission systems and not for distribution systems.

2.5.2.3 Support Vector Regression (SVR)

The method of Support Vector Classification can be extended to solve regression problems called SVR. One of the differences between SVR and SVC is the value of y_i . In SVC, y_i may equal to (+1,-1) or finite values. However, in SVR, y_i may be any real number. Thus, SVM handles numerical and nominal missing values. SVM can be applied to regression problems by the introduction of an alternative loss function ε. Thus, training the original SVR means solving

$$\text{Minimizing } \frac{1}{2}\left\|w^2\right\| \text{ subject to } \left\langle w, x_i \right\rangle + b - y_i \le \varepsilon \qquad (2.11)$$

The inner product plus intercept $\left\langle w, x_i \right\rangle + b$ is the prediction output, and ε is a free parameter that serves as a threshold. All predictions have to be within ε range of the true predictions. A graphical overview of the different steps in SVR is illustrated in Figure 2.6. The input pattern which a prediction is to be made is mapped into feature space by a map ϕ. Then, dot products are computed with the images of the training

patterns under the map ϕ. This corresponds to evaluating kernel functions. Finally the prediction output is given by solving the function $\sum_{i=1}^{l} \alpha_i y_i k(x, x_i) + b$

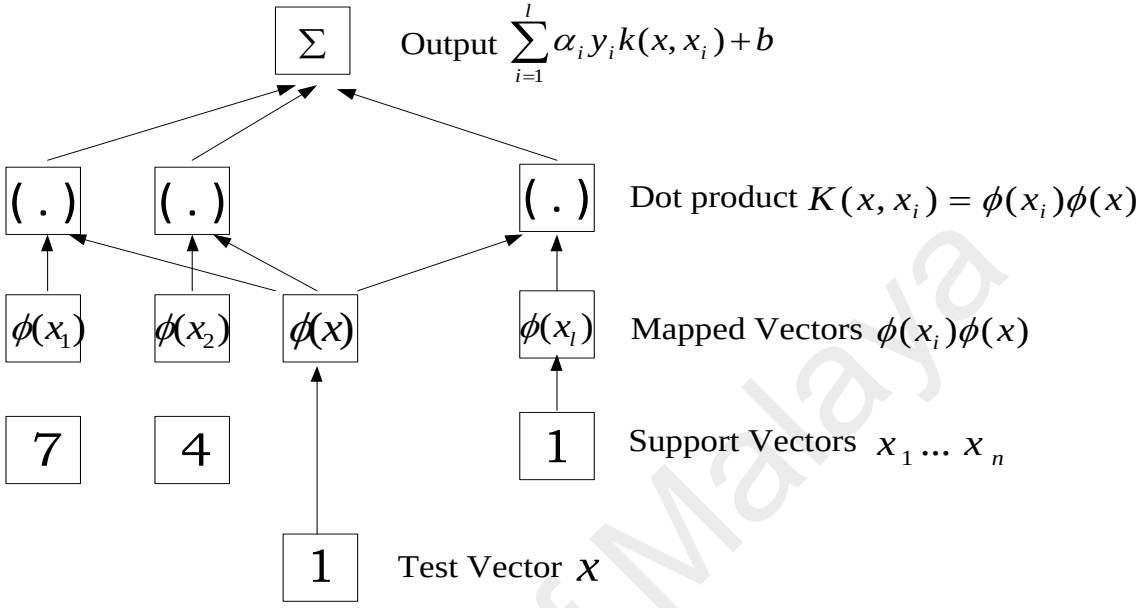

Figure 2.6 Architecture of SVR analysis

An effective method of fault location for transmission lines was proposed in (Salat & Osowski, 2004). The method uses the fundamental components of voltage and current at ill phases for fault location. The fault distance is identified using the high frequency range characteristics of voltage and current. In the work of (Janik & Lobos, 2006), RBF neural network and SVM are used to identify fault. The method uses three phase voltage signals to locate fault. The method utilizes SVM classifier and shows better classification rates than the RBF classifier, especially for oscillatory transients. By decreasing the number of training vectors, the difference between RBF and SVM classifiers grows in favor of SVM. This shows that the SVM network has satisfactory generalization ability and was able to recognize sags and other disturbances correctly, for the wide range of variable parameters.

In (Ravikumar et al., 2008), SVM was used as an intelligent tool to diagnose the fault type and distance in power transmission systems. The method uses the phasor values of line voltage and current to detect fault. The method is important for post fault diagnosis of any mal-operation of relays following a disturbance in the neighboring line connected to the same substation. The results are also compared with RBF neural network. It suggests that RBF kernel is a reasonable first choice for SVM training. Test results demonstrate that the SVMs have the potential to obtain a reliable post-fault diagnostic system.

SVM is used as an intelligent tool in (B., Thukaram, & Khincha, 2008) to discriminate between different zonal element faults in transmission systems. The method uses apparent impedance values from distance relay at different fault conditions. The method is successful for various operating conditions and fault resistance values.

An approach to predict the fault type and the fault distance using SVM and Wavelet transform was proposed in (Ekici, 2012). It uses voltage and current signals at one end of the transmission system to locate fault. It works in three stages. Firstly, wavelet transform is employed to extract the high frequency components of voltage and current. Secondly, fault type is identified using SVC. Finally, the fault distance is identified using SVR analysis. The accuracy of fault type identification is 1% and 0.7% for fault distance. The limitation of the method is that it does not consider the faulty phase in the system.

A hierarchical fault location method in neutral non-effectively grounded loop distribution system was proposed in (Deng, Yuan, Xiao, Li, & Wang, 2015). The method identifies faulty section and the fault distance. The faulty section is identified using the zero sequence current variation before and after closing the switch in ring network. The method also utilizes wavelet transform to extract eigenvalues from zero-

sequence current. The extracted values are then trained using SVM to identify the fault distance. The proposed method is analyzed only for single phase grounding fault and is not suitable for other types of fault.

The advantage of SVM is that it is faster even for large size problem and require less heuristics (B. et al., 2008). The main features of SVM are that the upper bound on the generalization error does not depend on the dimension of the space. Also, the error bound is minimized by maximizing the margin.

2.5.3 Fuzzy Logic

In fuzzy set theory, the concept of possibility is used instead of the concept of probability. Possibility is defined by a number between one (completely possible) and zero (totally impossible). Probability is an appropriate measure of uncertainty if statistical information is available. In uncommon situations where no statistics are available, an expert may be able to express degrees of confidence in various hypotheses.

A method to deal with the uncertainty involved in the process of locating fault was proposed in (Jarventausta, Verho, & Partanen, 1994). In this method, the heuristic knowledge and the information concerning the fault situation are modeled as member ship functions of fuzzy sets. By using fuzzy set, alternative places of fault can be identified. This method is proposed to enhance the information available to the operator for decision making and to perform necessary switching.

Fuzzy logic based classification scheme was proposed in (B. Das, 2006; B. Das & Reddy, 2005; A. K. Pradhan, Routray, & Biswal, 2004), which identified the type of fault in transmission systems. In (A. K. Pradhan et al., 2004), higher order statistics was developed to extract the features of fault signal and fault is categorized using fuzzy logic. Fault identification using the line current measurement of all 3 phases is proposed

in (B. Das & Reddy, 2005). Later, the method was developed in (B. Das, 2006) for fault type in unbalanced system. Although fuzzy logic based scheme is quite satisfactory, the drawback of fuzzy logic is in determining the global minimum using fuzzy membership functions. Also, feature definition and extraction have to be enhanced for classification algorithm.

2.5.4 Genetic Algorithm

Genetic algorithm (GA) is an intelligent technique that can be used to locate fault. The method searches possible fault location through selection, crossover and mutation operations to identify the exact location. An approach for faulty section estimation using GA was proposed in (Bedekar, Bhide, & Kale, 2011). In the faulty section, estimation is treated as an optimization problem. The objective function is identified using Hebb's rule and used by Continuous Genetic Algorithm (CGA) optimization for faulty section identification. The objective function reduces the time required by CGA to identify faulty section. The method uses less storage and is faster than Binary GA.

A new method using GA was proposed in (Jin & Ju, 2012), which divides the distribution system into main branch and into individual regions. The independent regions are detected using the fault current and GA was used to find fault for the main branch and fault independent regions. This method is only suitable for single fault or complex fault location of the single power source.

A fault location method using GA for transmission lines is proposed in (Li et al., 2012). It uses line parameters and asynchronous time at both the terminals of the line to identify the fault location. The method was tested with the actual fault recording data obtained from the south grid of China.

The disadvantage of GA for fault location in distribution systems is that the results are not consistent over time because in GA, almost all processes are random. There is a possibility that the GA may produce inaccurate results, hence on-line analysis using this method might not be appropriate.

2.5.5 Matching Approach

Another knowledge based technique is matching approach, which makes a comparison between measured and simulated data. Commonly, voltage sag or current data are recorded to identify the location of fault.

A fault location technique using voltage sag data was proposed in (Lamoree, Mueller, Vinett, Jones, & Samotyj, 1994). The underlying principal of this approach is based on the severity pattern of the voltage sag that can be clearly differentiated according to the location of the fault. A fault closer to the monitored node causes more severe sag as compared to fault occurring far from the monitored node, as shown in Figure 2.7.

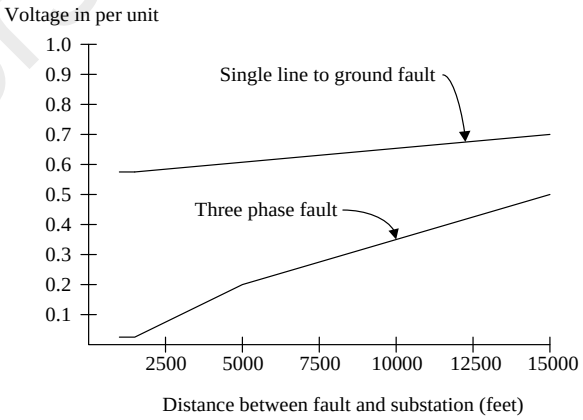

Figure 2.7 Voltage sag magnitude profile along a feeder due to Three Phase and Single Phase (Lamoree et al., 1994)

A method involving voltage sag to locate faults was reported in (R. A. Pereira, Kezunovic, & Mantovani, 2009). This method has been adopted for locating faults on

primary distribution feeders, and requires multiple meters to be integrated into the system. It has been tested on a 13.8 kV overhead line, with 238-node. Similar methods have been proposed in (R. A. F. Pereira, da Silva, Kezunovic, & Mantovani, 2009)but with a different test system of 13.8 kV with 134-nodes overhead lines. Different from other methods, the method in (A. Pradhan, Routray, & Madhan Gudipalli, 2007) is based on the difference in the phase angle between the positive sequence component of the current during fault and the pre-fault is being used to estimate the fault's direction. The direction is important for directional over-current relay operations.

A method to identify the faulty section was proposed in (Mokhlis H, 2010). The method utilizes voltage sag data at the primary substation to locate fault. Using simulation, a voltage sag database is created by generating fault at various sections. The method identifies the faulty section by matching the actual voltage sag during fault with the voltage sag pattern in database. Since these methods require the measurement of voltage sag at the primary substation, it is regarded as highly economical if it is to be implemented. The limitation is that the method identifies only the faulty section, maintenance crew needs to patrol along the suspected line section to find the exact location of fault. This process consumes time if the line section is long and delay the restoration process. Later, the method was further improved in (H. Mokhlis, Bakar, A., Talib, D., & Mohamad, H, 2010) for finding the fault distance. The method first identifies the faulty section and then the fault distance. The fault distance is calculated using a trigonometric equation considering a linear representation of voltage sag between two nodes.

A work in (Bollen, 1996) shows that the voltage sag variation can be linear or non-linear. Hence, a nonlinear representation of voltage sag variation is presented in (Hazlie Mokhlis & Li, 2011) to estimate the fault location. The method uses voltage sag at the

primary sub-station to locate fault. A set of two quadratic equations are framed using voltage phase and distance and also current phase and distance for fault distance calculation. The method also addresses the problem of multiple possibility of faulty section using a ranking process. The method considers the loading variation, fault resistance and measurement error.

An evaluation of fault location method in (Hazlie Mokhlis & Li, 2011) is presented in (H. Mokhlis, 2011). This work focuses on the influence of voltage sag pattern in finding the accurate fault distance. The performance of the method is analyzed using non-homogeneous and unbalanced distribution networks. The work shows the advantages and limitation of the method when applied for different fault resistance, loading variation and load models. (L. J. Awalin & Mokhlis, 2012) proposed an improved fault location considering multiple measurements in the distribution systems. A new method to identify faulty section and a ranking procedure to prioritize the faulty section was proposed.

The limitation of matching approach is that it is dependent on the simulated data stored in a database for matching the data with actual fault data. The process of creating database is time consuming since it is created through simulation for fault at all nodes.

2.5.6 Hybrid Method

Due to some limitations of the impedance and knowledge based techniques, fault location using a combination of both techniques is introduced, called as hybrid fault location method. The strength of each of the method is combined to increase the accuracy to fault location.

A novel method for online fault diagnosis was proposed in (Wen-Hui, Chih-Wen, & Men-Shen, 2000). The method identifies the fault type and the faulty section using

hybrid cause-effect network/fuzzy rule-based method. The proposed method has very fast inference speed, simple inference procedure and also robust in dealing with uncertainties.

A combination of ANN and SVM to locate fault in distribution systems was proposed in (Thukaram, Khincha, & Vijaynarasimha, 2005). Voltage and current grouping is used to detect the type of fault and to detect Short Circuit Current (SCC) levels using SVM. After this process, a feed forward neural network is used to determine the location of fault.

A fault location method using wavelet fuzzy neural network is presented in (Chunju, Li, Chan, Weiyong, & Zhaoning, 2007). The fault characteristics are identified using high frequency components and are extracted from fault signals using wavelet transform. Wavelet and fuzzy neural network were integrated to form wavelet fuzzy neural network (WFNN). The advantage of the method is that it is not influenced by the fault resistance and load current. The limitation is that it is implemented for only Single line to ground fault.

Another hybrid method has been proposed in (Salim, de Oliveira, Filomena, Resener, & Bretas, 2008) combining Impedance-based method, wavelet-based and ANN. The proposed method uses fundamental phasors of voltage and current to locate fault. Wavelet transforms were adopted for fault detection and classification. The fault location was identified using impedance based method and the faulty section was determined using ANN. The proposed fault diagnosis scheme was implemented in embedded software for distribution automation purposes and used by a Southern Brazilian power distribution company.

In (Sadinezhad, Oct 2008), parallel process of a novel Complex Least Error Squares (CLES) filter and Adaptive Linear Neural Networks were used to locate faults. The filter estimates the symmetrical components for fault location. Neural network estimates the fault location directly from time domain positive sequence components of transmission lines. The technique is robust and identifies fault location accurately.

A hybrid method using Wavelet analysis and ANN for detecting high impedance fault locations was proposed in (Moshtagh, 2009). EMTP/ATP software was applied to simulate a test system of 20kV underground power distribution systems. Another hybrid method using *k*-nearest neighbours (k-NN), and SVM was proposed in (Mora-Florez, Morales-Espana, & Perez-Londono, 2009). The method identified the fault zone and reduces multiple estimation of fault location. The voltage and current from primary substation were used as inputs. In this work, the fault locator is composed of two main stages:

1. Training is designed to obtain an associated object (as an input) and output (fault zone).
2. Testing is aimed to determine the best class (fault zone).

A new approach to predict the fault type and fault distance using WT and SVM was proposed in (Ekici, 2012). DWT was employed to extract the distinctive high-frequency components of the current and voltage signals. SVM was then used to identify the fault type and the fault distance. The method gave a very less percentage error of 1% in identifying the fault type and percentage error of 0.7% for fault distance.

A hybrid fault location with wavelet transform (WT) and wavelet packet transform (WPT) combining artificial neural network (ANN) is presented in (Ray, Panigrahi, & Senroy, 2013). The method uses current and voltage signal from the inception of fault.

The features of current and voltage signal are extracted by discrete WT and WPT. The extracted features are fed as input to ANN process for fault location. The method locates fault distance accurately with an absolute error of maximum 0.35%

Hybrid method requires extra information from various protective devices such as re-closer and fuses in order to rank the possible fault locations. However, problems in ranking the possible fault locations might occur if the setting time of protective devices is the same or if the device location is not known.

2.6 Summary

This chapter presents the overview of several fault location methods in distribution systems namely conventional technique, travelling wave-based method, impedance-based method and knowledge based method. From the reviewed articles, it can be summarized that every fault location method has its own advantages and limitations. However, it is observed that no single method has the capability to solve all the problems since each of them was developed based on specific conditions. Each method suits a problem depending on the complexity of network and the availability of monitoring devices.

Travelling wave method is more suitable for transmission system and not applicable for distribution system. The reason is distribution systems have more laterals compared to transmission systems. On the other hand, impedance-based method is more affected by circumstance such as the combined effect of fault resistance and load, system non-homogeneity and inaccurate measurement of relay. Fault location based on the intelligent approach may be suitable to be used for networks equipped with various monitoring equipment. Intelligent method includes Matching approach, Fuzzy logic, Genetic Algorithm, SVM and ANN. However, SVM is more popular among intelligent techniques due to its performance. It can be used for both classification and regression

analysis. Also, SVM is more advantageous than neural network since neural network uses trial and error method to identify hidden nodes, while SVM does not require any such trial and error. In addition, SVM does not require any training effort as like neural network for good performance.

The review also shows that many proposed technique involves mathematical equation to locate fault. The equations were derived based on particular assumptions of the system to simplify the problem. Thus, the equations may not be able to produce accurate results when applied on different system conditions. However, modeling all possible conditions of the system is difficult since configuration of distribution networks is complex. Considering this problem, matching approach is promising since it requires only training data and matches the simulated data with the actual fault data. To deal with limited measurement in distribution systems, the proposed method uses voltage sag data measured at the primary substation. These data can be further utilized for mathematical calculations, which identify the faulty section and fault distance. Thus, any possible conditions of the system can be modeled.

The proposed method considers the advantages of SVM, matching and mathematical approaches in identifying fault location. Using classification, SVM identifies faulty phase and fault type. The fault resistance for section identification and fault distance are calculated using regression analysis of SVM. The proposed method also formulates a fault distance equation using Euclidean approach. A comparison on fault distance using SVM and using mathematical equations is carried out for performance evaluation.

CHAPTER 3: FUNDAMENTALS OF FAULTS AND VOLTAGE SAG

3.1 Introduction

Various methods of fault location are briefly discussed in Chapter 2. The importance of accurate fault identification and the advantages and disadvantages of various methods are also discussed in the previous chapter. This chapter describes the fundamental theory related to voltage sag including the causes and characteristics related to fault in distribution systems. The faults under consideration are single line to ground fault (SLGF), line to line fault (LLF), double line to ground fault (DLGF) and three-phase to ground faults (LLLGF). Also, the influence of fault in the context of voltage sag profile is discussed since the proposed method utilizes voltage sag to locate fault. It also discusses the economic losses due to voltage sag in distribution systems.

3.2 Type of Faults

There are two types of faults in distribution lines namely, balanced faults and unbalanced faults also known as symmetrical and asymmetrical faults respectively. Most of the faults that occur on power systems are unbalanced faults and not balanced three-phase faults. Faults can also be categorized as series and shunt faults (Gonen, 2009).

3.2.1 Series Faults

Series fault occurs when unbalanced series impedance presents on lines. It represents an open conductor. It occurs when the system holds one or two broken lines, or impedance inserted in one or two lines. Series faults are characterized by increase of voltage and fall in current in the faulty phases.

3.2.2 Shunt Faults

Distribution systems generally experience shunt fault. Phase-overcurrent relays and ground-overcurrent relays are commonly used for detecting and isolating the faulted circuit in a distribution system. The important characteristic of shunt faults is the

increment the current suffers and fall in voltage and frequency. For a three phase line, shunt faults are classified as SLGF, LLF, DLGF and LLLGF.

3.2.2.1 Single Line to Ground Fault (SLGF)

Single line to ground fault is also known as short circuit fault. It occurs when one phase of transmission line falls to ground or makes contact with the neutral wire. Some of the reasons for SLGF are wind, falling tree or any other incident. 70% of faults in network are classified under this category (Saadat). Three types of SLGF are shown in Figure 3.1 where a, b and c represents the phases and R_f represents fault resistance.

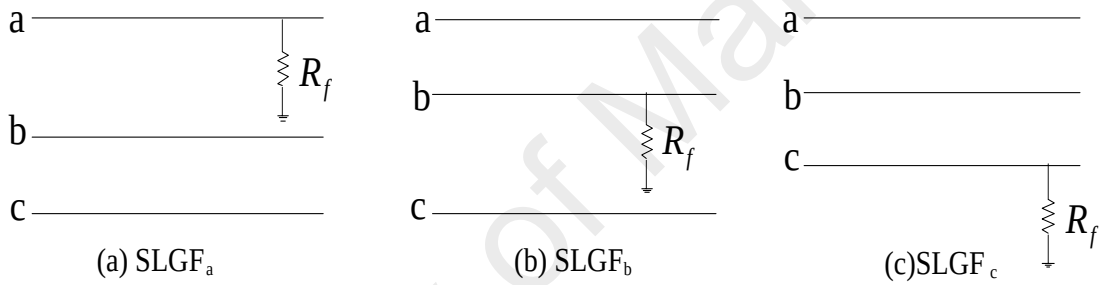

Figure 3.1 (a) Single line to ground fault at phase a ($SLGF_a$), (b) Single line to ground fault at phase b ($SLGF_b$) and (c) Single line to ground fault at phase c ($SLGF_c$)

3.2.2.2 Line to Line Fault (LLF)

Line to line fault occurs due to high winds or when two conductors are short circuited. It may take place either on overhead or underground transmission systems. Figure 3.2 represents line to line fault on three phase line conductors. One of the characteristics of this type of fault is that its fault impedance magnitude could vary over a wide range making very hard to predict its upper and lower limits. 15% of faults in network are considered as line to line faults (Saadat).

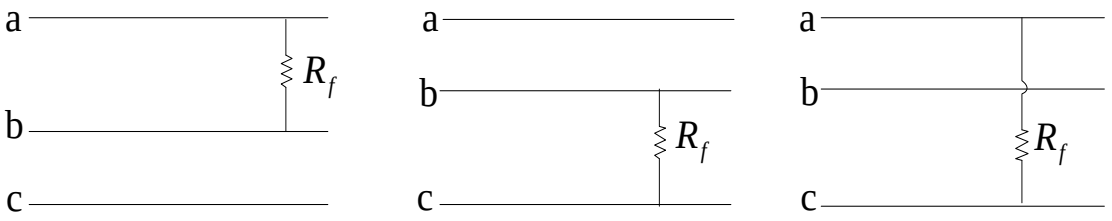

(a) LLF_{ab} (b) LLF_{bc} (c)LLF_{ca}

Figure 3.2 (a) Line to line fault at phase a and b (LLF_{ab}), (b) Line to line fault at phase b and c (LLF_{bc}) and (c) Line to line fault at phase c and a (LLF_{ca})

3.2.2.3 Double Line to Ground Fault (DLGF)

Double line to ground fault may occur when a falling tree connects two phases with the ground. In addition, two phases will be involved instead of one at the line-to-ground faults scenarios. A DLGF represents a serious event, which causes a significant asymmetry and it may spread into a three-phase fault when not clear in appropriate time. 10% of faults are classified under DLGF (Saadat). Figure 3.3 represents DLGF on three phase line conductors.

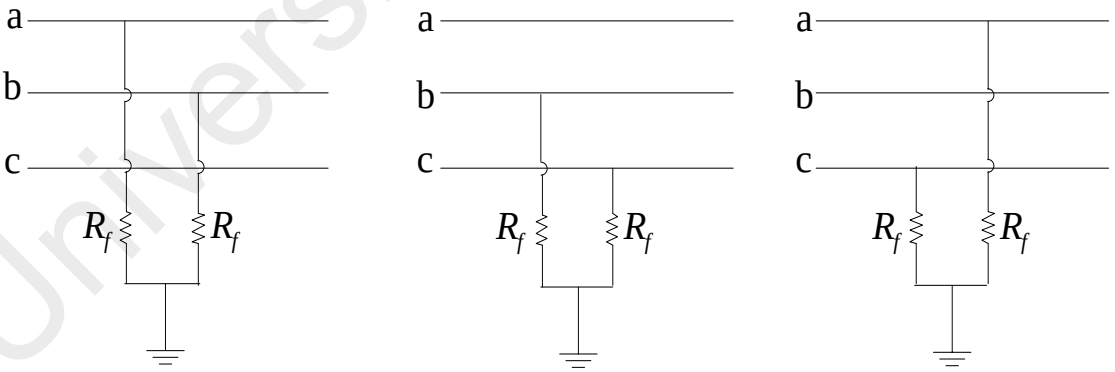

(a) $DLGF_{ab}$ (b) $DLGF_{bc}$ (c)$DLGF_{ca}$

Figure 3.3 (a) Double line to ground fault at phase a and b ($DLGF_{ab}$), (b) Double line to ground fault at phase b and c ($DLGF_{bc}$), and (c) Double line to ground fault at phase c and a ($DLGF_{ca}$)

3.2.2.4 Three Phase to Ground Fault (LLLGF)

Three-phase to ground fault is also known as symmetrical fault. It may occur due to a falling tower, failure of equipment or even a line breaking and touching the remaining phases. In reality, this type of fault does not often exist and occupies 5% of all transmission line faults (Saadat). Even though it is the least frequent fault, it is the most dangerous. Figure 3.4 shows a general representation of three-phase to ground fault at phase a, b and c. The characteristics of three-phase to ground fault are a very large fault current and a voltage level equals to zero.

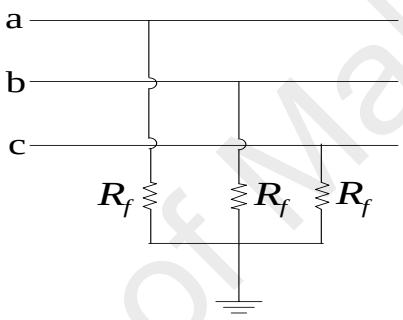

Figure 3.4 Three phase to ground fault at phase a, b and c ($LLLGF_{abc}$)

The percentage occurrence of the fault types and its severity are shown in Table 3.1. The severity of the fault can be expressed in terms of the magnitude of the fault current and its potential for causing damage. In power systems, three-phase to ground fault is caused by simultaneous short circuit between three lines and is the most severe while single line to ground fault is the least severe.

Table 3.1 Severity of fault occurrence

Fault	Percentage of Occurrence	Severity
SLGF	70%	Less severe
LLF	15%	Less severe
DLGF	10%	Less severe
LLLGF	5%	More severe

Also, the percentage occurrence of fault due to other elements of power system is shown in Table 3.2

Table 3.2 Fault occurrences due to power system elements

Power System Element	Percentage of fault occurrence
Overhead lines	50
Underground cables	9
Transformers	10
Generators	7
Switch Gear	12
CT, PT relays, Control equipment etc.	12

3.3 Fundamentals of Voltage Sag

Voltage sags are common phenomenon in power systems, which disturb the quality of the power supply. They are also known as voltage dip. Voltage sag in power systems is caused by a fault on the transmission or distribution systems and is the reduction in voltage for a short duration of time. They can also be caused by sudden load changes, or starting large motors and faults.

3.3.1 Definition of Voltage Sag

Voltage sag definitions are given in IEEE Standard 1159-1995 ("IEEE Recommended Practice for Monitoring Electric Power Quality," 1995) as “a decrease in voltage magnitude between 10 and 90 percent of nominal voltage during 0.5 cycles upto 1 minute”. The definition of voltage sag is illustrated in Figure 3.5. Events shorter than 0.5 cycles in duration are defined as ‘transients’ and magnitudes lower than 10 percent of nominal value are defined as ‘interruptions’. If the lower magnitude is maintained for longer than 1 minute, the problem is classified as an ‘under-voltage’. The voltage dip region is divided further depending on the dip duration. Between 0.5 and 30 cycles the dip is classified as ‘instantaneous’, between 30 cycles and 3 seconds, it is classified as

'momentary' and between 3 seconds and 1 minute, the dip is defined as 'temporary'. It is a natural conclusion that dips with longer duration cause bigger problems.

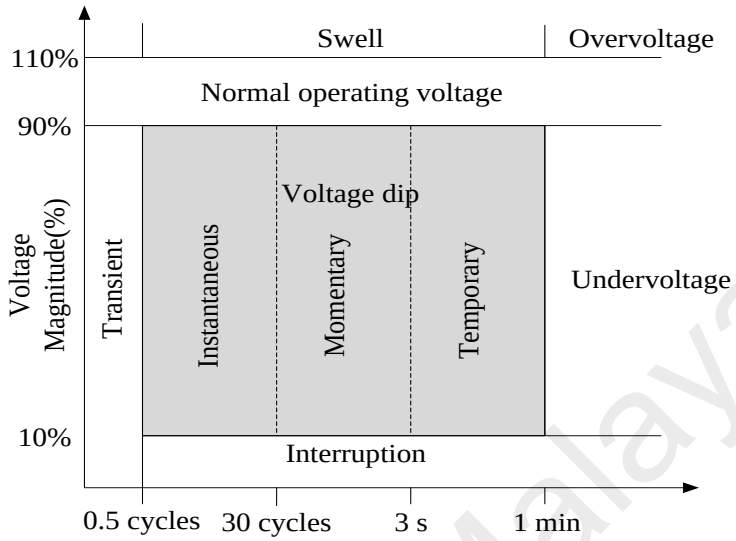

Figure 3.5 Definition of voltage dips according to IEEE Standard 1159-1995

3.3.2 Characteristics of Voltage Sag

The characteristics of voltage sag can be studied using the voltage sag magnitude, duration of voltage sag and phase angle jump.

3.3.2.1 Voltage Sags Magnitude

The voltage sag magnitude depends on the fault type, fault resistance, fault distance and the system configuration. Voltage sag magnitude can be calculated using a voltage divider model (Suresh Kamble, 2012). The principle of voltage divider model is shown in Figure 3.6. V_s and Z_s represent the source voltage and impedance. Z_f represents the fault impedance. The voltage sag V_{sag} can be calculated using

$$V_{sag} = \frac{Z_f}{Z_s + Z_f} V_s \tag{3.1}$$

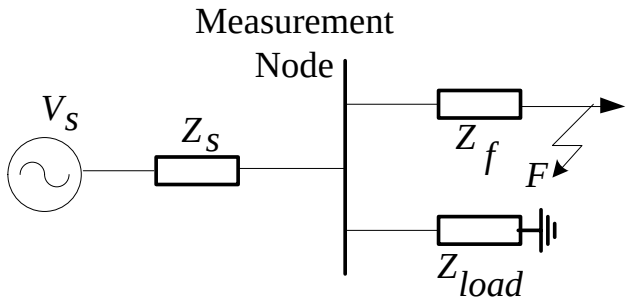

Figure 3.6 Voltage divider model

3.3.2.2 Voltage Sags Duration

The voltage sag duration is the period of time during RMS voltage magnitude is lower than a defined threshold limit. Figure 3.7 shows the voltage sag occurred at phase-a due to SLGF in a simple power system (Figure 3.8). The x-axis represents the time in seconds and y-axis represents the voltage in p.u.

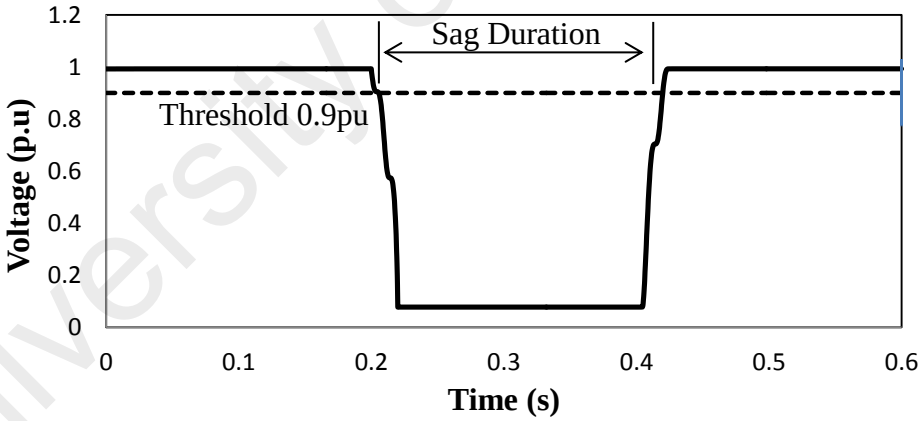

Figure 3.7 Voltage sag duration

The duration of the sag is mainly determined by the fault clearing time that relies on the protective equipment operation time. If the sag duration is long, it causes instability in the system, which may lead to black outs. Therefore, fast fault clearing time plays a critical role in power system. Once the protective device removes the fault from the system, the voltage magnitude will come back to its original state, as shown in Figure 3.7. Table 3.3 shows the fault clearing time for some conventional devices ("IEEE

Recommended Practice for the Design of Reliable Industrial and Commercial Power Systems - Redline," 2007).

Table 3.3 Typical fault clearing times

Fault clearing device	Clearing times (cycles)	
	Minimum	Time delay
Expulsion fuse	0.5	0.5 to 60
Current limiting fuse	0.25 or less	0.25 to 6
Electronic Recloser	3	1 to 30
Oil Circuit breaker	5	1 to 60
SF6 or vacuum breaker	2 to 5	1 to 60

3.3.2.3 Phase Angle Jump

Phase angle jump manifests itself as a shift in zero crossing of the instantaneous voltage during fault. Phase-angle jump during three-phase faults is due to the difference in X/R ratio between the source and the feeder. A second cause of phase angle jump is the transformation of sags through transformer to lower voltage level. Phase-angle jump is not of concern for most equipment except power electronics converter using phase-angle information for their firing instants (M. H. Bollen, 2000). The phase angle jump can be expressed using the following equations:

$$\Delta\phi = \arg\left(V_{sag}\right) \tag{3.2}$$

$$\Delta\phi = \arctan\left(\frac{X_F}{R_F}\right) - \arctan\left(\frac{X_s + X_F}{R_s + R_F}\right) \tag{3.3}$$

3.3.3 Voltage Sag in Distribution System

Voltage sags in transmission and distribution systems caused by faults have become one of the most important power quality problems. Figure 3.8 shows single line diagram of a power system. A, B, C and D represent a circuit breaker. F_1 and F_2 indicate fault at position 1 and 2. If a fault occurs at F_1, the protective relay identifies the fault and

operates the circuit breakers A and C to clear the fault. If fault is at F_2 then protective device 1 will open and all customers connected to this line will lose the power.

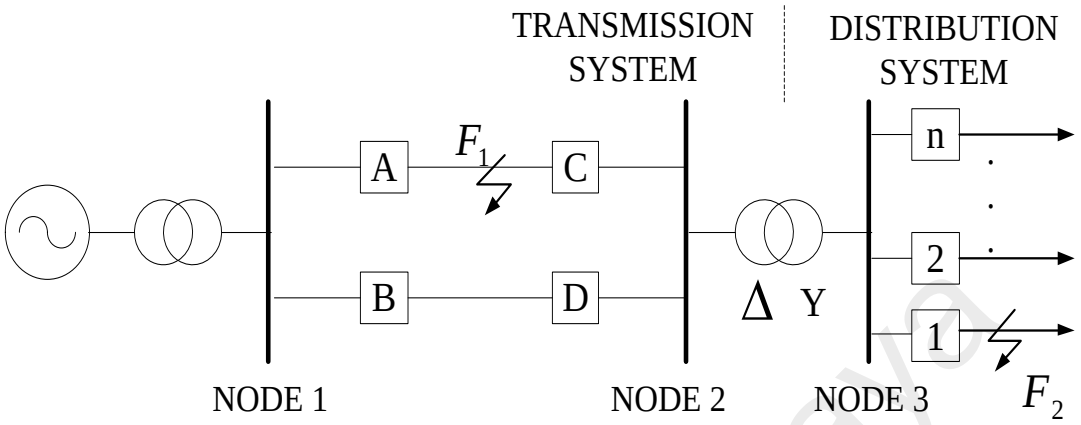

Figure 3.8 Single line diagram of power system

The monitored voltages at node 3 due to SLGF at phases a, b and c are shown in Figure 3.9. It shows the per unit values of voltage magnitude at phases a, b and c. The x-axis represents the time in seconds and y-axis represents the voltage in p.u.

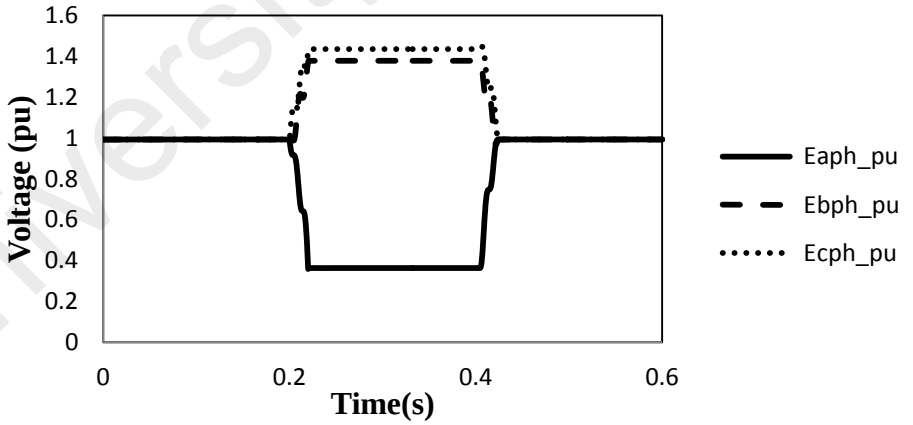

Figure 3.9 Voltage magnitude phases a, b and c for SLGF

The sag duration depends on the protective device setting operation time. Once the fuse or breaker operates to clear the fault from the system, the voltage magnitude at node 3 will return to normal. The sag duration due to a fault on transmission line systems is normally less than the duration of a fault on distribution systems because

protective device in transmission systems clears the fault faster than the protective device in distribution systems. This is crucial because transmission systems need to be well protected as they carry power supply to distribution systems. The severity of voltage sag depends on the location of the fault. Generally, a fault occurring near a substation will produce deeper sag than a fault located further from the substation.

3.4 Factors affecting Sag Characteristic

The type of fault in power systems is the major factor which affects sag characteristics. Depending whether the fault type is balanced or unbalanced, sag will be balanced or unbalanced in three phases. The magnitude and phase angle of sag will also depend on the type of fault (M. H. J. Bollen, 2000). Naturally, for LLLGF, the sag is symmetrical (balanced) in all three phases while for unbalanced faults like SLGF, LLF, DLGF the sag is unsymmetrical (unbalanced) in all three phases.

Figure 3.9 shows SLGF at phase a, where the pre fault voltage at phase a is greater than the fault voltage. The fault voltage at phase b and c is greater than the pre fault voltage. Hence, the pre-fault and fault voltage can be used to identify the fault type. Thus, for SLGF, the voltage sag magnitude at one of the phases is less while the other two remains higher than the pre-fault condition. For line to line fault, the voltage sag at two faulty phases is less and the voltage sag at third phase is equal to the pre fault voltage. For double line to ground faults, the voltage sag at two faulty phases is less and the third phase exceeds the pre-fault voltage. For three-phase to ground fault, voltage at all phases are equal and fault voltage is less than the pre-fault voltage. The fault type using the characteristics of voltage sag at fault and the pre fault condition is shown in Table 3.4.

Table 3.4 Voltage sag and fault type classification

Type of fault	Voltage sag characteristic
Single line to ground fault	$V_a^{fault} < V_a^{pre-fault}$ $V_{b,c}^{fault} > V_{bc}^{pre-fault}$
Line to line fault	$V_a^{fault} < V_a^{pre-fault}$ $V_b^{fault} < V_b^{pre-fault}$ $V_c^{fault} = V_c^{pre-fault}$
Double line to ground fault	$V_a^{fault} < V_a^{pre-fault}$ $V_b^{fault} < V_b^{pre-fault}$ $V_c^{fault} > V_c^{pre-fault}$
Three phase to ground fault	$V_a^{fault} = V_b^{fault} = V_c^{fault}$ $V_{a,b,c}^{fault} < V_{a,b,c}^{pre-fault}$

3.5 Voltage Sags Detection

In real time measurements, the voltage sag magnitude can be calculated using root mean square value and fundamental voltage component.

3.5.1 Root Mean Square (RMS)

The voltage waveforms are recorded as a sample of points from the monitoring node (Suresh Kamble, 2012). The formula to calculate RMS voltage magnitude is

$$V_{rms}(k) = \sqrt{\frac{1}{N}\sum_{n=1}^{N} v(n)^2} \tag{3.4}$$

where N is the number of samples per cycle, and $v(n)$ is the sample's voltage in the time domain. In practical applications, the data window slides along the time sequence in a specific sample interval. The window length must be an integer multiple of one half-cycle because other window lengths will produce an oscillation in the result with

frequencies equal to twice the fundamental frequency. In some power quality monitors, the approach is typically made for every cycle, as given by

$$V_{rms}(kN) = \sqrt{\frac{1}{N}\sum_{i=(k-1)N+1}^{i=kN} v(n)^2} \tag{3.5}$$

where *k* is the cycle number.

3.5.2 Fundamental Voltage Components Using Fourier Transforms

Voltage sag can also be characterized using fundamental voltage. The fundamental voltage is a complex quantity obtained from the decomposition of the instantaneous voltage into Fourier components. The second component of the series corresponds to the fundamental frequency signals. The decomposition for sampled vector data is calculated using Discrete Fourier Transform (DFT). The application of fundamental voltage to estimate voltage sag magnitude and duration was claimed to be accurate for most sag analysis (Ohrstrom & Soder, 2003). Fourier coefficients in a one-cycle window can be expressed in DFT form as

$$V(h) = \frac{1}{N}\sum_{n=1}^{N} v(n) e^{-i\frac{2\pi}{N}(n-1)h} \quad h = 1,2,3,\ldots N \tag{3.6}$$

where *h* is the harmonic component of the signal, *N* is the number of samples per cycle, and *v(n)* is the sample voltage in the time domain. This equation can be further extended as in (Wang & Zhu, 2002) to calculate the amplitude of the real and imaginary parts of the frequency component. The equation to calculate the real part (a_h) and the imaginary part (b_h) are given in (3.7) and (3.8), respectively.

$$a_h = \frac{2}{N}\sum_{n=1}^{N} v(n)\cos\left[\frac{2\pi}{N}(n-1)h\right] \tag{3.7}$$

$$b_h = \frac{2}{N}\sum_{n=1}^{N} v(n)\sin\left[\frac{2\pi}{N}(n-1)h\right] \tag{3.8}$$

The magnitude of the signal (m_h) and phase angle (φ_h) of the *h* harmonic component are given in (3.9) and (3.10), respectively.

$$m_h = \sqrt{a_h^2 + b_h^2} \tag{3.9}$$

$$\varphi_h = \arctan\left[\frac{b_h}{a_h}\right] \tag{3.10}$$

3.6 Economic Cost due to Voltage Sag

In recent years, the attention towards the economic consequences of voltage sag is focused. It is of course difficult to make accurate estimations of the total costs related to voltage dips. A recommendation for an individual customer to estimate the economic consequences due to voltage dips and interruptions is found in ("IEEE Recommended Practice for Evaluating Electric Power System Compatibility With Electronic Process Equipment," 1998). Here, the costs are divided into different categories like idled labor, lost production, cost to repair damaged equipment and cost of recovery. These are immediate consequences but delayed costs can appear like increased labor costs due to downtime, lost business due to customer's dissatisfaction and fines and penalties due to delays. The disruption cost is analyzed for 120V DPDT relay ("IEEE Recommended Practice for Evaluating Electric Power System Compatibility With Electronic Process Equipment," 1998) and identified that each disruption costs about $14 300.

Another study in Sweden gives the economic consequences of voltage dips and the estimation of the costs was done due to short duration interruptions (Akerlund, 2004). The estimated cost is given in Table 3.5.

Table 3.5 Estimated cost for short duration interruptions

Interruption time	Estimated cost (per year)
<3 minutes	1000 to 1500 million Swedish Krona (SEK)
>3 minutes	1400 million SEK
Total	2400 -2900 million SEK

3.7 Summary

Faults in systems are the main reason for voltage sags in power systems. This chapter discusses the type of shunt faults, namely single line to ground fault, line to line fault, double line to ground fault and three-phase to ground faults. Also, the fundamental theories of voltage sag, voltage sag in distribution system and its relation with faults are studied in detail. The voltage sag detection using root mean square value and Fourier transform are discussed. The voltage sag characteristics due to faults are discussed since the proposed method utilizes voltage sag to locate fault. It also discusses the economic losses due to voltage sag in distribution system.

CHAPTER 4: PROPOSED FAULT LOCATION METHOD

4.1 Introduction

Previous chapter explains the fundamental theory of voltage sag and the fault types. It can be seen that there exists a relationship between the voltage sag and fault location as explained in Chapter 3, section 3.4. Based on this relationship, a fault location method for radial distribution network is proposed. Different from the previous work, this method considers the limitation in simulating voltage sag database and thus, estimates voltage sag data using SVR, thereby reducing the simulation time. A new fault location equation using Euclidean distance was also formulated to find the possible fault distance. The work also proposed a method to locate fault using two-dimensional (2D) SVM which identified the fault type, faulty section and fault distance, where the faulty phase was not considered. For analysis considering the faulty phase, three-dimensional (3D) analysis of voltage sag data was carried out.

4.2 Review of Existing Method

The idea of the proposed method using Euclidean distance approach is based on an earlier work reported in (H Mokhlis, Mohamad, Bakarl, & Li, 2011). The method uses voltage sags profile observed in the primary substation to locate fault. In order to highlight the differences between the proposed work and the previous works, this section will review the earlier method, which is based on voltage sags profile.

A simple distribution network in Figure 4.1 is taken as an example to describe the method. The system consists of one main feeder and two branches, tapped at nodes 1 and 2. A fault is assumed to occur in line section *s* (between node *i* and *j*) with distance f_d from sending node *i*. The measurement node is available in the primary substation. Whenever a fault occurs at any location in the network, the measurement node will record the voltage sag events.

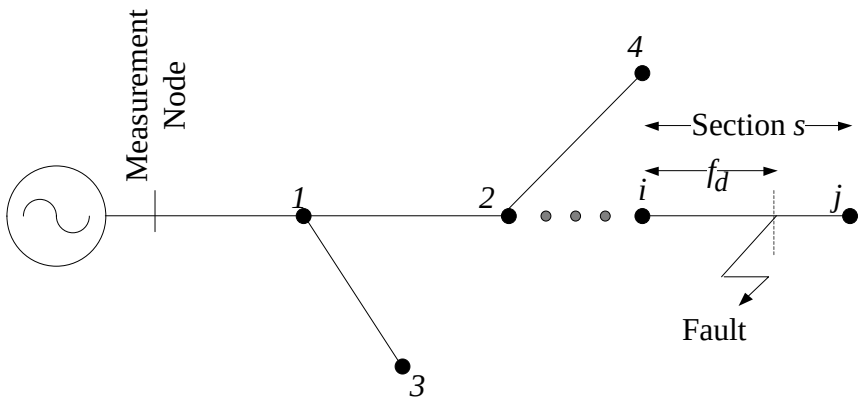

Figure 4.1 Simple distribution network

Basically, the algorithm of the method consists of four main tasks; the training data establishment, faulty section identification, ranking process and finally fault distance calculation.

4.2.1 Training Data Establishment

The training set of voltage sag data can be used for finding the fault location. The following are the steps involved in training data establishment:

1. SLGF is simulated at the nodes of the system with 0Ω resistance.
2. Voltage phase and angle of the fault are recorded from the measurement node. V and ϕ are corresponding to voltage phase and angle.
3. The recorded values are stored in a database.
4. Steps 2 and 3 are repeated for fault at all the n nodes of the system.
5. Steps 1 to 4 are repeated for fault resistance of 20Ω, 40Ω and 60Ω resistance.
6. Steps 1 to 5 are repeated for other fault types of LLF, DLGF and LLLGF.

Meanwhile, overall database for all types of fault is illustrated in Figure 4.2. The databases and the network parameters have to be updated whenever necessary, such as when changes are made in the system in the form of network reconfiguration or loading variation.

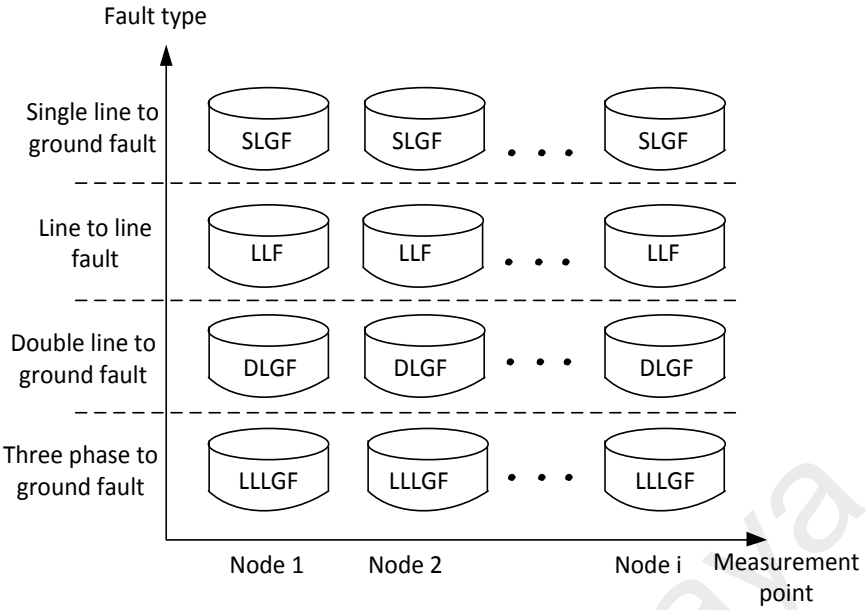

Figure 4.2 Illustration of analytical databases-2D analysis

4.2.2 Faulty Section Identification

Faulty section in distribution system is identified using a method of comparing the voltage sag phase and angle of adjacent fault resistance with the actual voltage sag phase and angle (Hazlie Mokhlis & Li, 2011). Since the establishment of databases is using a discrete value of fault resistance, there is possibility that the actual fault resistance is none of the simulated one. If the actual fault resistance R_f lies between the adjacent fault resistance in database ($R_f(x)$ and $R_f(x+1)$) where $R_f(x) < R_f(x+1)$ x=1…nr and (nr) is the total number of simulated fault resistance, the voltage sag data of $R_f(x)$ and $R_f(x+1)$ are used for faulty section identification, as shown in Eq. (4.1),

$$R_f(x) < R_f < R_f(x+1) \tag{4.1}$$

A faulty section s between nodes i and j, with a fault resistance between $R_f(x)$ and $R_f(x+1)$ is taken as an example. The possible voltage sag magnitude ($V_{i,\min}^{R_f(x)}$, $V_{i,\max}^{R_f(x+1)}$, $V_{j,\min}^{R_f(x)}$, $V_{j,\max}^{R_f(x+1)}$) and angle ($\phi_{i,\min}^{R_f(x)}$, $\phi_{i,\max}^{R_f(x+1)}$, $\phi_{j,\min}^{R_f(x)}$, $\phi_{j,\max}^{R_f(x+1)}$) are shown in Table 4.1.

Table 4.1 Voltage sag data for section identification in 2D analysis

	$R_f(x)$	$R_f(x+1)$
Node *i*	$V_{i,\min}^{R_f(x)}, \phi_{i,\min}^{R_f(x)}$	$V_{i,\max}^{R_f(x+1)}, \phi_{i,\max}^{R_f(x+1)}$
Node *j*	$V_{j,\min}^{R_f(x)}, \phi_{j,\min}^{R_f(x)}$	$V_{j,\max}^{R_f(x+1)}, \phi_{j,\max}^{R_f(x+1)}$

The illustration of selection boundary is shown in Figure 4.3. The shaded area represents the search boundary at resistance value $R_f(x)$ and $R_f(x+1)$. (V_f, ϕ_f) is the measured voltage phase and angle during fault condition. It can be seen that the measured voltage sag is not within the shaded area. To address this problem, the search boundary needs to be expanded by identifying the minimum and maximum voltage sag profiles of two adjacent fault resistances.

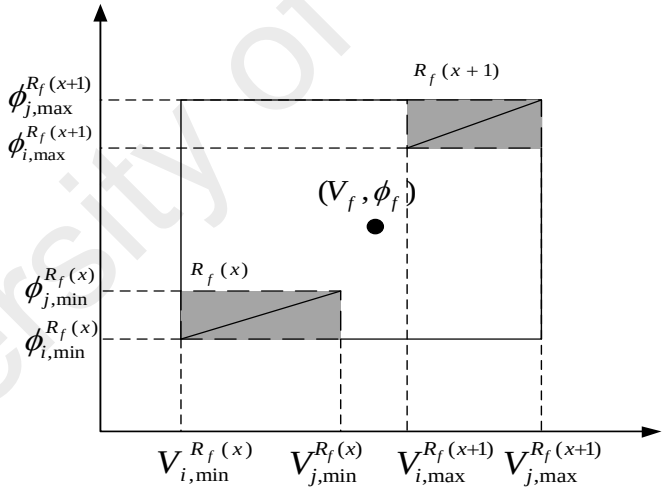

Figure 4.3 Voltage sag for section *s* and two different resistances - 2D analysis

The minimum and maximum values of voltage sag phase and angle are obtained for each section. If the faulted values of voltage phase and angle lie between the minimum and maximum values of each section, then the corresponding section is chosen as the faulty section (Hazlie Mokhlis & Li, 2011) as shown in Eq. (4.2) and (4.3),

$$V_{i,\min}^{R_f(x)} \le V_f \le V_{j,\max}^{R_f(x+1)} \tag{4.2}$$

$$\phi_{i,\min}^{R_f(x)} \le \phi_f \le \phi_{j,\max}^{R_f(x+1)} \quad (4.3)$$

These conditions determine the possible faulty section together with the fault resistances interval $R_f(x)$ and $R_f(x+1)$. The next pair of databases is read to find other fault section candidates and their corresponding fault resistance interval. The process is repeated until all of the sections and measurements of the databases are compared. The process ends when all the databases have been evaluated. For example, in Figure 4.1, faults occur at section *i-j*, the method may choose section *1-3*, section *2-4* and section *i-j* as the possible faulty section. This problem is addressed via the application of a ranking process.

4.2.3 Ranking Process

The ranking process utilizes a mathematical approach to find the most possible faulty section. This process is important since faulty section identification generates multiple faulty sections. This is due to the complexity of the distribution system, such as lateral branches and sub branches. For the ranking process, the voltage sag magnitude and phase shift are assumed to possess a linear function of a fault distance between two adjacent nodes. This assumption is only applicable for a short distance cable.

Figure 4.4 illustrates the linear relationship of the voltage sag magnitude and angle. It is assumed that there are three possible selected faulty sections; section *1-3*, section *2-4* and section *i-j*. To rank the faulty section among these selected sections, the rank algorithm will calculate the shortest distance d_{s1}, d_{s2} and d_{sn} between the measured voltage sags (V_f, ϕ_f) to the selected possible faulty sections.

Using a trigonometric method, the shortest distance d_{sn} (from node *i* to node *j*) can be calculated by identifying the perpendicular distance from measured point (V_f, ϕ_f)

perpendicular to the linear line. The shortest distance d_{sn} is given in Eq. (4.4) of section 4.2.4.

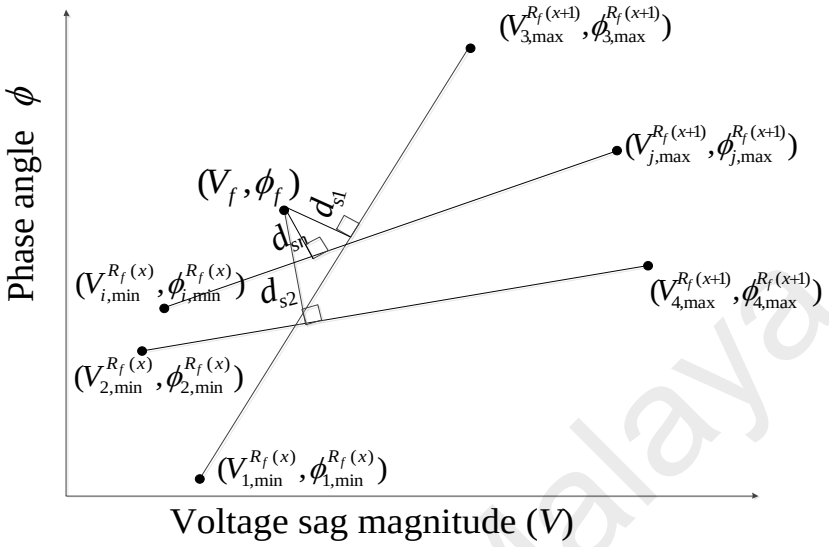

Figure 4.4 Ranking process in 2D analysis

The calculation is repeated for all possible faulty sections. The line section with the shortest distance will be determined as the first rank of possible faulty section, followed by the second shortest distance and so on. Based on the ranking of the section, the first rank faulty section will be inspected first. In case the first section is incorrect upon inspection, the second possible section will then be inspected. This process is repeated for the next section until the actual faulty section is found.

4.2.4 Fault Distance Calculation

The fault distance is determined by assuming that the length of a faulty section *i-j* (any two adjacent nodes of a section) corresponds to the distance between points *i* and *j* of the voltage sags data, as shown in Figure 4.5. The fault distance is estimated by considering the intersection of line d_{sn} (the shortest distance) to the line *i-j* (Lilik Jamilatul Awalin et al., 2013).

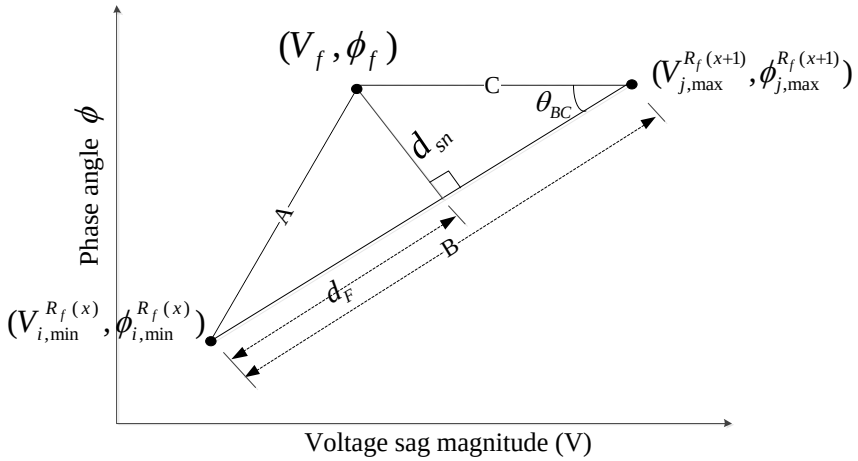

Figure 4.5 Fault distance calculation

The shortest distance d_{sn} is calculated using

$$d_{sn} = \left|\sin\theta_{BC} * C\right| \tag{4.4}$$

The distance d_F can be calculated based on the cosine rule. The fault distance d_F from node *i* is given as

$$d_F = \sqrt{A^2 - d_{sn}^2} \tag{4.5}$$

Finally actual length f_d can be calculated using

$$f_d = \frac{\left|d_F \times l_{i-j}\right|}{B} \tag{4.6}$$

where $\theta_{BC} = \cos^{-1}[(B^2 + C^2 - A^2)/(2 * B * C)]$ (4.7)

$$A = \sqrt{(\phi_f - \phi_{i,\min}^{R_f(x)})^2 + (V_f - V_{i,\min}^{R_f(x)})^2} \tag{4.8}$$

$$B = \sqrt{(\phi_{j,\max}^{R_f(x+1)} - \phi_{i,\min}^{R_f(x)})^2 + (V_{j,\max}^{R_f(x+1)} - V_{i,\min}^{R_f(x)})^2} \tag{4.9}$$

$$C = \sqrt{(\phi_{j,\max}^{R_f(x+1)} - \phi_f)^2 + (V_{j,\max}^{R_f(x+1)} - V_f)^2} \tag{4.10}$$

l_{i-j} is the length of cable/line for section *i-j* in km.

4.3 Difference between the Proposed and Existing methods

This work proposed a new method by improving the method discussed in section 4.2. The following are the differences between the existing method and the proposed method for fault location identification:

1. Establishment of voltage sag data

   In the existing method, voltage sag data required for calculation purpose are simulated using PSCAD software by creating fault at each node of the distribution system. The process of creating this database is time consuming. Furthermore, huge information may need to be stored to ensure accurate fault location. Hence, with the objective of minimizing the database size, SVR is used to estimate data that are not simulated or stored in the database.

2. Faulty section

   a) In existing method, faulty section is identified from the stored voltage sag data. Different from the previous methods, the proposed method uses the estimated voltage sag data and the stored data for identifying the faulty section.

   b) The proposed method considers faulty phase and identifies faulty section using 3D analysis of voltage sag data.

3. Ranking process

   a) The existing method ranks the possible faulty sections by finding the shortest distance from the fault to the linear line joining voltage phase and angle of a section using trigonometric principle. Different from the existing methods, a new equation to find the shortest distance is proposed in 2D analysis by

finding the perpendicular distance from fault to linear line joining voltage phase and angle.

b) A new ranking equation is formulated to rank the possible sections using 3D analysis considering faulty phase is proposed.

4. Fault distance calculation

a) The existing method (Lilik Jamilatul Awalin et al., 2013) for fault distance calculation is not accurate for fault resistance nearer to the stored database. Hence, a new approach using Euclidean distance of voltage sag profile is proposed. This approach considers the voltage sag at each node of the section and identifies the possible fault distance for all values of fault resistance.

b) In addition, fault distance in 2D and 3D analysis using SVR is proposed, which also considers the voltage sag at each node of the section

4.4 Algorithm of Proposed Method

The algorithm of the proposed fault location method is presented in this section. The implementation is divided into two main processes; (a) database establishment and (b) fault location identification. The flowchart of the proposed method is shown in Figure 4.6.

The database establishment includes creating a training set of data to locate the fault. Faults are simulated at all the nodes of the distribution system. The proposed method uses voltage sag magnitude and angle for 2D analysis and voltage sag magnitude at phases a, b and c for 3D analysis. The network parameters such as line impedance, load values and transformer parameters are obtained from the network parameter database. The database of voltage sag functions and network parameters will be updated

whenever there are changes in the studied distribution networks, such as loading variation or reconfiguration of the lines.

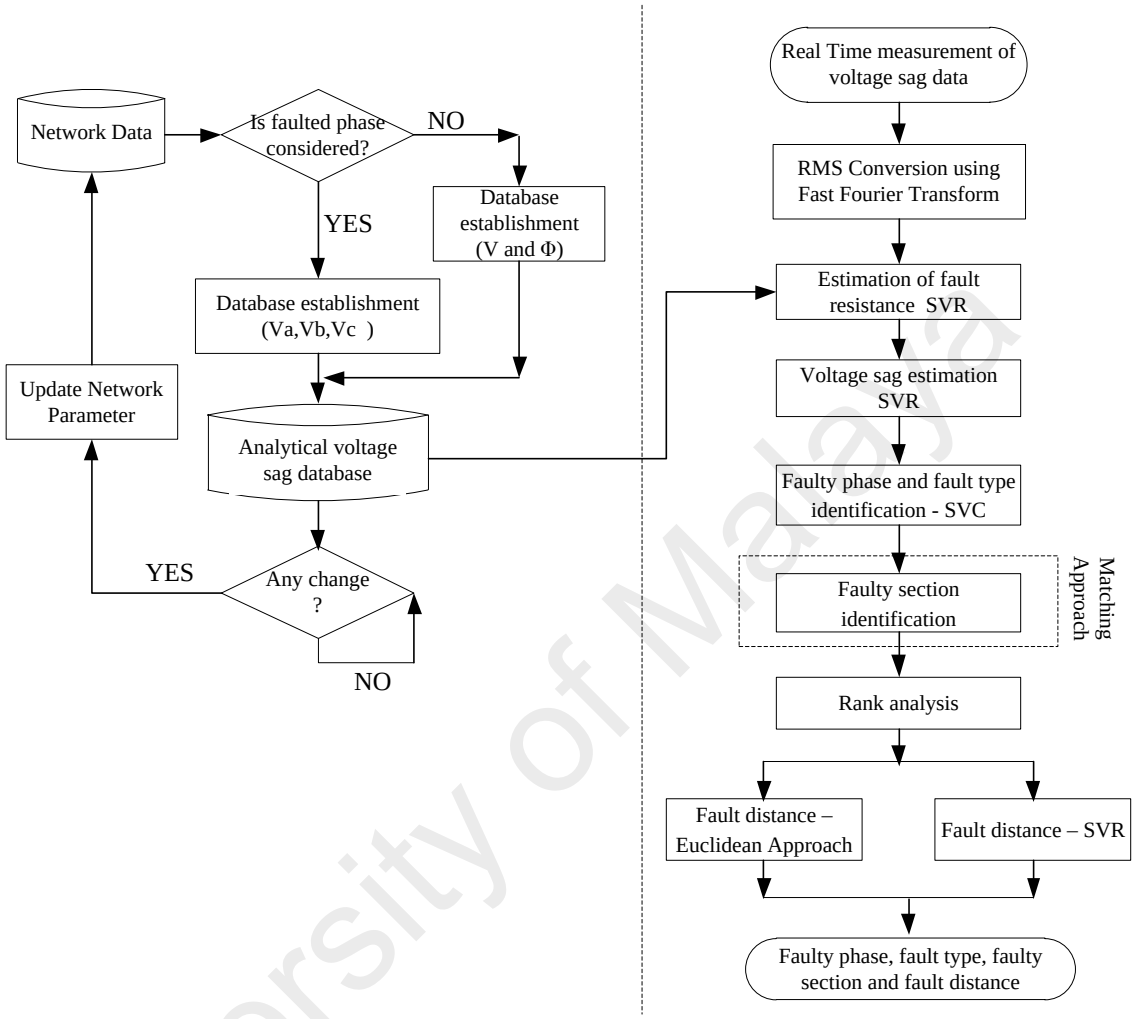

a) Database Establishment b) Fault location identification

Figure 4.6 Flow chart of proposed method

The fault location identification algorithms begin from real time measurement of the voltage sag data from measurement node when a fault occurs. During the fault, the waveform data of voltage sags are stored. The voltage sag waveform is then extracted to obtain the fundamental voltage sag magnitude and angle using Fourier Transformation. SVR is trained using simulated voltage sag to calculate the fault resistance and voltage sag nearer to the calculated fault resistance. The fault type is then identified using SVC as discussed in section 4.6. The matching approach finds the possible faulty section

which matches between the actual voltage sag data with the simulated voltage sag. The ranking of possible sections are discussed in sections 4.7.1.4 and 4.7.2.3. The ranked faulty sections are then used as a reference section in order to calculate the fault distance. In case the first rank is not the real faulty section, the second ranking is then selected, followed by the third rank and so on. The proposed method improves the existing method of locating the fault distance by using Euclidean approach. This approach considers the voltage sag at each node of the section. The work also proposes a method to identify fault distance using 2D and 3D analysis of SVR.

4.5 Training Data Establishment for 3D Analysis

The training data establishment for 2D analysis is explained in section 4.2.1. For analysis considering the faulty phase, 3D analysis of voltage sag data is carried out. The illustration of analytical databases is given in Figure 4.7. The following are the steps involved in training data establishment for 3D analysis:

a. $SLGF_a$ is simulated at all nodes of distribution system with 0Ω resistance. Voltage sag at phase a, b and c are recorded from the measurement node. The simulation is repeated for fault resistance of 20Ω, 40Ω and 60Ω resistance. The simulated fault resistance is expressed as $R_f(x)$, $R_f(x+1)$, $R_f(x+2)$ and $R_f(x+3)$.

b. Step (a) is repeated for other fault types of $SLGF_b$, $SLGF_c$, LLF_{ab}, LLF_{bc}, LLF_{ca}, $DLGF_{ab}$, $DLGF_{bc}$, $DLGF_{ca}$ and $LLLGF_{abc}$. The subscripts of SLGF, LLF, DLGF and LLLGF represents the faulty phase.

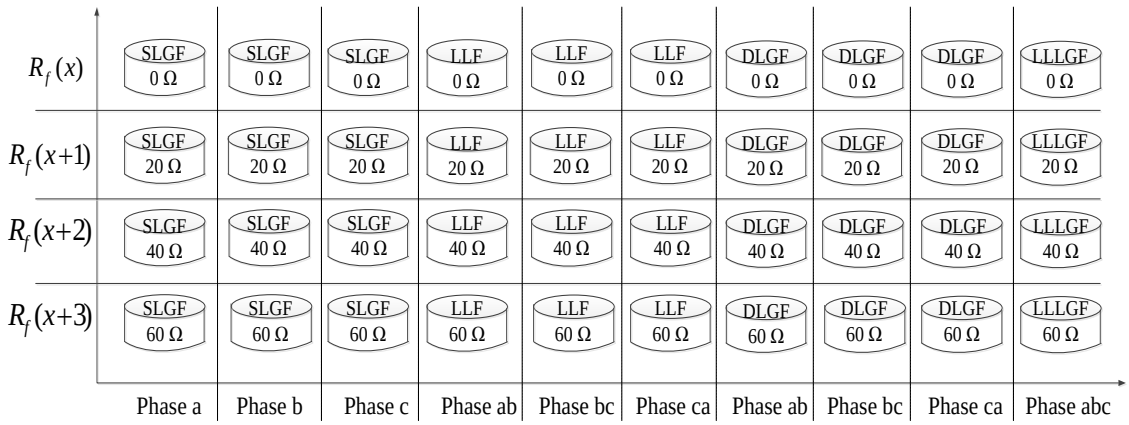

Figure 4.7 Illustration of analytical databases in 3D analysis

4.6 Proposed Fault Type Classification

This section presents the details of the proposed method to locate fault type of distribution system. The faulty type classification for 2D and 3D analysis are described.

4.6.1 Fault Type Classification in 2D Analysis

The proposed method identifies fault type for SLGF, LLF, DLGF and LLLGF using SVC. Since there are four types of fault, the method uses multiclass SVC with four classes (C1, C2, C3, C4). C1 corresponds to SLGF; C2 corresponds to LLF; C3 to DLGF and C4 to LLLGF.

The voltage samples (V and ϕ) are trained using RBF kernel and classified based on the classes. The classification uses one-versus-all concept. Figure 4.8 describes the fault type classification using multiclass SVC. V_f and ϕ_f correspond to voltage phase and angle at the fault. Class 1 and Class 0 are the two classes used in Matlab for classification. At first, the voltage sag data of SLGF is considered as Class 1 and the remaining (LLF, DLGF, LLLGF) are considered as Class 0. If the fault type is identified under Class 0 then a second step of classification takes place, else the fault type is finalized as SLGF. The second step of classification is done between LLF and remaining fault types (DLGF, LLLGF). If the fault type is not LLF, a third step of

classification is done between DLGF and LLLGF. Hence the corresponding output is the type of fault.

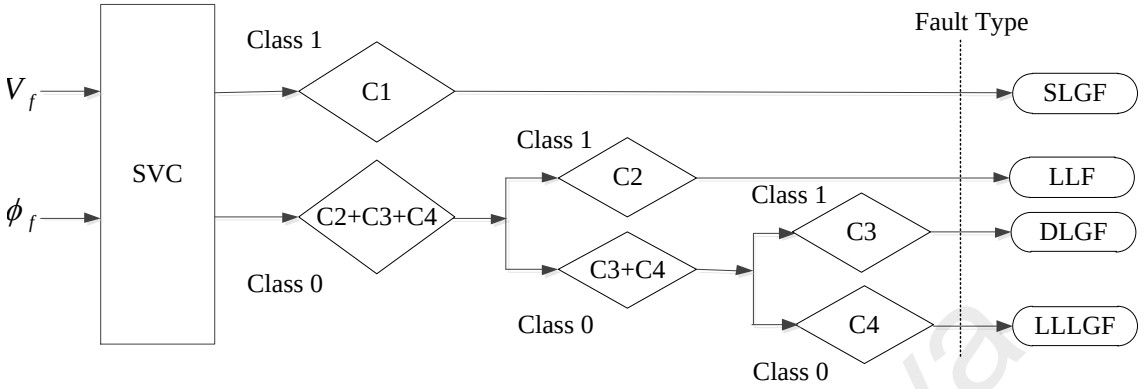

Figure 4.8 Fault type classification using 2D analysis of SVC

4.6.2 Fault Type Classification considering Faulty Phase in 3D Analysis

Considering faulty phase, 10 types of fault may occur in distribution systems, which are $SLGF_a$, $SLGF_b$, $SLGF_c$, LLF_{ab}, LLF_{bc}, LLF_{ca}, $DLGF_{ab}$, $DLGF_{bc}$, $DLGF_{ca}$ and $LLLGF_{abc}$. The voltage sag data at fault condition V_{af}, V_{bf} and V_{cf} serves as the input for SVC. The desired output is the type of fault. Figure 4.9 describes the 3D analysis of fault type classification using multiclass SVC.

At first, the voltage sag data of $SLGF_a$ is considered as Class 1 and the remaining ($SLGF_b$, $SLGF_c$, LLF_{ab}, LLF_{bc}, LLF_{ca}, $DLGF_{ab}$, $DLGF_{bc}$, $DLGF_{ca}$ and $LLLGF_{abc}$) are considered as Class 0. SVC finds the optimal hyper-plane between two classes and identifies if the input data falls in Class 1 or in Class 0. If the fault type is identified under Class 1 then the fault type is finalized as $SLGF_a$. If the fault type is identified under Class 0 then a second step of classification takes place by considering $SLGF_b$ as Class 1 and the remaining ($SLGF_c$, LLF_{ab}, LLF_{bc}, LLF_{ca}, $DLGF_{ab}$, $DLGF_{bc}$, $DLGF_{ca}$ and $LLLGF_{abc}$) as Class 0. The process is continued until the actual fault type is identified.

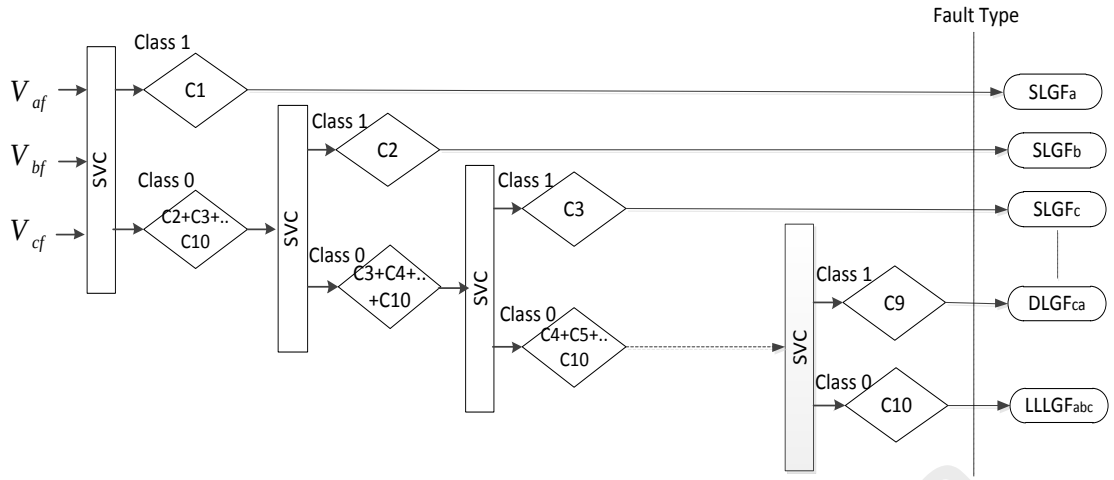

Figure 4.9 Fault type classification using 3D analysis of SVC

4.7 Proposed Faulty Section Identification

This section presents the details of the proposed method to locate faulty sections. The faulty section identification in 2D and 3D analysis are described in this section.

4.7.1 Faulty Section in 2D Analysis

The illustration of faulty section identification is shown in Figure 4.10. The process of identifying faulty section involves fault resistance estimation using SVR. The voltage sag for the estimated fault resistance is then identified. The possible faulty sections are identified from the estimated voltage sag and ranked using a shortest distance equation.

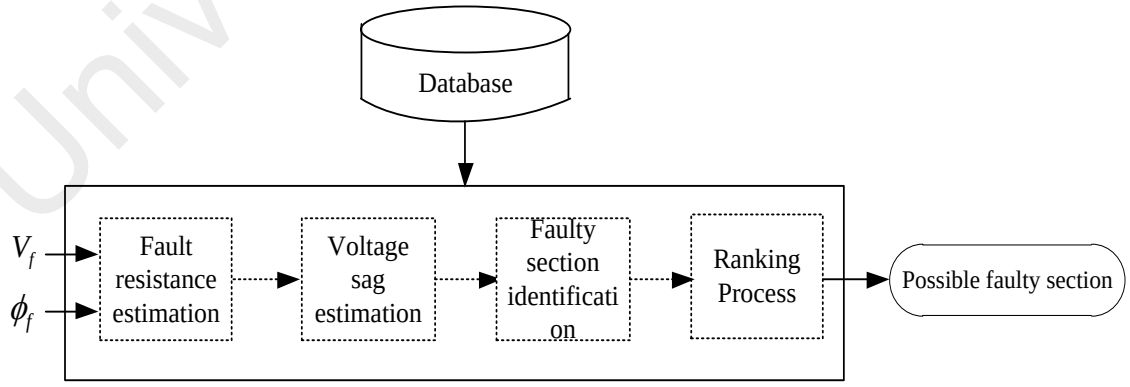

Figure 4.10 Illustration of faulty section in 2D analysis

4.7.1.1 Fault Resistance Estimation in 2D Analysis

Fault resistance is estimated by training the voltage sag data using SVR. The RBF kernel is adopted to train the simulated voltage sag samples. The voltage sag phase and angle during fault are given as input to SVR process. The corresponding output is the fault resistance as depicted in Figure 4.11. V_f and ϕ_f correspond to voltage phase and angle during the fault and R_f is the estimated fault resistance.

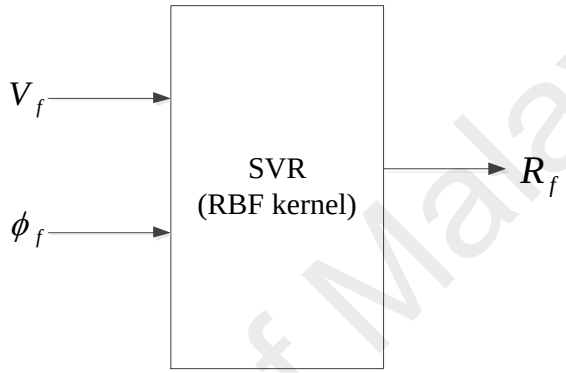

Figure 4.11 Fault resistance estimation in 2D analysis

4.7.1.2 Establishment of Voltage Sag Data

After estimating fault resistance, the voltage sag nearer to the estimated fault resistance has to be identified. For this reason, two adjacent resistances in the database, $R_f(x)$ and $R_f(x+1)$ nearer to the estimated fault resistance R_f are selected. The average of the two adjacent fault resistances is calculated as in Eq. (4.11),

$$R_f(x+k) = \frac{R_f(x) + R_f(x+1)}{2} \tag{4.11}$$

$R_f(x+k)$ is the average of adjacent fault resistance for which the voltage sag has to be calculated. The voltage sag data for $R_f(x+k)$ is estimated using SVR for all nodes of a distribution system. This estimation reduces the simulation time and also reduces the possibility of faulty section. The illustration of voltage sag estimation is shown in

Figure 4.12. The fault resistance and the number of node are given as input to SVR. The corresponding output of this process is the voltage sag magnitude and angle.

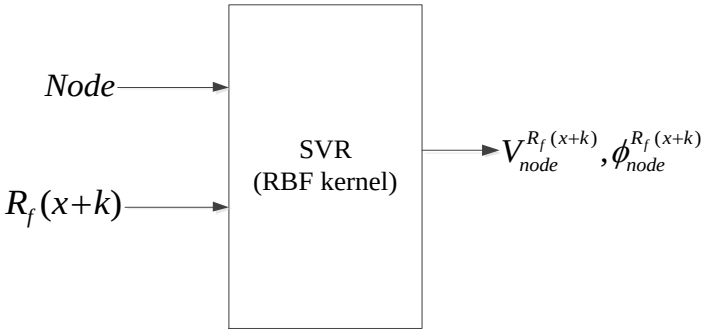

Figure 4.12 Voltage sag estimation using SVR

4.7.1.3 Possible Faulty Sections in 2D Analysis

The possible faulty sections identification in 2D analysis of voltage sag phase and angle is explained in section 4.2.2. The voltage sag data of $R_f(x)$ and $R_f(x+k)$ are used for faulty section identification by using

$$R_f(x) < R_f < R_f(x+k) \tag{4.12}$$

The minimum and maximum values of voltage sag phase and angle are obtained for each section. If the faulted values of voltage phase and angle lie between the minimum and maximum values of each section, the corresponding section is chosen as the faulty section (Hazlie Mokhlis & Li, 2011) as shown in Eq. (4.13) and (4.14),

$$V_{i,\min}^{R_f(x)} \le V_f \le V_{j,\max}^{R_f(x+k)} \tag{4.13}$$

$$\phi_{i,\min}^{R_f(x)} \le \phi_f \le \phi_{j,\max}^{R_f(x+k)} \tag{4.14}$$

4.7.1.4 Ranking Process in 2D Analysis

A shortest distance equation is proposed to find the most possible faulty section using the approach as in (Lilik Jamilatul Awalin et al., 2013). Figure 4.4 illustrates the linear relationship of the voltage sag magnitude and angle. It is assumed that there are three possible selected faulty sections; section *1-3*, section *2-4* and section *i-j*. The

shortest distance prioritizes the most possible faulty section among these selected sections by calculating the shortest distance d_{s1}, d_{s2} and d_{sn} between the measured voltage sags (V_f, ϕ_f) to the selected possible faulty sections.

The shortest distance will be determined as the first rank of possible faulty section, followed by the second shortest distance and so on. The shortest distance d_{sn} at section *i-j* can be calculated by identifying the perpendicular distance from point (V_f, ϕ_f) to the linear line joining $(V_{i,\min}^{R_f(x)}, \phi_{i,\min}^{R_f(x)})$ to $(V_{j,\max}^{R_f(x+k)}, \phi_{j,\max}^{R_f(x+k)})$.

$$d_{sn} = \frac{m_1 - (\phi_f - m_2 V_f)}{\sqrt{m_2^2 + 1}} \tag{4.15}$$

where

$$m_1 = \frac{V_{j,\max}^{R_f(x+k)} \phi_{i,\min}^{R_f(x)} - V_{i,\min}^{R_f(x)} \phi_{j,\max}^{R_f(x+k)}}{V_{j,\max}^{R_f(x+k)} - V_{i,\min}^{R_f(x)}} \tag{4.16}$$

$$m_2 = \frac{\phi_{i,\min}^{R_f(x)} - \phi_{j,\max}^{R_f(x+k)}}{V_{i,\min}^{R_f(x)} - V_{j,\max}^{R_f(x+k)}} \tag{4.17}$$

The shortest distance is given in Eq. (4.15). The calculation is repeated for *ns* number of possible sections and ranked from 1 to *ns*. Based on the ranking priority, the fault distance is calculated.

4.7.2 Faulty Section in 3D Analysis

Faulty section identification in 3D analysis consists of fault resistance estimation, selection of possible sections and ranking process. Fault resistance is estimated using SVR analysis. Using the fault resistance, the voltage sag data from database is selected and compared with the actual voltage sag data to identify the possible faulty sections. After that, the most possible faulty sections can be identified and ranked using ranking process. The illustration of faulty section identification is shown in Figure 4.13.

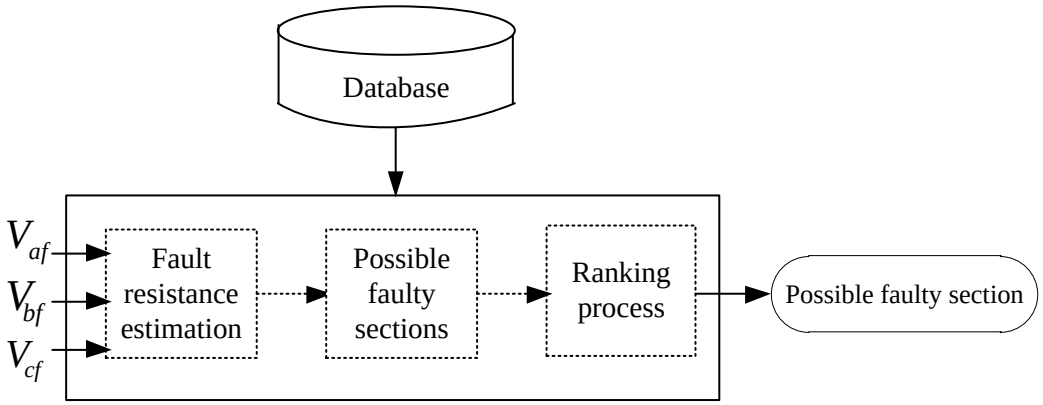

Figure 4.13 Illustration of faulty section identification in 3D analysis

4.7.2.1 Fault Resistance Estimation in 3D Analysis

Fault resistance is estimated using SVR analysis. The voltage sag data from database is trained using radial basis function in SVR. The voltage sags at fault conditions (V_{af}, V_{bf} and V_{cf}) are assigned as the input to SVR. The corresponding output (R_f) is the estimated fault resistance. The illustration of the fault resistance estimation is depicted in Figure 4.14.

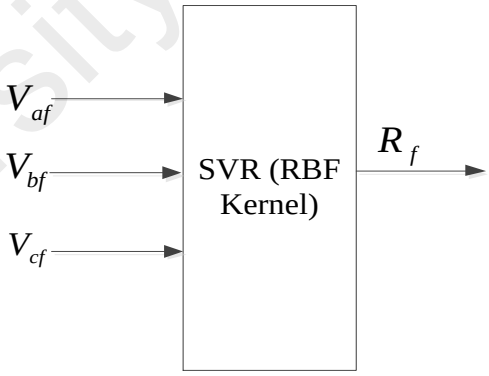

Figure 4.14 Fault resistance estimation in 3D analysis

4.7.2.2 Possible Faulty Sections in 3D Analysis

The possible faulty sections in a distribution system are identified by comparing the voltage sag phase and angle of adjacent fault resistance with the actual of voltage sag phase and angle (Mokhlis H, 2010; Hazlie Mokhlis & Li, 2011). This process is vital since multiple faulty sections are usually identified in distribution systems. This is due

to the complexity of distribution systems having parallel branches and sub branches which make many sections, overlap with each other. Hence, multiple possible faulty sections occur due to the equivalent electrical distance, as seen from the measurement location. A faulty section *s* between nodes *i* and *j*, with a fault resistance between $R_f(x)$ and $R_f(x+1)$ is considered. The voltage sag magnitudes are shown in Table 4.2.

Table 4.2 Voltage sag data for section identification in 3D analysis

Node	$R_f(x)$	$R_f(x+1)$
Node *i*	$V_{a,i}^{R_f(x)}, V_{b,i}^{R_f(x)}, V_{c,i}^{R_f(x)}$	$V_{a,i}^{R_f(x+1)}, V_{b,i}^{R_f(x+1)}, V_{c,i}^{R_f(x+1)}$
Node *j*	$V_{a,j}^{R_f(x)}, V_{b,j}^{R_f(x)}, V_{c,j}^{R_f(x)}$	$V_{a,j}^{R_f(x+1)}, V_{b,j}^{R_f(x+1)}, V_{c,j}^{R_f(x+1)}$

The search boundary at resistance values, $R_f(x)$ and $R_f(x+1)$ in 3D analysis is given in Figure 4.15. (V_{af}, V_{bf}, V_{cf}) corresponds to the measured voltage sag magnitude in phase a, b and c at fault condition. It can be seen that the measured voltage sag is not within the search boundary. To address this problem, the minimum and maximum voltage sag profiles of two adjacent fault resistances are considered.

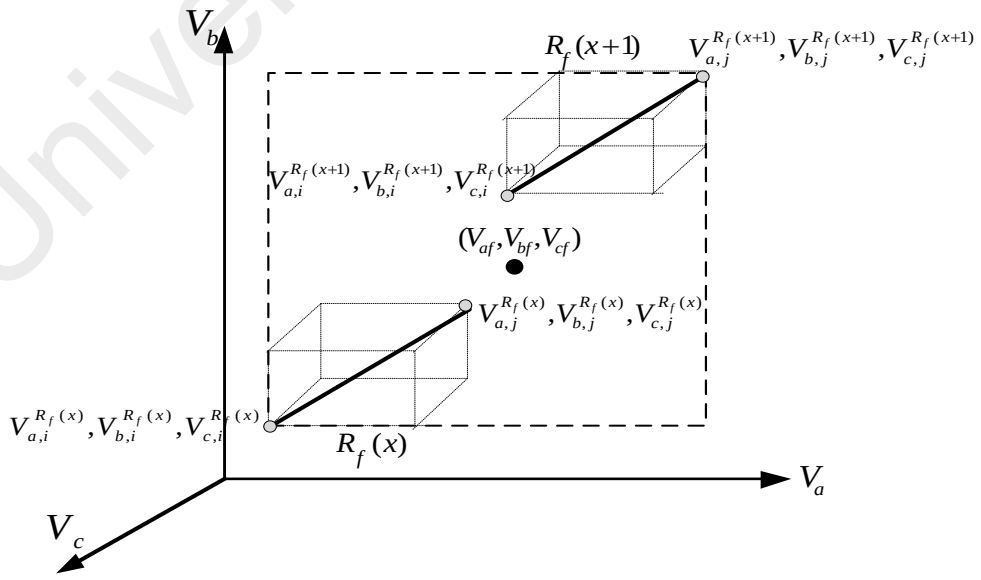

Figure 4.15 Voltage sag for section *s* and two different resistances - 3D analysis

The minimum and maximum of node *i* and *j* at section *s* are obtained. If the voltage sag at fault lies between minimum and maximum voltage sag at two nodes of a section, the corresponding section is chosen as the faulty section (Hazlie Mokhlis & Li, 2011).

The faulty section is identified using Eqs. (4.18) to (4.20),

$$V_{a,i}^{R_f(x)} \le V_{af} \le V_{a,j}^{R_f(x+1)} \tag{4.18}$$

$$V_{b,i}^{R_f(x)} \le V_{bf} \le V_{b,j}^{R_f(x+1)} \tag{4.19}$$

$$V_{c,i}^{R_f(x)} \le V_{cf} \le V_{c,j}^{R_f(x+1)} \tag{4.20}$$

4.7.2.3 Ranking Process in 3D Analysis

The most possible faulty section is identified using ranking process. The shortest distance d_{sn} between the fault point and the faulty line section (*i-j*) is calculated. The faulty section, which yields the shortest distance among all possible faulty section has a high priority of the most possible faulty section (Ali, Abu Bakar, Mokhlis, Arof, & Azil Illias, 2014).

Figure 4.16 shows a possible faulty section *s* between nodes *i* and *j*. $(V_{a,\min}^{i}, V_{b,\min}^{i}, V_{c,\min}^{i})$ and $(V_{a,\max}^{j}, V_{b,\max}^{j}, V_{c,\max}^{j})$ represent the minimum and maximum values of voltage sag at section *s*. (V_{af}, V_{bf}, V_{cf}) represents the voltage sag data identified during the fault. d_{sn} represent the shortest distance between the fault point and the line joining minimum and maximum values of sections *s*.

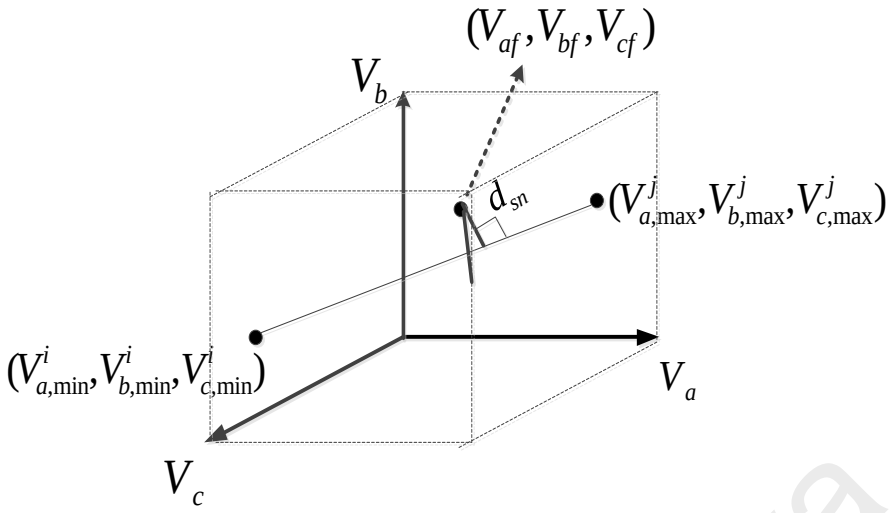

Figure 4.16 Ranking process in 3D analysis

The shortest distance d_{sn} is calculated using

$$S_x = V^i_{a,\min} - V^j_{a,\max} \tag{4.21}$$

$$S_y = V^i_{b,\min} - V^j_{b,\max} \tag{4.22}$$

$$S_z = V^i_{c,\min} - V^j_{c,\max} \tag{4.23}$$

where $\bar{S} = \{S_x, S_y, S_z\}$ is the directing vector of line joining $(V^i_{a,\min}, V^i_{b,\min}, V^i_{c,\min})$ and $(V^j_{a,\max}, V^j_{b,\max}, V^j_{c,\max})$.

$$N_x = V^i_{a,\min} - V_{af} \tag{4.24}$$

$$N_y = V^i_{b,\min} - V_{bf} \tag{4.25}$$

$$N_z = V^i_{c,\min} - V_{cf} \tag{4.26}$$

where $\overline{N} = \{N_x, N_y, N_z\}$ is the directing vector of line joining $(V^i_{a,\min}, V^i_{b,\min}, V^i_{c,\min})$ and (V_{af}, V_{bf}, V_{cf}).

$$\overline{M} = \{M_x, M_y, M_z\} = \overline{N} * \overline{S} \tag{4.27}$$

$$M_x = N_y S_z - S_y N_z \tag{4.28}$$

$$M_y = -(N_x S_z - S_x N_z) \tag{4.29}$$

$$M_z = N_x S_y - S_x N_y \tag{4.30}$$

$\overline{M}$ is the cross product of vectors $\overline{N}$ and $\overline{S}$. The shortest distance d_{sn} is given by

$$d_{sn} = \frac{|\overline{M}|}{|\overline{S}|} = \frac{\sqrt{M_x^2 + M_y^2 + M_z^2}}{\sqrt{S_x^2 + S_y^2 + S_z^2}} \tag{4.31}$$

4.8 Proposed Fault Distance Calculation

After the faulty sections are identified, the fault distance is calculated. The fault distances are calculated based on the number of candidates of the faulty section. The proposed method of fault distance calculation is implemented using Euclidean distance approach and using 2D and 3D analysis of SVR.

4.8.1 Fault Distance Calculation using Euclidean Distance Approach

In (Lilik Jamilatul Awalin et al., 2013), a method considering the minimum and maximum value of voltage sag data of a section is used to locate fault. The existing method is accurate for fault at the middle of the section and average of adjacent fault resistance. Since the fault resistance is not predictable in actual case, the method is not appropriate for other fault resistances. Hence, a new approach (as shown in Figure 4.17)

is proposed considering the voltage sag at each node of the section. The proposed method will find the possible fault distance for all values of fault resistance.

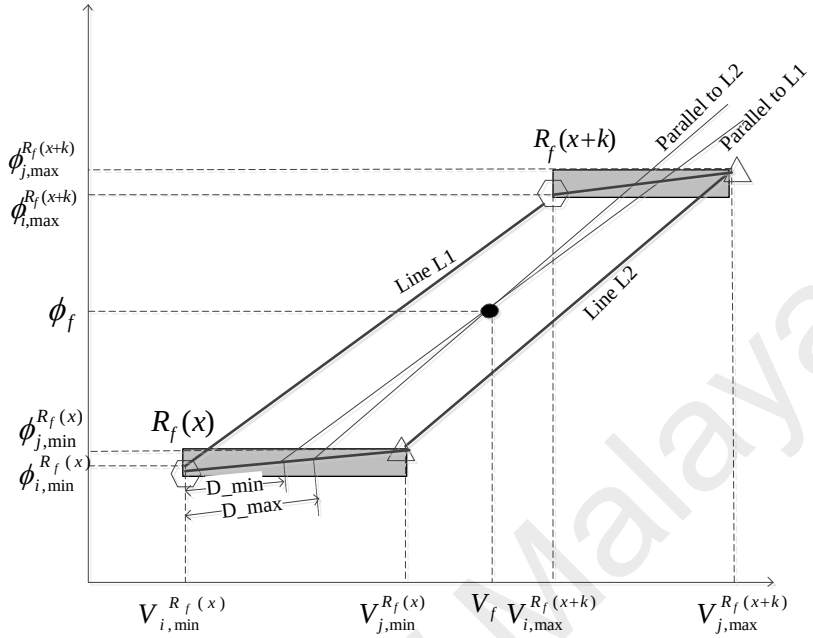

Figure 4.17 Mathematical analysis of voltage sag profile

At first, a linear line is created with the minimum and maximum values of voltage phase and angle of node i. The equation of line L1 connecting $(V_{i,\min}^{R_f(x)}, \phi_{i,\min}^{R_f(x)})$ and $(V_{i,\max}^{R_f(x+k)}, \phi_{i,\max}^{R_f(x+k)})$ is given as

$$y = m_1 x + c_1 \tag{4.32}$$

where m_1 is the slope and c_1 is the constant,

$$m_1 = \frac{\phi_{i,\max}^{R_f(x+k)} - \phi_{i,\min}^{R_f(x)}}{V_{i,\max}^{R_f(x+k)} - V_{i,\min}^{R_f(x)}} \tag{4.33}$$

$$c_1 = \phi_{i,\min}^{R_f(x)} - mV_{i,\min}^{R_f(x)} \tag{4.34}$$

The next linear line L2 is created between the maximum values of voltage phase and angle of node *j*. The equation of line connecting $(V_{j,\min}^{R_f(x)}, \phi_{j,\min}^{R_f(x)})$ and $(V_{j,\max}^{R_f(x+k)}, \phi_{j,\max}^{R_f(x+k)})$ are

$$y = m_2 x + c_2 \tag{4.35}$$

$$m_2 = \frac{\phi_{j,\max}^{R_f(x+k)} - \phi_{j,\min}^{R_f(x)}}{V_{j,\max}^{R_f(x+k)} - V_{j,\min}^{R_f(x)}} \tag{4.36}$$

$$c_2 = \phi_{j,\min}^{R_f(x)} - mV_{i,\min}^{R_f(x)} \tag{4.37}$$

Similarly, the line joining $(V_{i,\min}^{R_f(x)}, \phi_{i,\min}^{R_f(x)})$ and $(V_{j,\min}^{R_f(x)}, \phi_{j,\min}^{R_f(x)})$ is given as $y = m_3 x + c_3$ Then, a line parallel to Line 1 and passing through (V_f, ϕ_f) is created. Equation of line parallel to $y = m_1 x + c_1$ and passing through the fault point (V_f, ϕ_f) is given as $y = m_{f1} x + c_{f1}$ and has the same slope as that of $y = m_1 x + c_1$.

The constant c_{f1} is given as

$$c_{f1} = \phi_f - m_f V_f \tag{4.38}$$

The point of intersection of $y = m_3 x + c_3$ and $y = m_{f1} x + c_{f1}$ is the point (V_{f_1}, ϕ_{f_1})

$$\phi_{f\_1} = \frac{c_{f1} m_3 - c_3 m_{f1}}{m_3 - m_1} \tag{4.39}$$

$$V_{f\_1} = \frac{\phi_{f\_1} - c_{f1}}{m_{f1}} \tag{4.40}$$

The fault distance D_min can be calculated using equation (4.41),

$$D\_\min = \frac{(D_1^{line1} * L)}{D_2} \tag{4.41}$$

where $D_1^{line1} = \sqrt{(V_{f\_1} - V_{i,\min}^{R_f(x)})^2 + (\phi_{f\_1} - \phi_{i,\min}^{R_f(x)})^2}$ (4.42)

$$D_2 = \sqrt{(V_{j,\min}^{R_f(x)} - V_{i,\min}^{R_f(x)})^2 + (\phi_{j,\min}^{R_f(x)} - \phi_{i,\min}^{R_f(x)})^2} \tag{4.43}$$

and L is the length of the section.

Also, the same set of calculations are repeated by creating a parallel line to Line 2 and passing through (V_f, ϕ_f). The line parallel to $y = m_2 x + c_2$ is given as $y = m_{f2} x + c_{f2}$ where

$$c_{f2} = \phi_f - m_{f2} V_f \tag{4.44}$$

The point of intersection of $y = m_3 x + c_3$ and $y = m_{f2} x + c_{f2}$ is the point (V_{f_2}, ϕ_{f_2}) and the fault distance D_max can be calculated using equation (4.45),

$$D\_\max = \frac{(D_1^{line2} * L)}{D_2} \tag{4.45}$$

where $D_1^{line2} = \sqrt{(V_{f\_2} - V_{i,\min}^{R_f(x)})^2 + (\phi_{f\_2} - \phi_{i,\min}^{R_f(x)})^2}$ (4.46)

Finally, the fault distance f_d is calculated using the average of D_min and D_max

$$f_d = \frac{D\_\min + D\_\max}{2} \tag{4.47}$$

4.8.2 Fault Distance using SVR in 2D Analysis

Fault distance using SVR analysis is discussed in this section. The two adjacent fault resistances $R_f(x)$ and $R_f(x+1)$ from database nearer to the estimated fault resistance are selected for training using SVR. For each possible faulty section, the voltage sag data from database is considered as in Table 4.1 and trained using SVR.

The illustration for fault distance estimation is shown in Figure 4.18. Here, l represents the length of the line section *s*. The voltage sag data during fault (V_f, ϕ_f) and estimated fault resistance R_f are given as input to SVR, which maps the input data with the training data for finding the fault distance f_d.

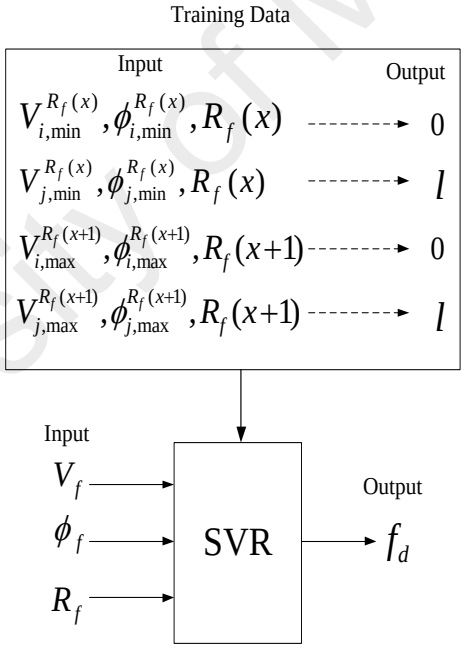

Figure 4.18 Fault distance estimation in 2D analysis

4.8.3 Fault Distance using SVR in 3D Analysis

The voltage sag data for the selected faulty section (Table 4.2) is trained using SVR to estimate the fault distance. The illustration for fault distance estimation in 3D analysis is shown in Figure 4.19. The voltage sag data during the fault (V_{af}, V_{bf}, V_{cf})

and the estimated fault resistance R_f are assigned as input to SVR. The corresponding output is the fault distance f_d.

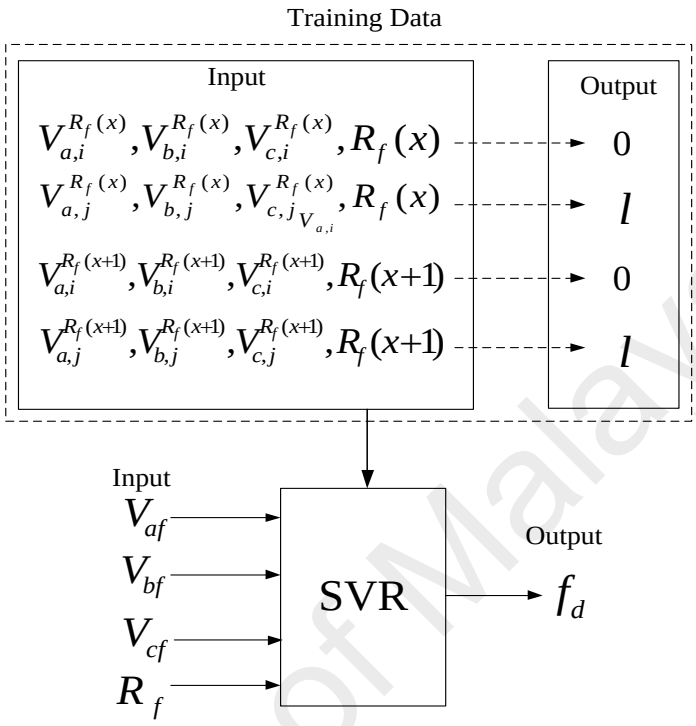

Figure 4.19 Fault distance estimation in 3D analysis

4.9 Summary

This chapter presents a comprehensive fault location method consisting of faulty phase, fault type, faulty section and fault distance determination from one-ended bus using limited simulation of voltage sag data. Although the basic principle of the proposed method is similar to previous fault location methods, many improvements have been made. The most important improvements are the voltage sag estimation using limited simulated data and consideration of faulty phase for locating fault.

Most of the intelligent methods require database for training purpose or for matching the simulated data and the actual data. The database is created by simulation, which is time consuming. Thus, a method to estimate voltage sag database using Support vector

machine is proposed. This estimates the voltage sag data that are not simulated and thus, helps to reduce the simulation time in creating database.

None of the researches, mainly using SVM focus on finding fault type by considering the faulty phase, faulty section and distance at the same time in distribution system. Considering these opportunity of improvement, this work tends to identify faulty phase, fault type, faulty section and fault distance in a single method. This chapter has presented the fault type classification using multiclass SVC. Fault type for classification of SLGF, LLF, DLGF and LLLGF is proposed using 2D SVC. Considering faulty phase, classification of fault type for $SLGF_a$, $SLGF_b$, $SLGF_c$, LLF_{ab}, LLF_{bc}, LLF_{ca}, $DLGF_{ab}$, $DLGF_{bc}$, $DLGF_{ca}$ and $LLLGF_{abc}$ is proposed using 3D SVC.

Faulty phase and fault type classification helps in calculating faulty section and fault distance. The possible faulty section identification using matching approach is discussed. The proposed method suggests new formulation of the faulty section and ranking process in 3D analysis. Based on the voltage sag magnitudes, the proposed methods are able to identify the candidate of the faulty section. A new fault distance method based on voltage sags has been proposed here. Each of the process of fault distance calculation has been explained in detail. The proposed method of fault distance calculation overcomes the limitation of existing trigonometric method and calculates fault distance for all values of fault resistance. Also, the proposed method calculates fault distance using SVR by considering the voltage sag at each node of a section.

CHAPTER 5: IMPLEMENTATION OF THE PROPOSED METHOD

5.1 Introduction

In this chapter, the algorithms of the proposed method to locate fault in a distribution network are presented. The algorithm of the faulty phase, fault type, faulty section and fault distance was implemented in Matlab to validate the proposed method. The test data to validate the algorithms were generated by performing fault simulations on actual distribution network from Tenaga Nasional Berhad (TNB) Malaysia and SaskPower distribution network from Canada. For this simulation, an industrial power system software PSCAD version 4.5.0 was used. All of the tests and simulation were performed on a Personal Computer, with a processor Intel(R) Core(TM)2 Quad CPU Q8400 @2.66GHz 2.67GHz.

5.2 Implementation Procedures

5.2.1 Database Establishment

The flowchart of establishing the analytical database for all types of fault is presented in Figure 5.1. Faults are simulated at nodes as described in section 4.2.1 and section 4.5, with the first fault resistance value set to $R_f(x) = 0\Omega$. The voltage sags are measured at the monitoring node and are stored in database. The process is repeated until all nodes in the test network have been evaluated. Once the database for the first fault resistance has been established, the process is repeated with the new fault resistance, ie. $R_f(x+1) = R_f(x) + \Delta R_f$, where $R_f(x)$ is the previous fault resistance, ΔR_f is the defined increment of new fault resistance from the previous one and $R_f(x+1)$ is the new fault resistance. The process is repeated until the simulated fault resistance $R_f(x)$ reaches the maximum defined fault resistance $\max(R_f(x))$. The maximum fault resistance value is determined from simulation study; it can be identified when it makes the voltage sag become a nominal value when simulating a fault.

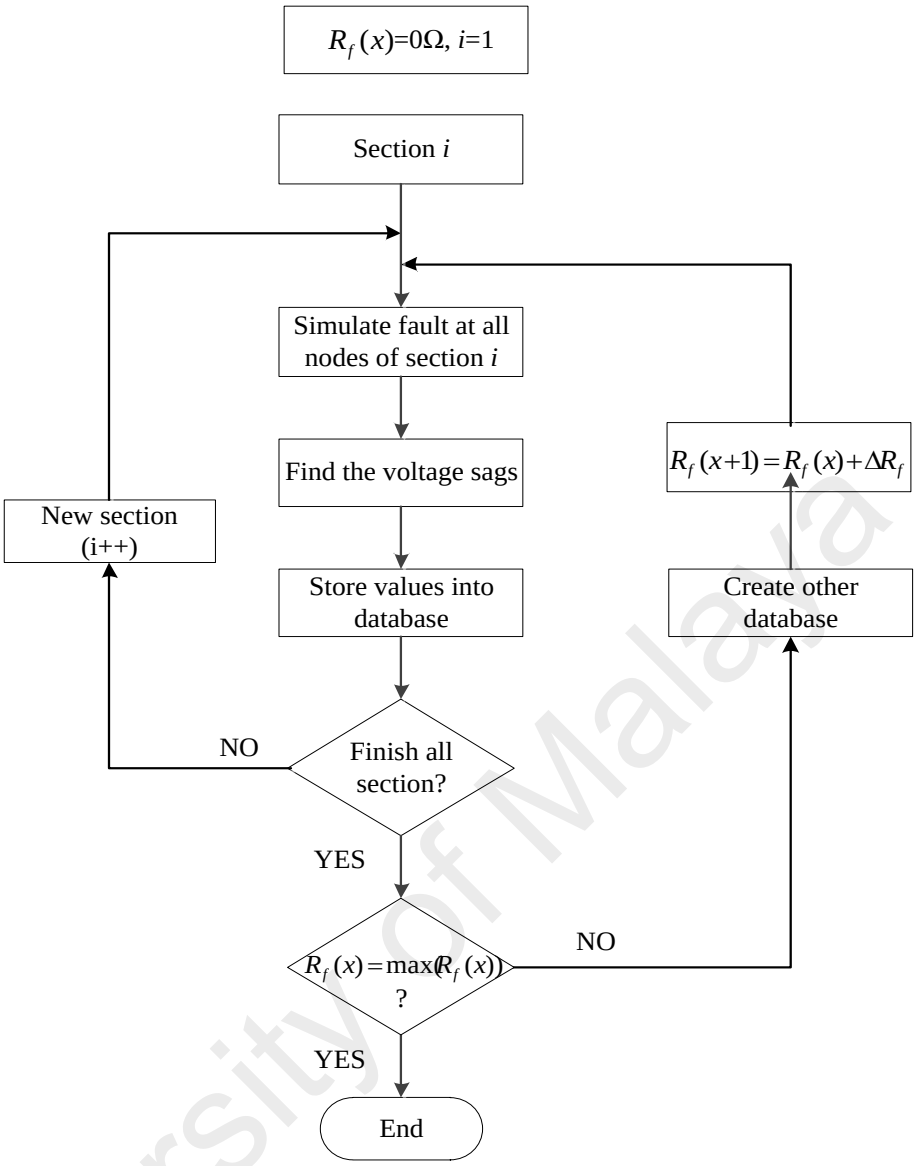

Figure 5.1 Flowchart of Database establishment

In this study, the minimum fault resistance is assumed to be 0Ω and the maximum $\max(R_f(x))$ is set to 60Ω. The fault resistance increment ΔR_f is set to be 20Ω. Thus, there will be a total of 40 database representing 10 fault types and 4 different values of fault resistance. The proposed method locates fault for two different considerations; (a) Identifying fault type, faulty section and fault distance; (b) Identifying faulty phase, fault type, faulty section and fault distance. For case (a), the method is implemented using voltage sag magnitude and phase angle. For case (b), the proposed method requires voltage sag magnitude at all three phases. This is due to the faulty phase can be

identified if the data at all three phases are known. Hence, for case (a), two dimensional (2D) analysis is performed, and for case (b), three dimensional (3D) analysis is carried out. The established database for SLGF at 2D analysis is illustrated in Table 5.1 and 3D analysis is illustrated in Table 5.2.

Table 5.1 Example of 2D analysis of voltage sag for SLGF database

Node	Voltage sag magnitude	Phase angle
1	V_1	ϕ_1
2	V_2	ϕ_2
.	.	.
.	.	.
n	V_n	ϕ_n

Table 5.2 Example of 3D analysis of voltage sag for SLGF database

Node	Voltage sag magnitude		
	Phase a	Phase b	Phase c
1	V_{a1}	V_{b1}	V_{c1}
2	V_{a2}	V_{b2}	V_{c2}
3	V_{a3}	V_{b3}	V_{c3}
.	.	.	.
.	.	.	.
n	V_{an}	V_{bn}	V_{cn}

5.2.2 Faulty Section Identification

The voltage sag data are used in the search algorithm to find the possible faulty sections. Figure 5.2 illustrates the flowchart of the algorithm to determine the possible faulty sections. The search process starts by reading the specific databases of the fault type. The database corresponding to fault resistance $R_f(x)$ and the second database for fault resistance $R_f(x+1)$ are read to obtain the voltage sags as described in section 4.7.1.3 and section 4.7.2.2.

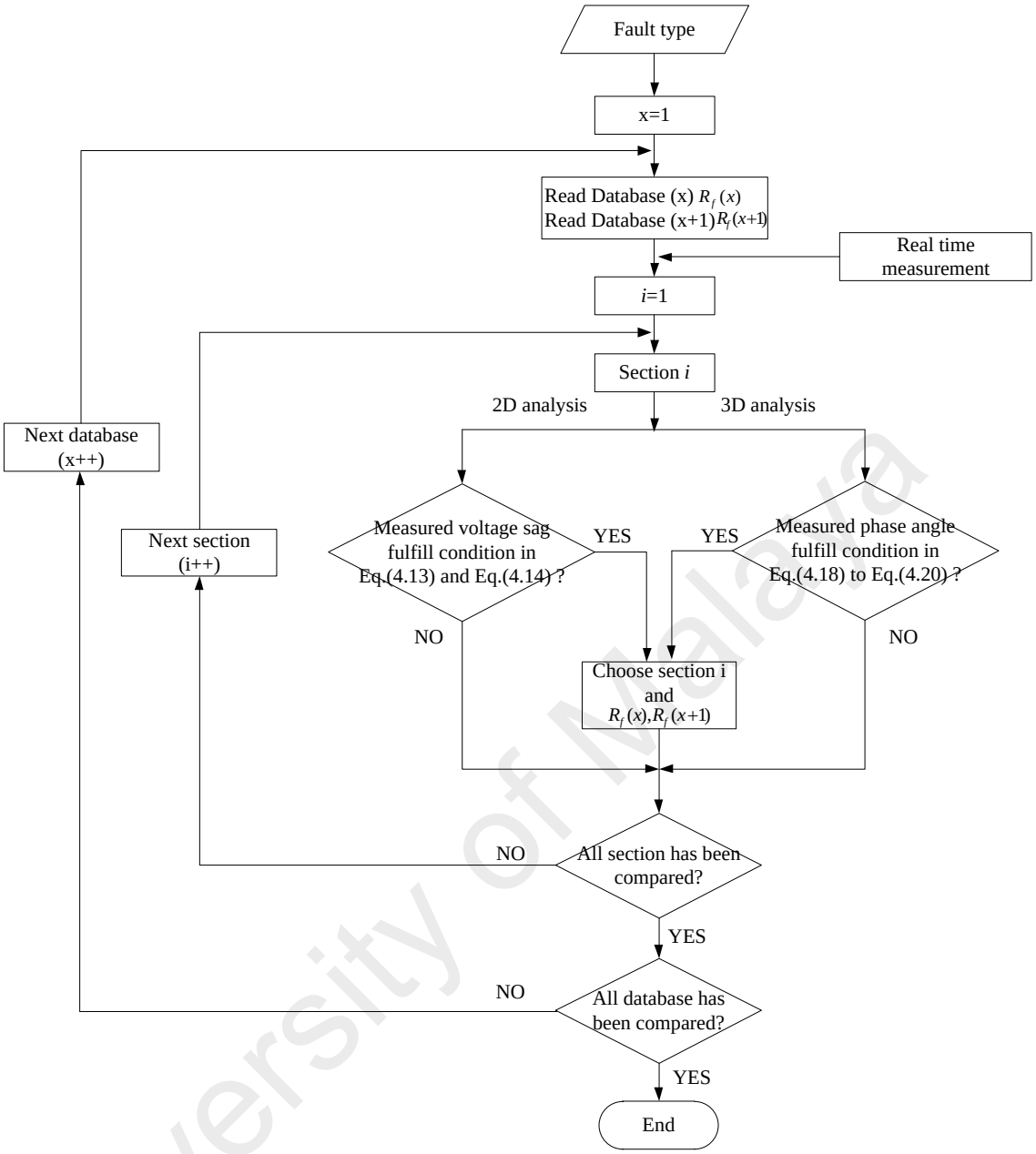

Figure 5.2 Flowchart to find the faulty section candidates

Once the voltage sag databases have been determined, the measured voltage sag is compared with the voltage sag in database. For 2D analysis, if the real time measurement of voltage sag magnitude (V_f) and phase angle (ϕ_f) lie between two adjacent nodes as in Equations (4.13) to (4.14), the section will be selected as a candidate of faulty section. For 3D analysis, if the real time measurement of voltage sag magnitude at three phases (V_{af}, V_{bf}, V_{cf}) lie between two adjacent nodes as in Equations (4.18) to (4.20), the section will be selected as a candidate of faulty section. The next

pair of databases is read to find other fault section candidates. The process is repeated until all of the sections in databases are compared. The process ends when all databases have been evaluated.

5.2.3 Ranking Process

After the candidates of the faulty section have been selected, the faulty sections are ranked using shortest distance approach. The illustration on the flowchart of ranking process is given in Figure 5.3.

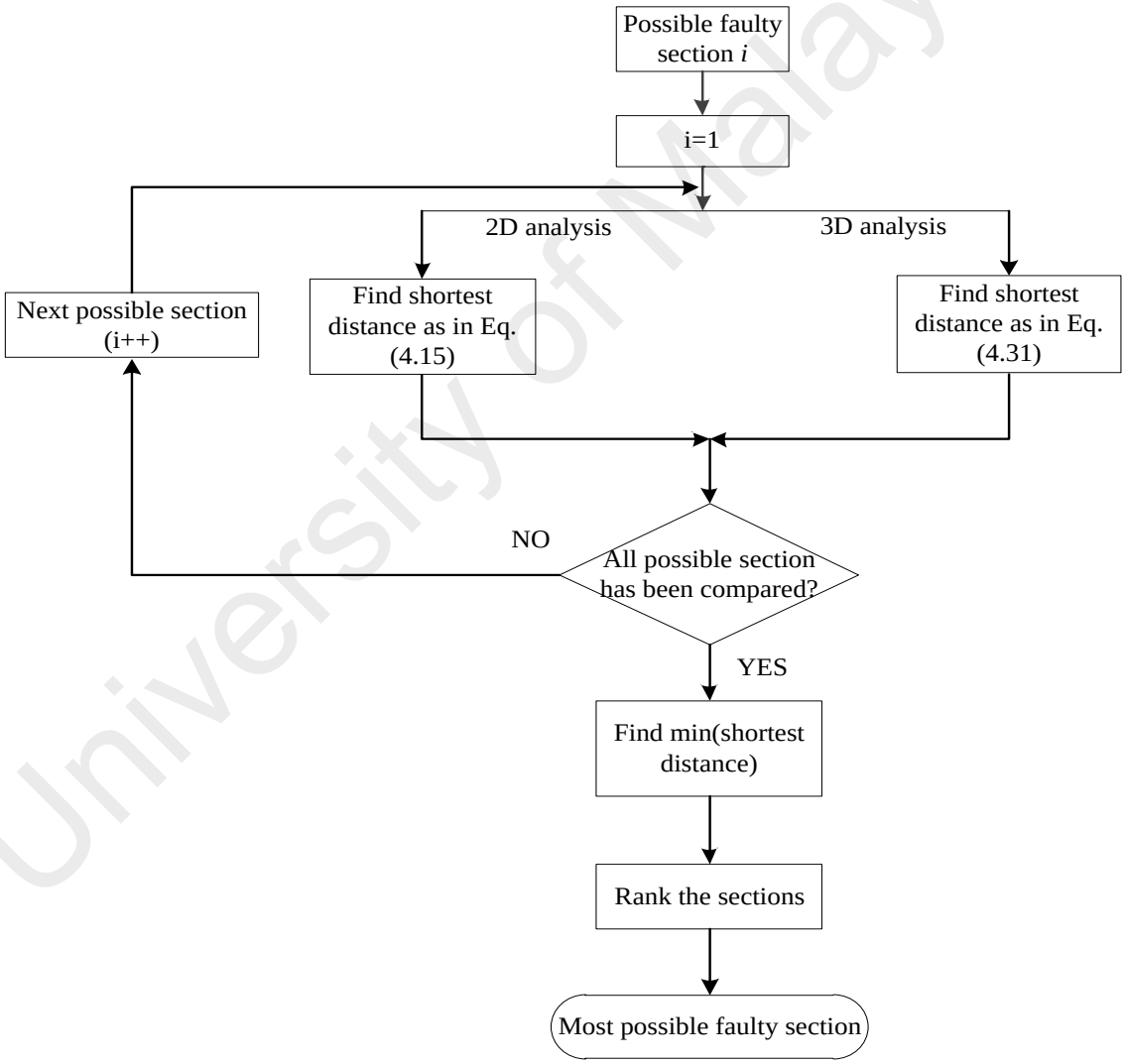

Figure 5.3 Flowchart for ranking process

For 2D analysis, the shortest distance is given in Eq. (4.15) and for 3D analysis the shortest distance is given in Eq. (4.31). The shortest distance is identified for all possible faulty sections. The faulty section corresponding to the minimum of the calculated shortest distance is ranked as the most possible faulty section. The second possible shortest distance is ranked as the second possible faulty section. The steps are repeated until all the possible faulty sections are ranked.

5.2.4 Fault Distance Calculation

The faulty section candidates are evaluated to find the fault distance of each candidate. The algorithm of fault distance of a faulty section candidate is shown in Figure 5.4.

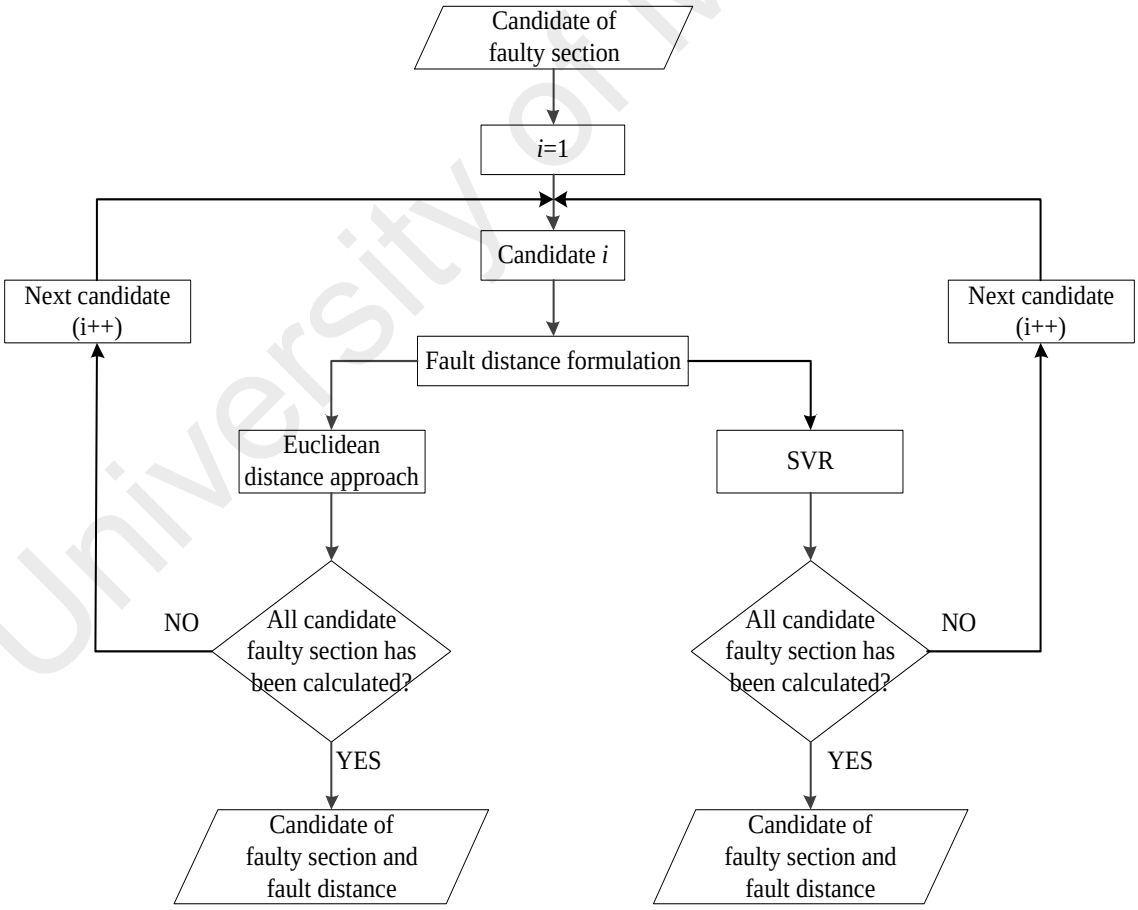

Figure 5.4 Algorithm of Fault Distance

The fault distances are calculated based on the number of candidates of the faulty section. The process starts by evaluating the first candidate *i* with fault resistance values between $R_f(x)$ and $R_f(x+1)$. Data from real time measurements are utilized as the input for the purpose of calculating the fault distance. Two methods that are based on Euclidean distance approach and SVR are adopted for this purpose. From this algorithm, the candidate of the faulty section and the fault distance are obtained together. The whole process is repeated for other faulty section candidates.

5.3 Test Network

In order to analyze the performance of the proposed method, two different distribution networks, namely Tenaga National Berhad (TNB), a Malaysian power utility company (Figure 5.5) and SaskPower distribution network from Canada (Figure 5.6) are used. These networks were chosen because they have different network configurations. The TNB network is an existing radial distribution network in Malaysia. It consists of a balanced three phase underground cable system and three-phase balanced loads. The SaskPower network is also a radial distribution network (Hazlie Mokhlis & Li, 2011; Mora-Flòrez et al., 2008; Seung-Jae et al., 2004) consisting of unbalanced lines and unbalanced loads. By having two different types of test network, the ability of the method to locate fault can be studied thoroughly.

5.3.1 TNB Distribution Network

The TNB distribution network is shown in Figure 5.5. It consists of 132 kV source representing the grid, frequency 50 Hz, a step down transformer (Y-Δ) 132/11kV and 8 branches considering the sub branches, 39 line sections (represented in Figure 5.5 as s1, s2 till s39) and 40 nodes. The network is made up of cables that are three-phase balanced and fully underground. The measurement node is placed in the primary substation, which gives the voltage sag during fault in distribution system. The total

length of the distribution system is 25.533 km. The parameters of the test network are given in Appendix A.1.

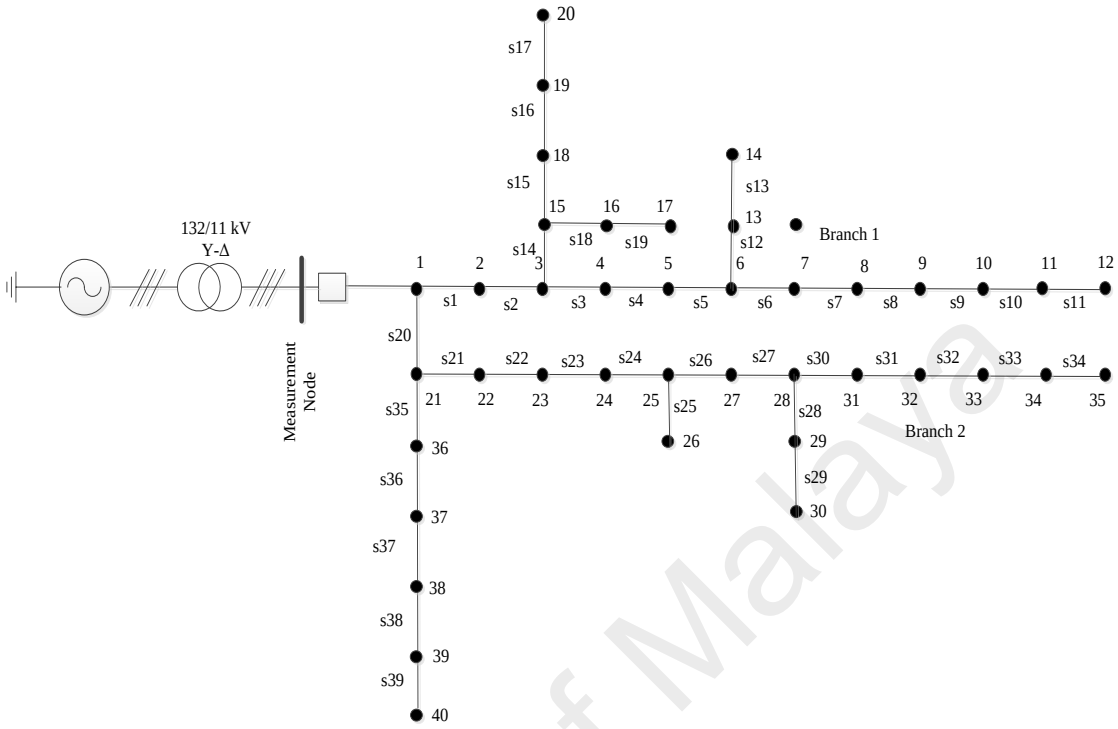

Figure 5.5 TNB Distribution Network

5.3.2 SaskPower Distribution Network

The SaskPower distribution network is depicted in Figure 5.6.

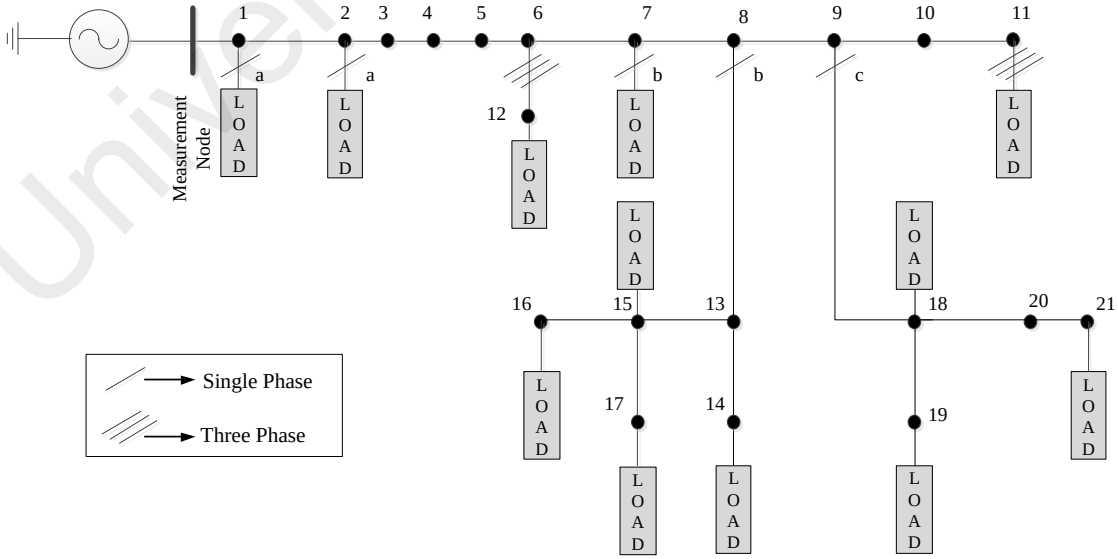

Figure 5.6 SaskPower Distribution Network

The network consists of a 25kV equivalent source, 21 nodes and several line sections made up of different conductor. The main feeder of the network is from node 1 to node 11 and is 37 km long. Along the main feeder, single phase or three-phase lines and loads are tapped. Voltage sags can be obtained from the measurement node installed at node number 1. The details of the network data are provided in Appendix A.2.

5.3.3 PSCAD Simulation of Test Distribution Network

PSCAD simulation software was used with the objective to develop an analytical database for training and to generate test data of voltage sag in order to validate the proposed method. For the purpose of developing database, faults were simulated at all nodes. For testing, faults were simulated at the middle of each line section of the distribution networks.

The network modeling of TNB and SaskPower distribution network using PSCAD software is shown in Figure 5.7 and Figure 5.8. The 132kV source is modeled using an equivalent three-phase voltage source model and the transformer using a three phase 2-winding transformer. The line cables are modelled using the π model. All of these models are retrieved from the PSCAD master library. Meanwhile, the loads are modelled as constant impedance loads with equivalent resistance (R) and inductance (L). Single phase breaker is included in all three phase of the network for protection.

The measurement node for both the test distribution network is placed in the primary substation. The measurement node records the voltage sag data. If the distribution system experiences a fault, the voltage data at measurement node reduces. This causes voltage sag magnitude and also changes the corresponding phase angle. The severity of voltage sag varies according to the fault distance. Using the characteristic of voltage sag, the fault distance can be identified.

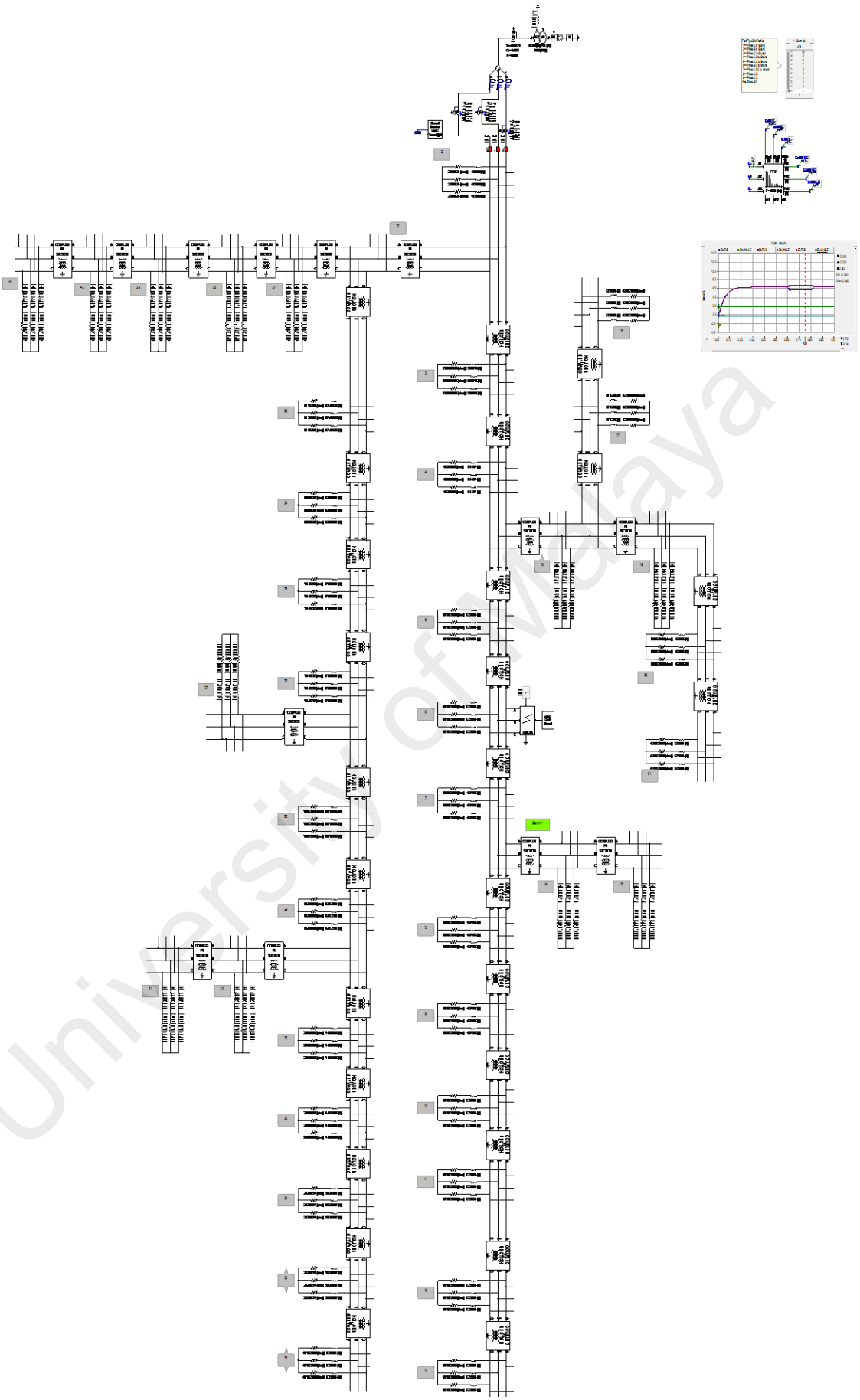

Figure 5.7 PSCAD simulation of TNB distribution network

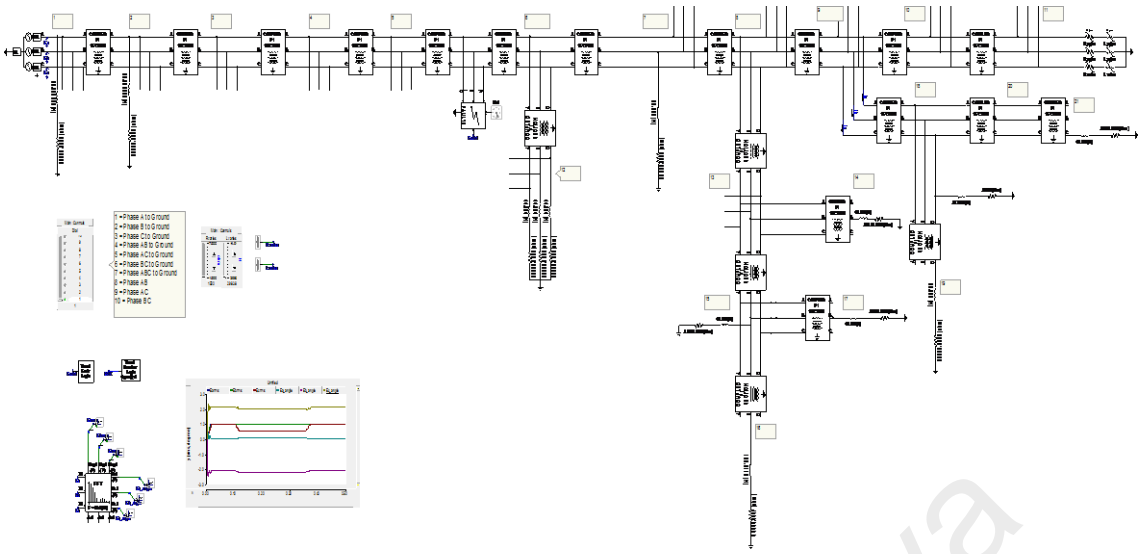

Figure 5.8 PSCAD simulation of SaskPower distribution network

The sinusoidal values of voltage sag are converted to root mean square values using an online frequency scanner as shown in Figure 5.9. The online frequency scanner performs online FFT, which determines the fundamental RMS value of voltage signal. The model of FFT is available and retrieved from PSCAD master library.

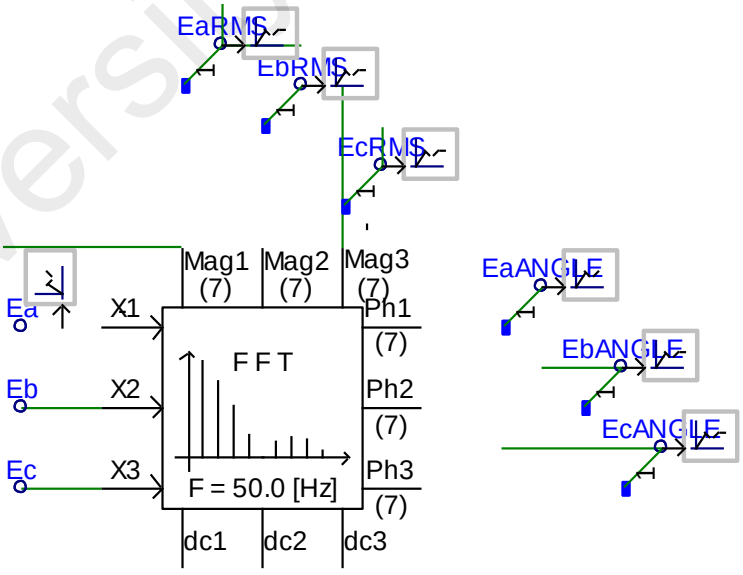

Figure 5.9 Fast Fourier Transform (FFT) model

An example of voltage sag magnitude and its corresponding phase angle from fault simulation of TNB network is depicted in Figure 5.10 and Figure 5.11. These voltage

sags are due to SLGF at mid-point of nodes 1-2. For this example, the lowest voltage magnitude 0.2596 V (0.04089 p.u) and its corresponding phase angle 1.8275 radians are used for 2D analysis. For analysis considering faulty phase (3D analysis), the voltage sag magnitude at three phases a, b and c are considered, which are 0. 04089 p.u, 1.6131 p.u and 1.7179 p.u.

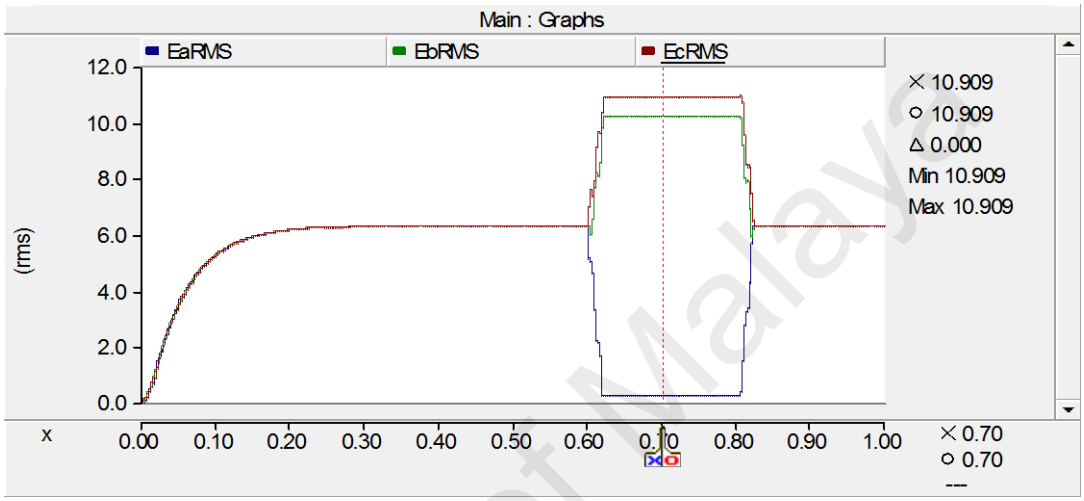

Figure 5.10 Voltage sag magnitude from fault simulation

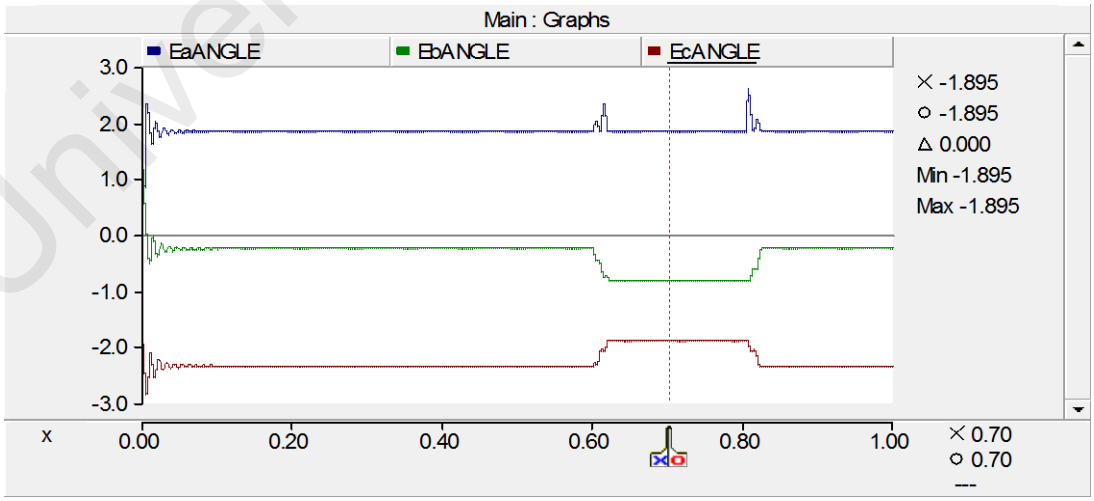

Figure 5.11 Phase angle from fault simulation

5.4 Verification of using Voltage Sag Pattern to Locate Fault

5.4.1 Voltage Sag for Different Distance

In order to justify the use of voltage sag data for locating faults, studies on the voltage sag magnitude and angle for different locations were conducted. For this purpose, faults are created at different nodes, from nodes 1 to 12 of the TNB network (Figure 5.5) in the main feeder. The patterns of voltage sag magnitude and phase angle due to faults at different distances are shown in Figure 5.12 and Figure 5.13.

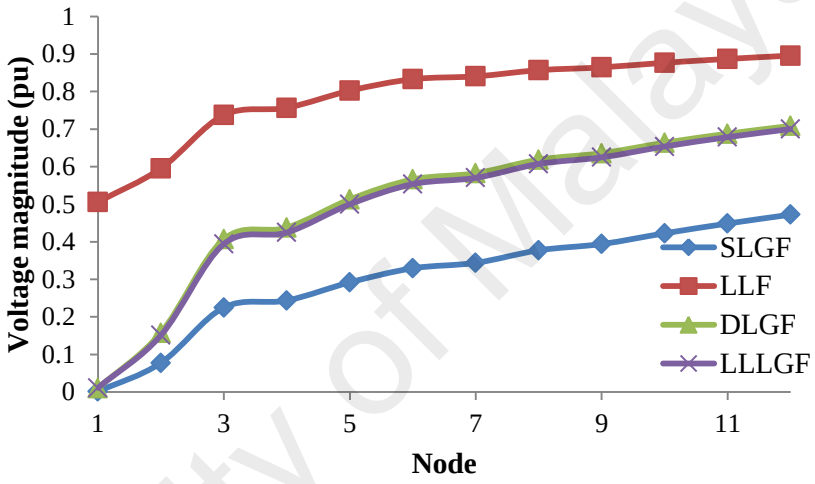

Figure 5.12 Voltage sag magnitude at different nodes

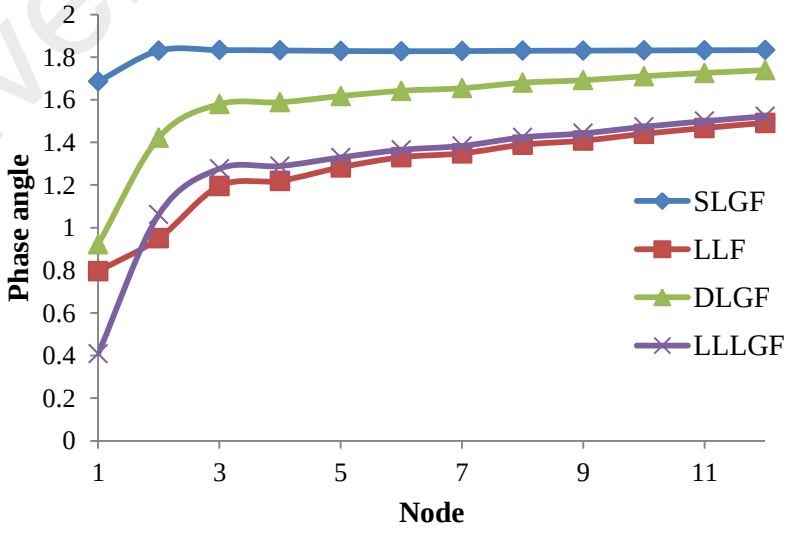

Figure 5.13 Phase angle at different nodes

From Figure 5.12, it can be observed that the voltage magnitude decreases as the fault distance is closer to the monitoring node. SLGF has the smallest value compared to other types of fault. Similar values of voltage sag were obtained for DLGF and LLLGF, followed by LLF, which has higher voltage sag value for each distance. From Figure 5.13, it can be noted that the phase angle increases slightly as the fault distance increases. It can be summarised that the use of voltage sag magnitude and phase angle is justified since it reflects the location of fault, i.e whether near or far from the measurement point.

5.4.2 Voltage Sag for Different Types of Fault

To analyze the pattern of voltage magnitudes due to faults, faults are simulated on section 1-2 of the TNB network at the mid-point with 0Ω fault resistance. The results are depicted in Figure 5.14. For this example, the voltage sag magnitude occurred for SLGF for phase a at 0.62 second until 0.81 second, with the voltage sag magnitude in phase a is 0.040894 p.u, phase b is 1.613093 p.u and phase c is 1.717879 p.u. It can be seen that due to SLGF, the voltage sag is experienced by phase a only. For other types of fault, for example DLGF (ab to ground fault), the voltage sag is experienced by phases a and b. Based on these observations, types of fault can be easily identified from the patterns of voltage.

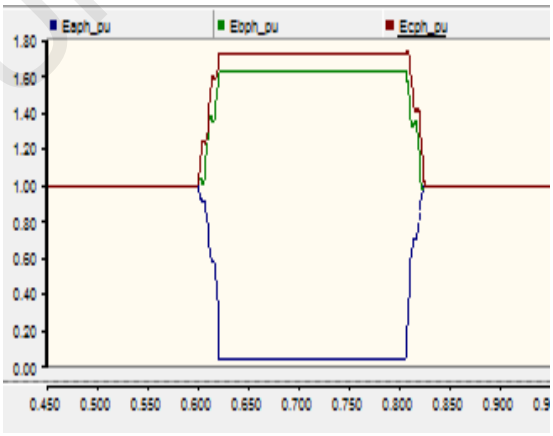

(a)

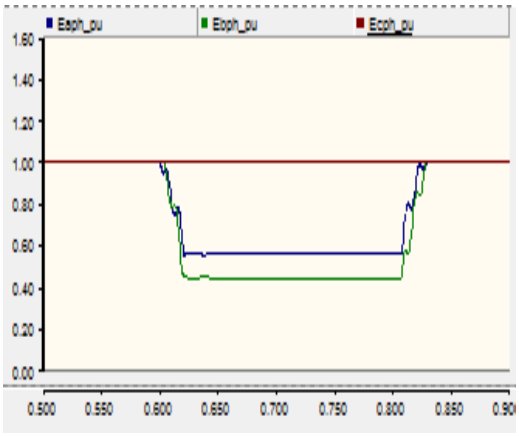

(b)

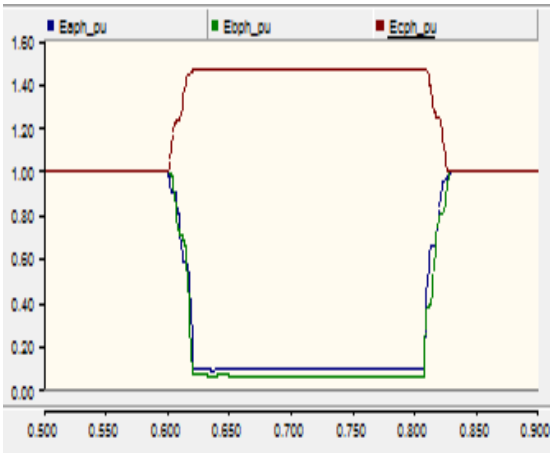

(c)

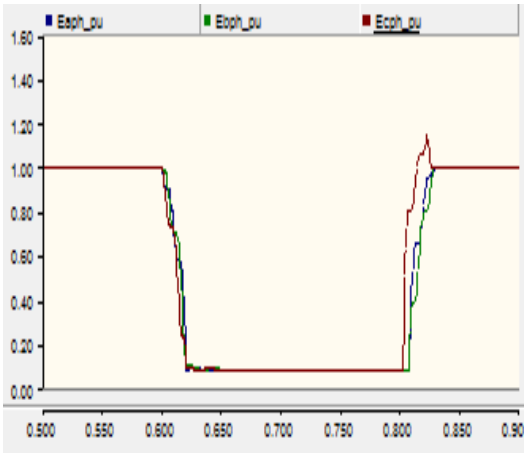

(d)

Figure 5.14 Voltage Sag magnitude waveform due to fault (a) SLGF (b) LLF (c) DLGF (d) LLLGF

5.5 Testing on TNB Network

For the case study, training data is obtained by simulating fault at all the 40 nodes of the distribution system at a fault resistance of 0 Ω. The simulated data is recorded in database. Hence, a total of 160 voltage samples are created using simulation for 2D analysis (SLGF, LLF, DLGF and LLLGF) and 400 voltage samples for 3D analysis ($SLGF_a$, $SLGF_b$, $SLGF_c$, LLF_{ab}, LLF_{bc}, LLF_{ca}, $DLGF_{ab}$, $DLGF_{bc}$, $DLGF_{ca}$ and $LLLGF_{abc}$). The voltage sag data is trained using SVM and the proposed method is implemented using MATLAB.

Test cases were carried out by simulating fault at the midpoint of line section between nodes. Hence, a total of 156 voltage samples are tested for 2D analysis and 390 voltage samples for 3D analysis. The line section, the length of all line sections and the distance of simulated fault from sending node are shown in Table 5.3. All types of fault were taken into account due to the network consists of three-phase lines. The performance of the proposed method was investigated and test results are discussed in following section.

Table 5.3 Test case for fault at mid-points of section on TNB network

Section number	Line section	Line length (km)	Simulated fault location from sending node (km)
1	1-2	0.5	0.25
2	2-3	1.25	0.625
3	3-4	0.14	0.07
4	4-5	0.4	0.2
5	5-6	0.35	0.175
6	6-7	0.2	0.1
7	7-8	0.5	0.25
8	8-9	0.27	0.135
9	9-10	0.5	0.25
10	10-11	0.5	0.25
11	11-12	0.5	0.25
12	6-13	0.3	0.15
13	13-14	0.75	0.375
14	3-15	1.29	0.645
15	15-18	0.5	0.25
16	18-19	0.5	0.25
17	19-20	0.25	0.125
18	15-16	0.395	0.1975
19	16-17	0.51	0.255
20	1-21	5	2.5
21	21-22	0.04	0.02
22	22-23	0.884	0.442
23	23-24	0.54	0.27
24	24-25	0.716	0.358
25	25-26	0.9	0.45
26	25-27	0.1	0.05
27	27-28	0.5	0.25
28	28-29	0.723	0.3615
29	29-30	0.45	0.225
30	28-31	0.594	0.297
31	31-32	0.908	0.454
32	32-33	0.5	0.25
33	33-34	0.5	0.25
34	34-35	0.5	0.25
35	21-36	0.5	0.25
36	36-37	0.473	0.2365
37	37-38	1.3	0.65
38	38-39	0.3	0.15
39	39-40	0.5	0.25

5.5.1 Voltage Sag Pattern of Characteristic Analysis

Before discussing the test results, the pattern of voltage sag variation between two adjacent nodes in a distribution system are analyzed. This is necessary to study the impact of the voltage sag pattern in the identification of fault type, faulty section and fault distance. For this purpose, the voltage sag data for fault at all nodes of the distribution system are considered. The lowest voltage magnitude versus phase angle is plotted into a graph to create a variation pattern. The voltage sag pattern variation in TNB network for all fault types with zero fault resistance is depicted in Figure 5.15. It shows that the voltage sag phase and magnitude varies for different types of fault and thus can be used to identify fault.

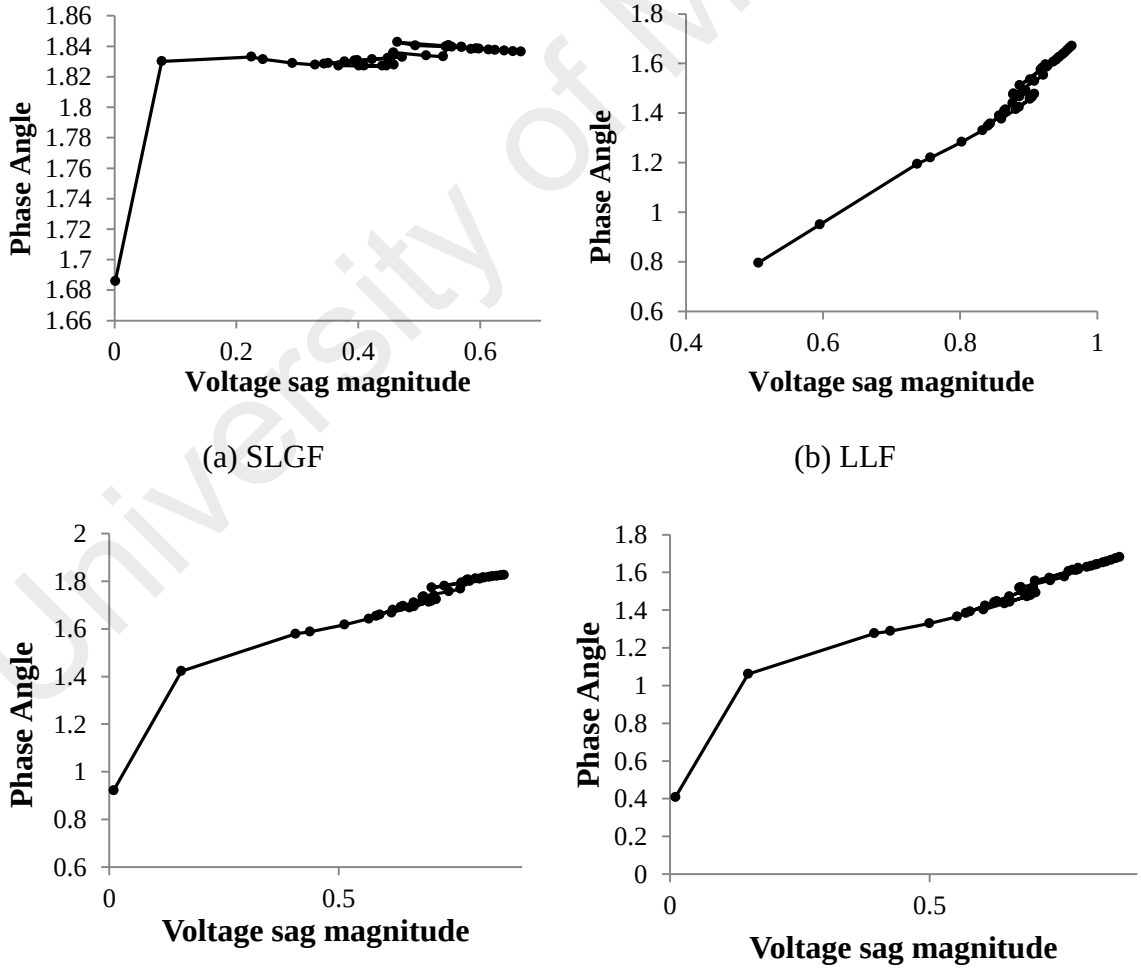

(a) SLGF (b) LLF

(c) DLGF (d) LLLGF

Figure 5.15 Voltage sag magnitude versus phase angle –TNB Network

Also the voltage sag variation pattern for each fault type was analyzed using the voltage sag magnitude at phase a, b and c. For this purpose, all of the nodes in TNB network are taken into account. The voltage sag pattern variation for all of types (SLGF, LLF, DLGF and LLLGF) with zero fault resistance is depicted in Figure 5.16. It can be noted that there is significant difference when fault occurs at different nodes in the distribution system. Also the pattern of voltage sag varies if the type of fault is different. Thus this variation can be used to identify fault in distribution system.

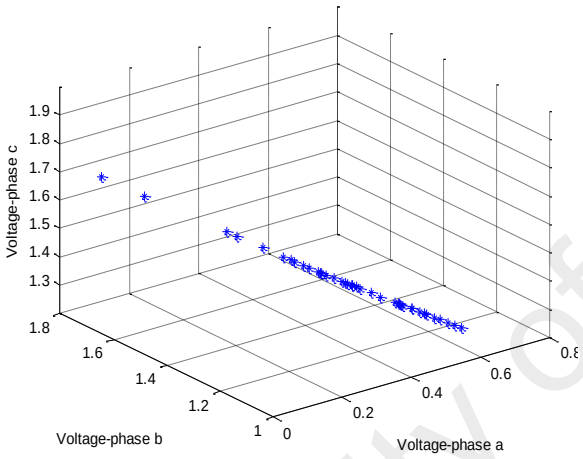

(a) SLGF

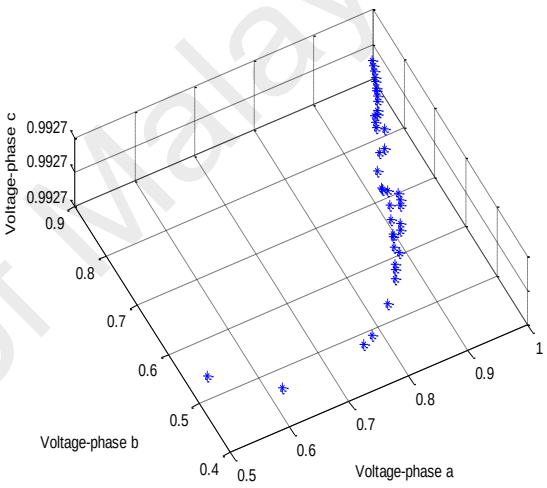

(b) LLF

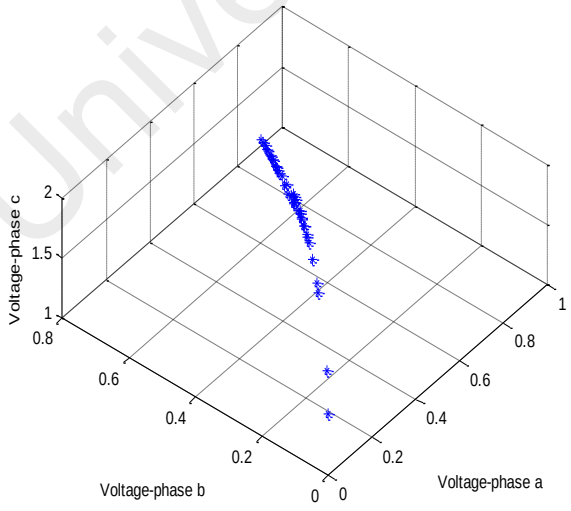

(c) DLGF

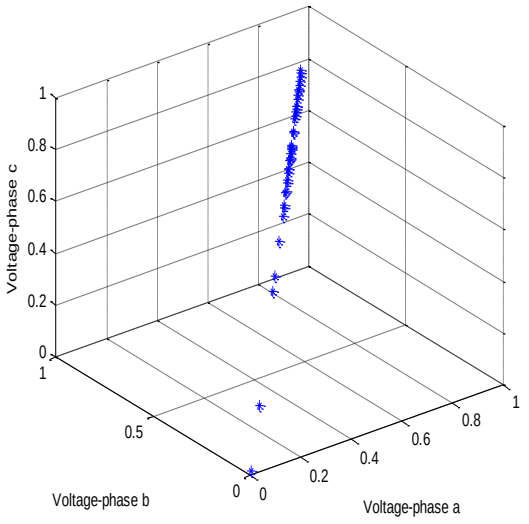

(d) LLLGF

Figure 5.16 Voltage sag pattern at phase a, b and c-TNB network

5.5.2 Case Studies

The test results of the possible faulty sections and rank of the correct section are summarized in Table 5.4 to Table 5.7. The tables show the faulty section candidate for test section (1-2, 4-5, 9-10, 13-14, 15-16, 27-28 and 36-37) and the ranking number where the actual faulty section can be found. The complete results for all sections are summarized in Appendix B. The results are analyzed considering phases a, b and c at a fault resistance of 0Ω.

The rank for the fault types of $SLGF_a$, $SLGF_b$ and $SLGF_c$; LLF_{ab}, LLF_{bc} and LLF_{ca}; $DLGF_{ab}$, $DLGF_{bc}$ and $DLGF_{ca}$ are the same. This is due to only the faulty phase is interchanged.

Table 5.4 Faulty sections and rank of the correct section for $SLGF_a$/ $SLGF_b$/ $SLGF_c$

Section number	Test section	Possible faulty section	Rank number of the actual faulty section
1	1-2	1-2, 1-21	1
4	4-5	4-5, 3-15, 1-21	1
9	9-10	9-10, 15-18, 16-17, 1-21	1
13	13-14	7-8, 13-14, 15-18, 15-16, 1-21	1
18	15-16	8-9, 13-14, 15-18, 15-16, 1-21	1
27	27-28	25-26, 27-28, 38-39	1
36	36-37	22-23, 36-37	1

Table 5.5 Faulty sections and rank of the correct section for LLF_{ab}/ LLF_{bc}/ LLF_{ca}

Section number	Test section	Possible faulty section	Rank number of the actual faulty section
1	1-2	1-2, 1-21	1
4	4-5	4-5, 3-15, 1-21	1
9	9-10	9-10, 15-18, 15-16, 1-21	1
13	13-14	7-8, 13-14, 3-15, 1-21	2
18	15-16	9-10, 15-18, 15-16, 1-21	1
27	27-28	25-26, 27-28	1
36	36-37	11-12, 18-19, 16-17, 22-23,36-37	1

Table 5.6 Faulty sections and rank of the correct section for $DLGF_{ab}$/ $DLGF_{bc}$/ $DLGF_{ca}$

Section number	Test section	Possible faulty section	Rank number of the actual faulty section
1	1-2	1-2, 1-21	1
4	4-5	4-5, 3-15, 1-21	1
9	9-10	9-10, 15-18, 15-16, 1-21	1
13	13-14	7-8, 13-14, 15-18, 15-16, 1-21	2
18	15-16	9-10, 13-14, 15-18, 15-16, 1-21	1
27	27-28	25-26, 27-28	1
36	36-37	22-23, 36-37	1

Table 5.7 Faulty sections and rank number of the correct section for $LLLGF_{abc}$

Section number	Test section	Possible faulty section	Rank number of the actual faulty section
1	1-2	1-2, 1-21	1
4	4-5	4-5, 3-15, 1-21	1
9	9-10	9-10, 15-18, 15-16, 1-21	1
13	13-14	7-8, 13-14, 15-18, 15-16, 1-21	2
18	15-16	9-10, 13-14, 15-18, 15-16, 1-21	1
27	27-28	25-26, 27-28	1
36	36-37	22-23, 36-37	1

Generally, the test results show that the test sections have multiple possible faulty sections due to complex patterns. The overlapping and close pattern in many places in the test network causes the selection of multiple faulty sections. From the results of Table 5.4 to Table 5.7, it can also be seen that the correct faulty sections were found in either the first rank or second rank for all tested sections and fault types. This shows that the method can accurately identify faulty section in a low ranking number from the possible faulty sections. This is very important for speeding up the fault location process.

Figure 5.17 shows the overall ranking for mid-point tests at all test sections at 0Ω resistance. The results indicate that no 100% test section can be found in the first rank.

30 faulty sections are correctly identified in the first rank for SLGF, DLGF and LLLGF and 29 line sections for LLF. 8 to 9 faulty sections are identified in rank 2 and 1 section is identified in rank 3 for all types of fault. These results indicate that for lower fault resistance the voltage sag during fault deviates much from the pre-fault voltage. When the fault resistance increases, the voltage sag is very close to the pre-fault voltage. Hence, the possibility of identifying the faulty section at rank1 is higher for 0Ω resistance.

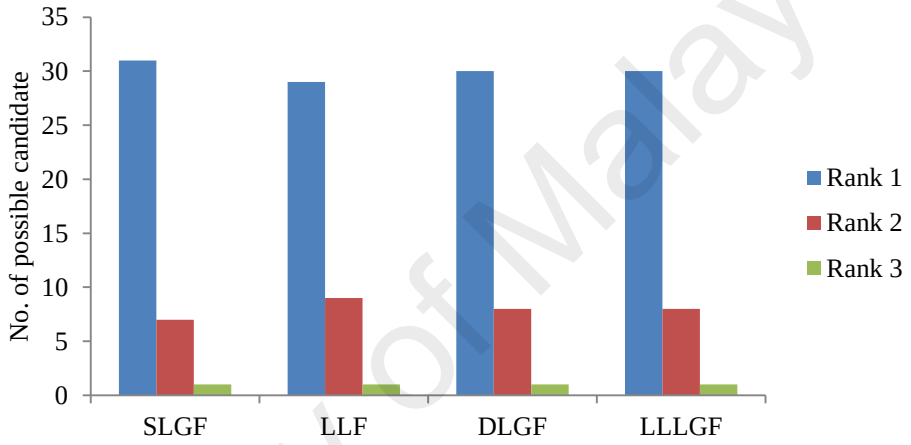

Figure 5.17 Overall test results of ranking at 0Ω resistance – TNB Network

The test result of fault distance by using SVR is given in Table 5.8 to Table 5.11. The results are analyzed for all fault types such as SLGF, LLF, DLGF and LLLGF.

Table 5.8 Fault distance of SLGF at 0Ω resistance-TNB Network

Section number	Test section	Actual fault distance (km)	Fault distance 2D analysis-SVR (km)	Fault distance 3D analysis-SVR (km)
1	1-2	0.25	0.263807	0.25913
4	4-5	0.2	0.204732	0.205104
9	9-10	0.25	0.252754	0.253031
13	13-14	0.375	0.385142	0.385977
18	15-16	0.1975	0.200394	0.20068
27	27-28	0.25	0.252075	0.252191
36	36-37	0.2365	0.239642	0.239859

Table 5.9 Fault distance of LLF at 0Ω resistance-TNB Network

Section number	Test section	Actual fault distance (km)	Fault distance 2D analysis-SVR (km)	Fault distance 3D analysis-SVR (km)
1	1-2	0.25	0.268074	0.276411
4	4-5	0.2	0.208973	0.202644
9	9-10	0.25	0.255131	0.252707
13	13-14	0.375	0.393346	0.386179
18	15-16	0.1975	0.203233	0.20067
27	27-28	0.25	0.251877	0.251126
36	36-37	0.2365	0.240539	0.238917

Table 5.10 Fault distance of DLGF at 0Ω resistance-TNB Network

Section number	Test section	Actual fault distance (km)	Fault distance 2D analysis-SVR (km)	Fault distance 3D analysis-SVR (km)
1	1-2	0.25	0.272440	0.260059
4	4-5	0.2	0.208437	0.208479
9	9-10	0.25	0.255654	0.254042
13	13-14	0.375	0.395585	0.390197
18	15-16	0.1975	0.203754	0.202762
27	27-28	0.25	0.252032	0.252086
36	36-37	0.2365	0.241031	0.240663

Table 5.11 Fault distance of LLLGF at 0Ω resistance-TNB Network

Section number	Test section	Actual fault distance (km)	Fault distance 2D analysis-SVR (km)	Fault distance 3D analysis-SVR (km)
1	1-2	0.25	0.279601	0.260711
4	4-5	0.2	0.206616	0.209764
9	9-10	0.25	0.256331	0.25534
13	13-14	0.375	0.395747	0.393555
18	15-16	0.1975	0.203404	0.204249
27	27-28	0.25	0.252264	0.252634
36	36-37	0.2365	0.240701	0.241963

Generally, it can be seen that the highest fault distance estimation error by using SVR occurs on test section 1-2 on all fault types. Section 1-2 has a maximum error percentage of 11.8% for LLLGF in 2D analysis. It can be noted that the actual fault

distance is 0.25km while the calculated fault distance is 0.2796km. The difference between the actual and the calculated fault distance is 29.6 meters, which is a small distance compared to the whole distribution system.

5.6 Testing on SaskPower Network

The performance of proposed method was also tested using SaskPower distribution network, which the training data is obtained by simulating fault at all 21 nodes of the distribution system at a fault resistance of 0Ω. The simulated data is recorded in database. Hence, a total of 84 voltage samples are created using simulation for 2D analysis and 210 voltage samples for 3D analysis. The voltage sag data is trained using SVM and the proposed method is implemented using MATLAB. The line section, the length of all the line sections and the distance of simulated fault from sending node are shown in Table 5.12.

Table 5.12 Test case for fault at mid-points of section on SaskPower network

Test case	Line section	Line length (km)	Simulated fault location from sending node (km)
1	1–2	2.414	1.207
2	2–3	4	2
3	3-4	4	2
4	4-5	4	2
5	5-6	4	2
6	6–7	4.023	2.0115
7	7–8	5.15	2.575
8	8–9	2.414	1.207
9	9–10	4.506	2.253
10	10–11	2.414	1.207
11	6–12	2.414	1.207
12	8–13	2.414	1.207
13	13–14	2.414	1.207
14	13–15	2.414	1.207
15	15–16	2.414	1.207
16	15–17	2.414	1.207
17	9–18	2.414	1.207
18	18–19	2.414	1.207
19	18–20	3.219	1.6095
20	20–21	3.219	1.6095

Test cases were carried out by simulating fault at the midpoint of line section between nodes. Hence, a total of 80 voltage samples are tested for 2D analysis and 200 voltage samples for 3D analysis. All types of fault were takes into accounted due to the network consists of three-phase lines. The performance of the proposed method was investigated and test results are discussed in following section.

5.6.1 Voltage Sag Pattern of Characteristic Analysis

This section analyzes the pattern of voltage sag variation between two adjacent nodes for all sections in SaskPower network. The voltage sag variation pattern for each fault type was created at all nodes. The lowest voltage magnitude versus phase angle is plotted into a graph to create a variation pattern. The voltage sag pattern variation for all of types with zero fault resistance is depicted in Figure 5.18 (a), (b), (c) and (d). It can be noticed that there is an overlap of voltage sag data at some of the nodes. This overlap leads to multiple possible faulty section.

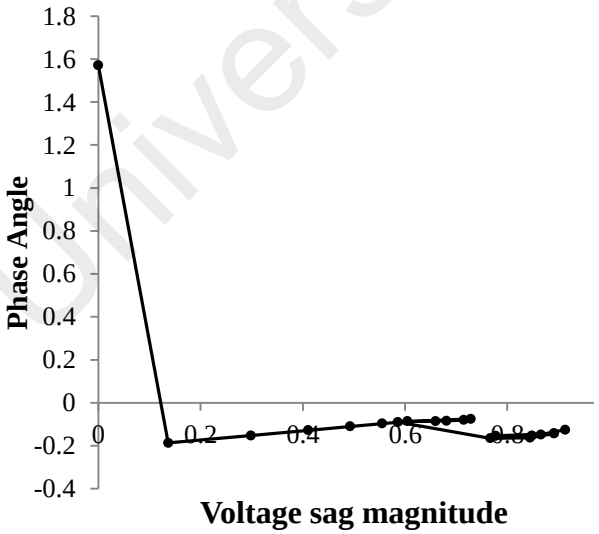

(a) SLGF

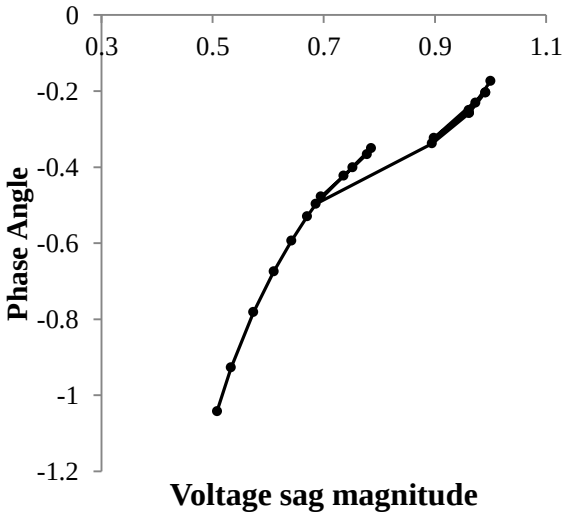

(b) LLF

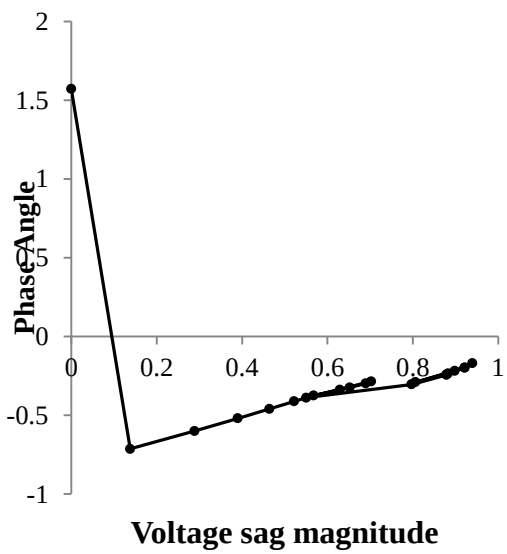

(c) DLGF

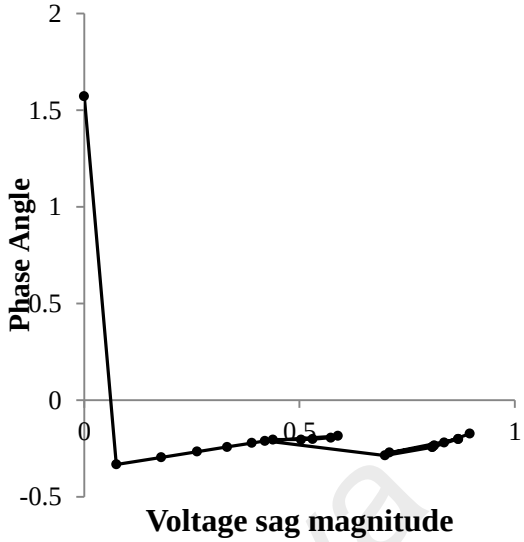

(d) LLLGF

Figure 5.18 Voltage sag magnitude versus phase angle -SaskPower Network

Also, the voltage sag variation pattern for each fault type is analyzed for 3D data using the voltage sag magnitude at phase a, b and c. For this purpose, all of the nodes in SaskPower network are taken into account. The voltage sag pattern variation for all of fault types (SLGF, LLF, DLGF and LLLGF) with zero fault resistance is depicted in Figure 5.19.

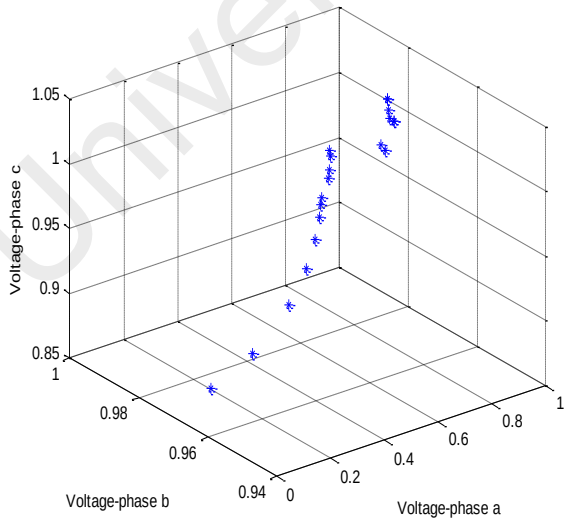

(a) SLGF

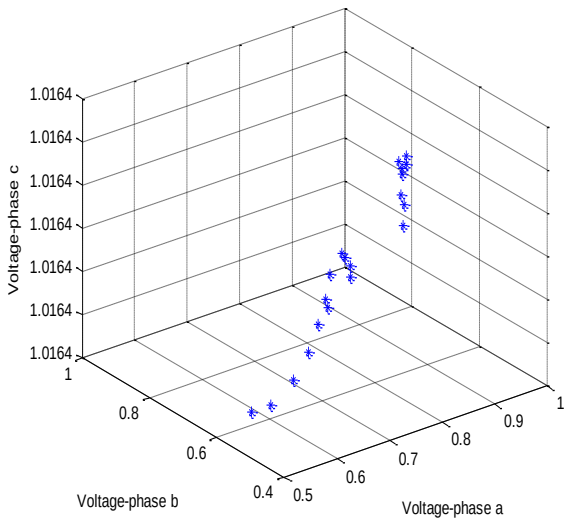

(b) LLF

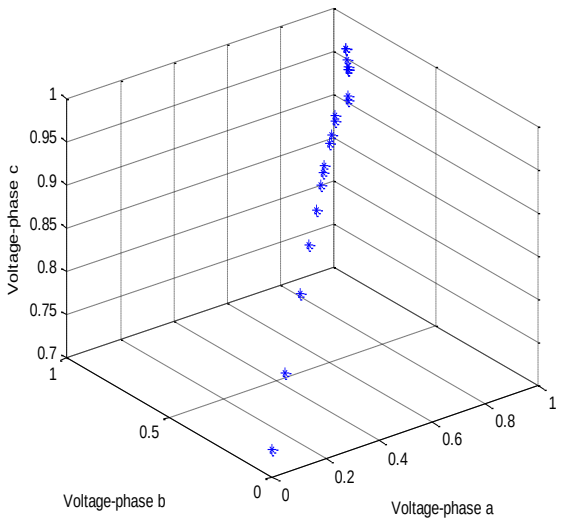

(c) DLGF

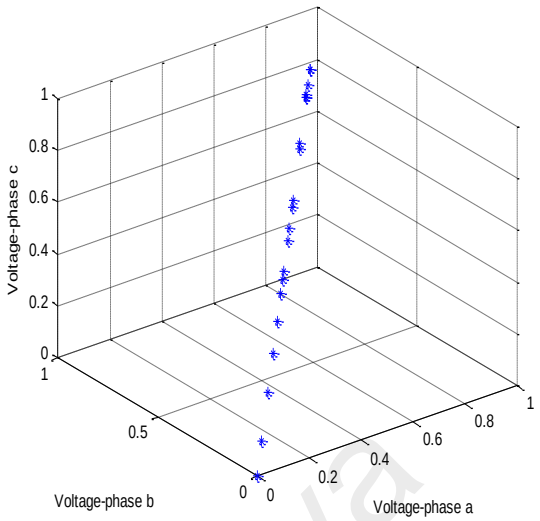

(d) LLLGF

Figure 5.19 Voltage sag at phase a, b and c -SaskPower Network

5.6.2 Case Studies

This section identifies the test results of the possible faulty sections, rank of the correct section and fault distance of the identified section at 0Ω resistance. Table 5.13 to Table 5.16 show the faulty section candidate for some of the test sections (1-2, 7-8, 13-14 and 18-20) and the ranking number where the actual faulty section can be found. The complete results for all sections are summarized in Appendix B.2 and fault distance in Appendix C.2.

From the results, it can be noted that single faulty sections were selected for test sections 1-2 and 7-8 for all types of fault. This is due to from node 1 to node 2 and node 7 to node 8 is completely a radial line and there are no parallel line sections here. The voltage sag pattern characteristics of SLGF also indicate this scenario as shown in Figure 5.19 (a). The rank for the fault type of $SLGF_a$, $SLGF_b$ and $SLGF_c$; LLF_{ab}, LLF_{bc} and LLF_{ca}; $DLGF_{ab}$, $DLGF_{bc}$ and $DLGF_{ca}$ are the same. This is due to only the faulty phase is interchanged.

Table 5.13 Faulty sections and rank of the correct section for $SLGF_a$/ $SLGF_b$/ $SLGF_c$

Section number	Test section	Possible faulty section	Rank number of the actual faulty section
1	1-2	1-2	1
7	7-8	7-8	1
13	13-14	13-14, 13-15, 18-19, 18-20	1
19	18-20	13-14, 13-15, 18-19, 18-20	2

Table 5.14 Faulty sections and rank of the correct section for LLF_{ab}/ LLF_{bc}/ LLF_{ca}

Section number	Test section	Possible faulty section	Rank number of the actual faulty section
1	1-2	1-2	1
7	7-8	7-8	1
13	13-14	13-14, 13-15, 18-19, 18-20	1
19	18-20	13-14, 13-15, 18-19, 18-20	3

Table 5.15 Faulty sections and rank of the correct section for $DLGF_{ab}$/ $DLGF_{bc}$/ $DLGF_{ca}$

Section number	Test section	Possible faulty section	Rank number of the actual faulty section
1	1-2	1-2	1
7	7-8	7-8	1
13	13-14	13-14, 13-15, 18-19, 18-20	1
19	18-20	13-14, 13-15, 18-19, 18-20	3

Table 5.16 Faulty sections and rank of the correct section for $LLLGF_{abc}$

Section number	Test section	Possible faulty section	Rank number of the actual faulty section
1	1-2	1-2	1
7	7-8	7-8	1
13	13-14	13-14, 13-15, 18-19, 18-20	1
19	18-20	13-14, 13-15, 18-19, 18-20	2

The ranking is analyzed for fault at the midpoint of all line sections and the rank results are illustrated in Figure 5.20. It shows that most of the possible faulty sections are found correctly at the first and second ranks for mid-point tests at all test sections. 14 faulty sections are correctly identified in the first rank for LLF, 15 sections for SLGF and DLGF and 18 sections for LLLGF. These results indicate that for lower fault resistance, the voltage sag during fault deviates much from the pre-fault voltage. When the fault resistance increases, the voltage sag is very close to the pre-fault voltage. Hence, the possibility of identifying the faulty section at rank 1 is higher for 0Ω resistance. The faulty section performances of LLF (2 sections) and DLGF (1 section) have rankings, up to the third rank. Generally, the result shows that all of the sections can be determined. The complete results and all possibility of faulty sections are shown in Appendices B.2.

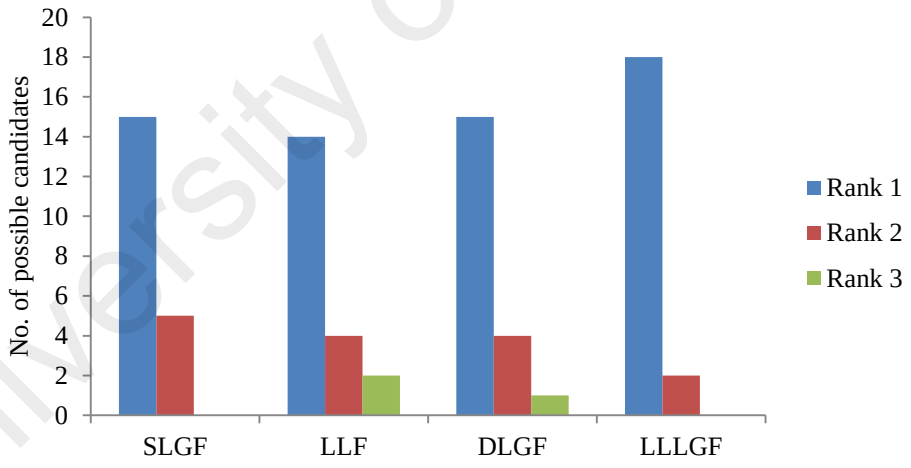

Figure 5.20 Overall test results test results of ranking at 0Ω resistance – SaskPower Network

The test results of fault distance for some of the test sections (1-2, 7-8, 13-14 and 18-20) are analyzed using SVR and are given in Table 5.17 to Table 5.20. It can be noticed that the calculated fault distance is closer to the actual distance in the analyzed test cases.

Table 5.17 Fault distance of SLGF at 0Ω resistance-SaskPower Network

Section number	Test section	Actual fault distance (km)	Fault distance 2D analysis-SVR (km)	Fault distance 3D analysis-SVR (km)
1	1–2	1.207	1.238148	1.248661
7	7–8	2.575	2.598596	2.59918
13	13–14	1.207	1.238479	1.240812
19	18–20	1.6095	1.673516	1.679025

Table 5.18 Fault distance of LLF at 0Ω resistance-SaskPower Network

Section Number	Test Section	Actual fault distance (km)	Fault distance 2D analysis-SVR (km)	Fault distance 3D analysis-SVR (km)
1	1–2	1.207	1.209373	1.210396
7	7–8	2.575	2.60419	2.585018
13	13–14	1.207	1.266509	1.266268
19	18–20	1.6095	1.727554	1.730491

Table 5.19 Fault distance of DLGF at 0Ω resistance-SaskPower Network

Section Number	Test Section	Actual fault distance (km)	Fault distance 2D analysis-SVR (km)	Fault distance 3D analysis-SVR (km)
1	1–2	1.207	1.2688	1.284594
7	7–8	2.575	2.604729	2.610853
13	13–14	1.207	1.261797	1.287734
19	18–20	1.6095	1.718968	1.765603

Table 5.20 Fault distance of LLLGF at 0Ω resistance-SaskPower Network

Section Number	Test Section	Actual fault distance (km)	Fault distance 2D analysis-SVR (km)	Fault distance 3D analysis-SVR (km)
1	1–2	1.207	1.21572	1.226618
7	7–8	2.575	2.599408	2.628671
13	13–14	1.207	1.269019	1.330834
19	18–20	1.6095	1.732743	1.83675

The fault distance errors are also analyzed for fault at the midpoint of all line sections and the results are tabulated. Appendix C.2 shows the calculated fault distance for all fault types at 0Ω resistance.

5.7 Summary

This chapter has described the algorithm of the proposed fault location method and the tests to evaluate it. The analytical voltage database establishment and fault location analysis were implemented separately in MATLAB programming code so that the database can be updated continuously to address any change, such as loading variation or reconfiguration of lines. This chapter have also discussed the voltage sag variation patterns between two adjacent nodes as seen from the substation. The pattern shows that there are overlapping areas and lines at few sections. In this chapter, the impact of the fault distance to the voltage sags was discussed in order to justify its usage in this work. The test results show that in most cases, the method is able to locate faults at the first rank, with some findings at the second and third rank. In SaskPower network, the best ranking is achieved for LLLGF, where 17 faulty sections are detected in the first attempt. This is possible due to the voltage sag patterns do not overlap much compared to another types of fault. The fault distance algorithm was also discussed. The calculated fault distance is much closer to the actual fault distance in the analyzed test cases.

CHAPTER 6: RESULTS AND DISCUSSION

6.1 Introduction

In Chapter 5, the implementation of the proposed method, test system and test cases are discussed. The main idea behind the proposed method is based on locating fault considering faulty phase, fault type, faulty section and fault distance. In this chapter, the test results of the proposed method to locate fault in a distribution network are presented. The test data to validate the algorithms were generated by performing fault simulation on actual distribution networks from Malaysia and Canada. The performance of the proposed method in terms of calculating faulty phase, fault type, fault resistance, voltage sag database, ranking the possible faulty section and fault distance was investigated and test results are discussed in this chapter.

6.2 Test on Fault Type Analysis

The training and test data for locating fault is shown in Table 6.1. For training purpose, simulations were performed for fault at the nodes of the distribution system at 0Ω, 20Ω, 40Ω and 60Ω resistance. For testing purpose, faults are simulated at the midpoint of the line section. The proposed method was also tested for three different fault resistances of 10Ω, 30Ω and 50Ω.

Table 6.1 Training and testing data for fault type classification

Parameters	**Training details**	**Testing details**
Voltage sag data for 3D analysis – TNB Network	1600	1170
Voltage sag data for 3D analysis -SaskPower Network	840	600
Voltage sag data for 2D analysis -TNB Network	640	468
Voltage sag data for 2D analysis - SaskPower Network	336	240
Fault point	At node	At middle of line section
Fault Resistance	0Ω, 20Ω, 40Ω and 60Ω	10Ω, 30Ω and 50Ω

6.2.1 Fault Type using 2D Analysis of SVC

Fault type is identified using 'one versus all' concept of SVC. The performance of fault type classification is tested using TNB and SaskPower distribution network.

6.2.1.1 Fault Type in TNB Distribution Network

SVC is trained with 640 voltage samples using radial basis function kernel for classification of 4 classes. After training, SVC identifies support vectors and hyper plane for fault type classification.

SVC and hyper plane for fault type classification are shown from Figure 6.1 to Figure 6.3. Figure 6.1 gives a total available 640 voltage sag data and the hyperplane for SLGF. The voltage sag data of SLGF are marked in green color. The x-axis represents the phase voltage and y-axis represents the angle of voltage sag data. The training data of SLGF is considered as class 1 and marked in green color. All remaining data (LLF, DLGF, LLLGF) are considered as class 0 and mentioned in red color. The support vectors are marked as circles and a total of 125 support vectors are identified by mapping using kernel function for SLGF identification.

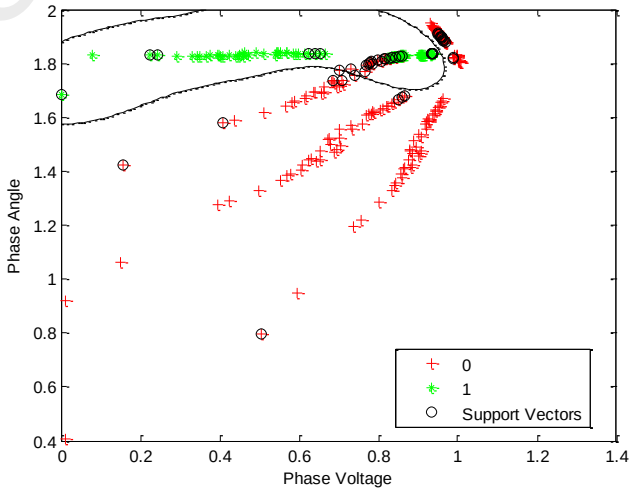

Figure 6.1 2D hyper plane for SLGF – TNB network

If the fault type is not SLGF, then the remaining fault types (LLF, DLGF, LLLGF - marked in red color) are selected for fault type classification purpose. Then SVC verifies for fault type of LLF. For this, the training data of SLGF is removed and the voltage sample of LLF is marked in green color. The data of LLF is chosen as class 1 (green color) and the remaining data (DLGF, LLLGF) as class 0 (red color). Figure 6.2 represents the nonlinear hyper plane for LLF classification. A total of 211 support vectors are identified by mapping using kernel function for classification of LLF.

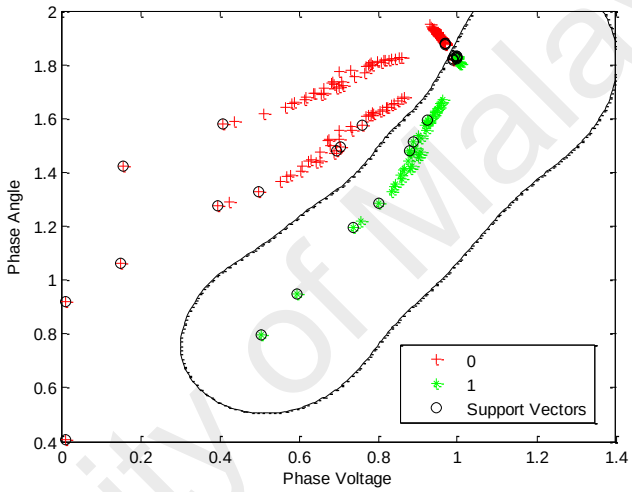

Figure 6.2 2D hyper plane for LLF– TNB network

If LLF is not identified as fault type, then the dataset of DLGF and LLLGF are considered for classification purpose. Figure 6.3 represents the voltage samples of DLGF and LLLGF and its separating hyper plane. A total of 55 support vectors are identified by mapping using kernel function.

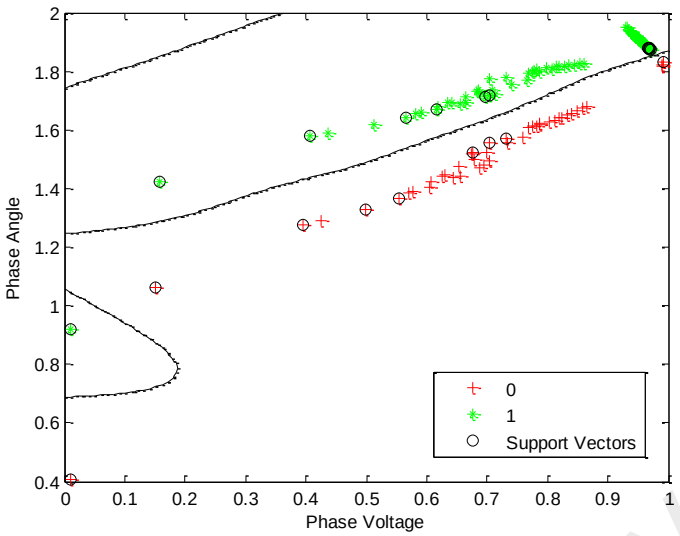

Figure 6.3 2D hyper plane for DLGF and LLLGF– TNB network

Test cases were carried out for fault at midpoint of each line section for fault resistances of 10Ω, 30Ω and 50Ω. The fault resistances of 10Ω, 30Ω and 50Ω are selected such that they are at the middle of the available set of database readings. The accuracy of the fault type using 2D SVC is tabulated in Table 6.2. It is noticed that DLGF at 0Ω identifies the fault type accurately for only 59% and the remaining 41% are identified as SLGF. Also, some of the fault types of LLLGF at 0Ω, 10Ω, 30Ω and 50Ω conflict with LLF. The reason is the hyper plane conflicts with the available data between SLGF and DLGF and between LLF and LLLGF. It happens since only the smallest voltage sag at the phase is considered. This limitation can be overcome when 3D analysis is carried out.

Table 6.2 Percentage accuracy of fault type in 2D analysis-TNB network

Type of fault	Percentage Accuracy of fault type classification			
	0Ω	10Ω	30Ω	50Ω
SLGF	100%	100%	100%	100%
LLF	100%	100%	100%	100%
DLGF	59%	100%	100%	100%
LLLGF	77%	82%	82%	92%

6.2.1.2 Fault Type in SaskPower Distribution Network

SVC is trained with 336 voltage samples using radial basis function kernel for classification of 4 classes (SLGF, LLF, DLGF, LLLGF). After training, SVC identifies support vectors and hyper plane for fault type classification using 'one versus all' concept.

The support vectors and the hyper plane for fault type classification are shown from Figure 6.4 to Figure 6.9. The x-axis represents the phase voltage in p.u and y-axis represents the phase angle of voltage sag data. Figure 6.4 shows the classification of voltage sag data for SLGF identification. It shows the voltage sag data of SLGF (class 1) in green, the remaining LLF, DLGF, LLLGF (class 0) in red and the separating hyper plane. The support vectors are marked as circles and a total of 190 support vectors are identified by mapping using kernel function for SLGF identification. The 3D view of Figure 6.4 is given in Figure 6.5 for better visibility.

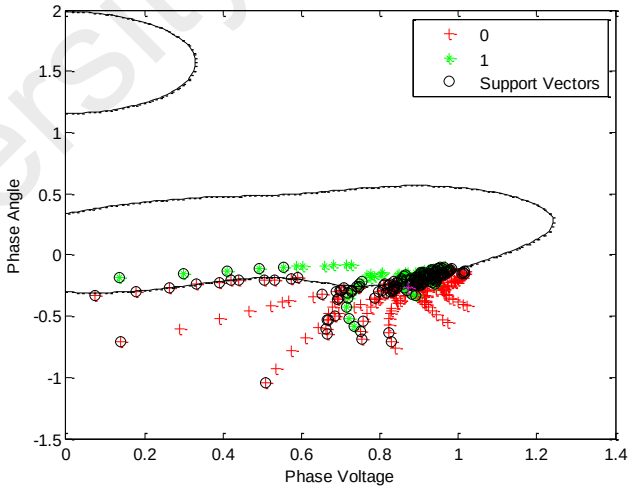

Figure 6.4 2D hyper plane for SLGF– SaskPower network

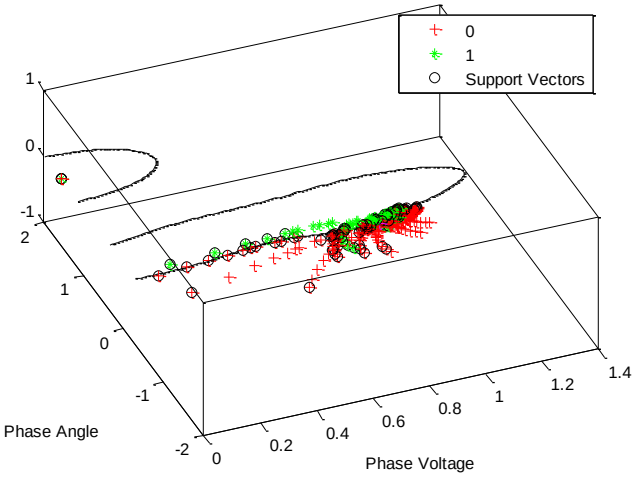

Figure 6.5 3D view of hyper plane for SLGF– SaskPower network

If the fault type is not SLGF then a second set of classification takes place between LLF and combination of DLGF and LLLGF. Figure 6.6 shows the classification of fault type for LLF and its 3D view is given in Figure 6.7. The voltage sag data of LLF is class 1 and the remaining fault types (DLGF, LLLGF) is class 0. A total of 121 support vectors are identified by mapping using kernel function for LLF identification.

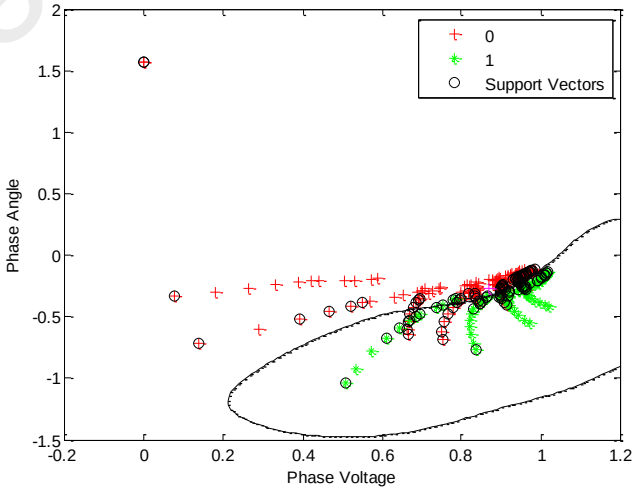

Figure 6.6 2D hyper plane for LLF– SaskPower network

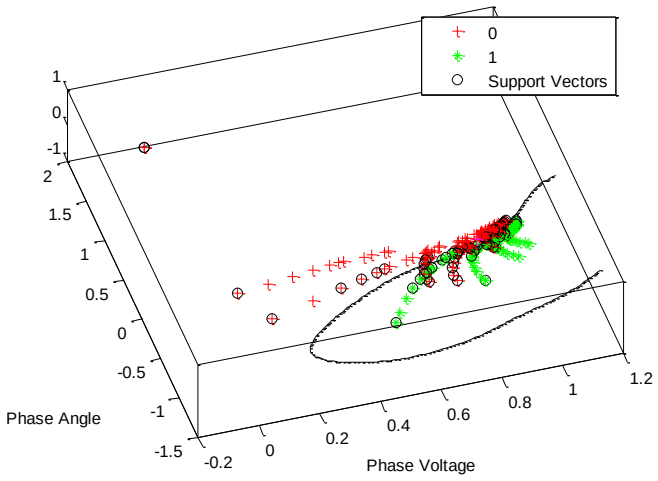

Figure 6.7 3D view of hyper plane for LLF– SaskPower network

Figure 6.8 shows the classification of voltage sag data between DLGF/LLLGF and its separating hyperplane. The voltage sag data of DLGF is represented as class 1 and LLLGF as class 0. A total of 138 support vectors are identified for DLGF/LLLGF classification. The 3D view on the classification of voltage sag data between DLGF/LLLGF is given in Figure 6.9.

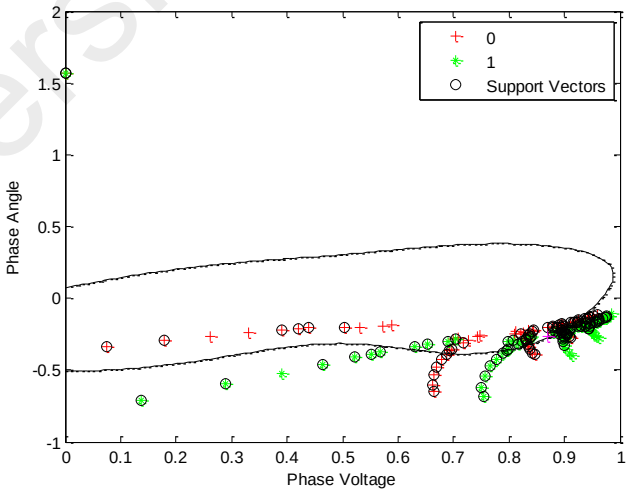

Figure 6.8 2D hyper plane for DLGF/LLLGF– SaskPower network

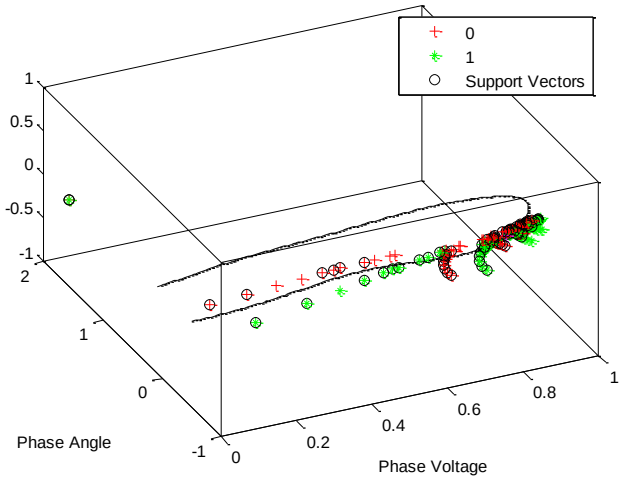

Figure 6.9 3D view of hyper plane for DLGF/LLLGF– SaskPower network

Test cases were carried for fault at midpoint of each line section for fault resistances of 0Ω, 10Ω, 30Ω and 50Ω and are tabulated in Table 6.3. It can be noticed that the percentage accuracy in 2D analysis (SaskPower network) varies between 60% and 100%. This happens because of the overlap of hyperplane, since the method considers only the smallest voltage sag at the phase. This limitation can be overcome when 3D analysis is carried out, which considers voltage sag at phases a, b and c.

Table 6.3 Percentage accuracy of fault type in 2D analysis - SaskPower network

Type of fault	Percentage Accuracy of fault type classification			
	0Ω	10Ω	30Ω	50Ω
SLGF	100%	75%	75%	75%
LLF	90%	95%	95%	95%
DLGF	70%	60%	60%	75%
LLLGF	70%	70%	80%	70%

6.2.2 Fault Type using 3D Analysis of SVC

Test on fault type classification for 3D analysis was performed for fault simulations on actual distribution networks from Malaysia and Canada. The performance results are given in section 6.2.2.1 and section 6.2.2.2.

6.2.2.1 Fault Type in TNB Distribution Network

Ten types of fault may occur in distribution systems, which are $SLGF_a$, $SLGF_b$, $SLGF_c$, LLF_{ab}, LLF_{bc}, LLF_{ca}, $DLGF_{ab}$, $DLGF_{bc}$, $DLGF_{ca}$ and $LLLGF_{abc}$. The subscript in the fault type represents the faulty phase. The faulty phase and the fault type are identified using 3D analysis of multiclass SVC. SVC is trained with 1600 voltage samples using radial basis (RBF) function for classification of 10 output. After training process, SVC identifies a hyper plane for fault type classification, as shown in Figure 6.10 to Figure 6.18.

Figure 6.10 shows a total available 1600 voltage sag data and 3D non-linear hyperplane identified using RBF. The voltage sag data of $SLGF_a$ are marked with dark blue color. The x-axis represents the voltage at phase a, y-axis represents the voltage at phase b and z-axis represents the voltage at phase c. The training data of $SLGF_a$ is considered as class 1. All remaining data ($SLGF_b$, $SLGF_c$, LLF_{ab}, LLF_{bc}, LLF_{ca}, $DLGF_{ab}$, $DLGF_{bc}$, $DLGF_{ca}$ and $LLLGF_{abc}$) are considered as class 0 and are marked with red color. A total of 175 support vectors are identified by mapping using kernel function for SLGF identification and are marked with green circles.

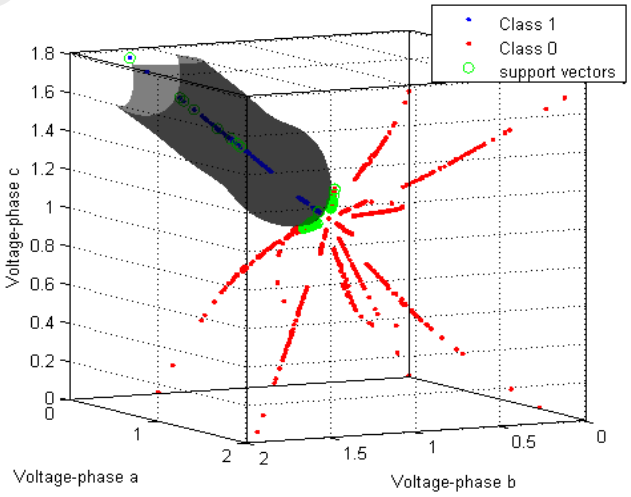

Figure 6.10 3D hyper plane for $SLGF_a$– TNB network

If the fault type is not $SLGF_a$, then the remaining fault types ($SLGF_b$, $SLGF_c$, LLF_{ab}, LLF_{bc}, LLF_{ca}, $DLGF_{ab}$, $DLGF_{bc}$, $DLGF_{ca}$ and $LLLGF_{abc}$) are selected for fault type classification purpose. A binary classification to identify $SLGF_b$ is considered. For this purpose, the training data of $SLGF_a$ is removed and the voltage sample of $SLGF_b$ is marked with dark blue color (class 1) and the remaining data ($SLGF_c$, LLF_{ab}, LLF_{bc}, LLF_{ca}, $DLGF_{ab}$, $DLGF_{bc}$, $DLGF_{ca}$ and $LLLGF_{abc}$) are marked with red color (class 0) as shown in Figure 6.11. A total of 162 support vectors are identified by mapping using RBF for classification of $SLGF_b$.

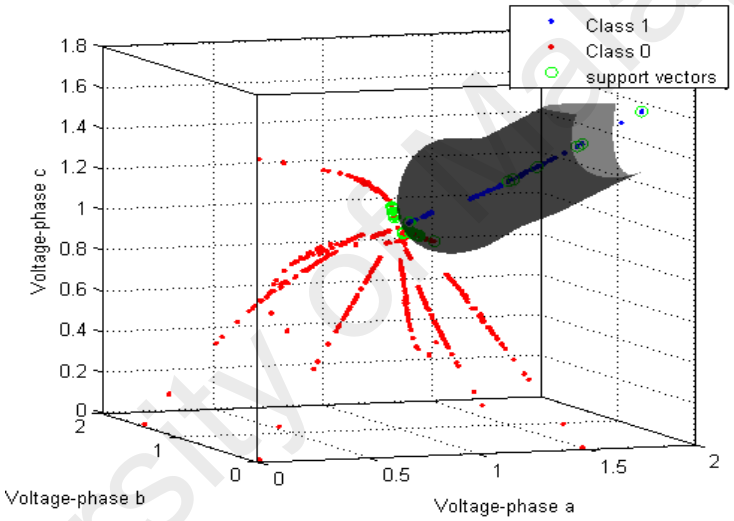

Figure 6.11 3D hyper plane for $SLGF_b$– TNB network

Figure 6.12 shows the 3D hyper plane identified for $SLGF_c$. The support vectors are identified using RBF and marked with green circles. A total of 159 support vectors are identified by mapping using kernel function for classification of $SLGF_c$.

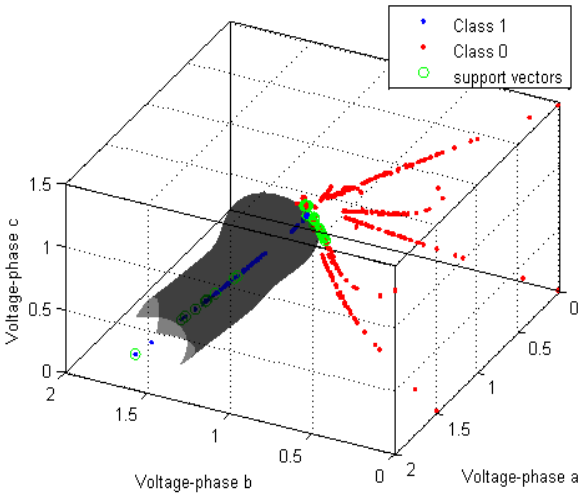

Figure 6.12 3D hyper plane for $SLGF_c$– TNB network

Figure 6.13, Figure 6.14 and Figure 6.15 show the 3D hyper plane identified for LLF_{ab}, LLF_{bc} and LLF_{ca} respectively. A total of 50 support vectors are identified by mapping using kernel function for classification of LLF_{ab}, 36 support vectors for LLF_{bc} and 40 support vectors for LLF_{ca}.

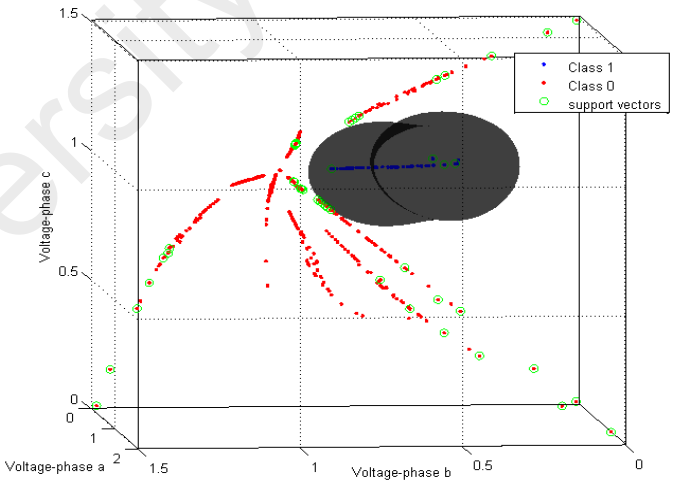

Figure 6.13 3D hyper plane for LLF_{ab}– TNB network

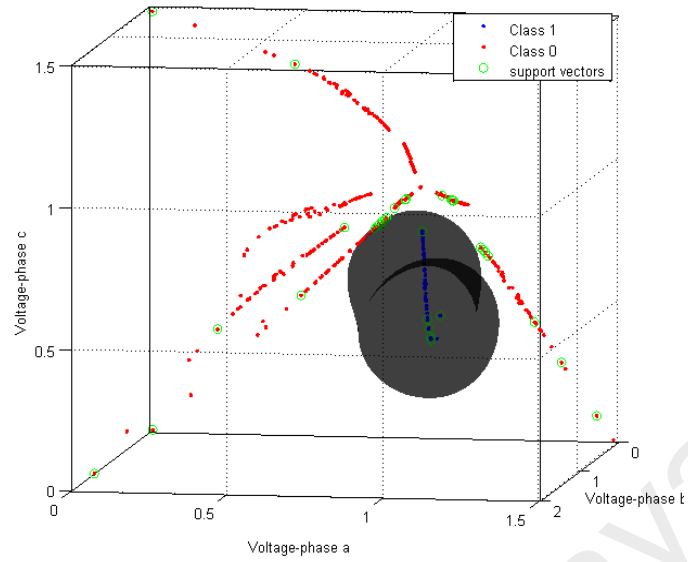

Figure 6.14 3D hyper plane for LLF_{bc}– TNB network

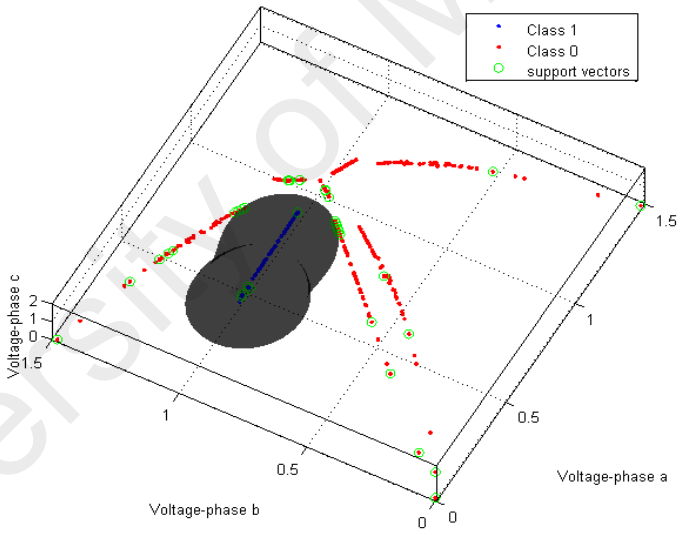

Figure 6.15 3D hyper plane for LLF_{ca}– TNB network

Figure 6.16 and Figure 6.17 show the 3D hyper plane identified for $DLGF_{ab}$ and $DLGF_{bc}$. 66 support vectors are identified for $DLGF_{ab}$ and 58 support vectors for $DLGF_{bc}$ using RBF kernel function. It can be noticed that the hyper plane clearly separates class 1 and class 0.

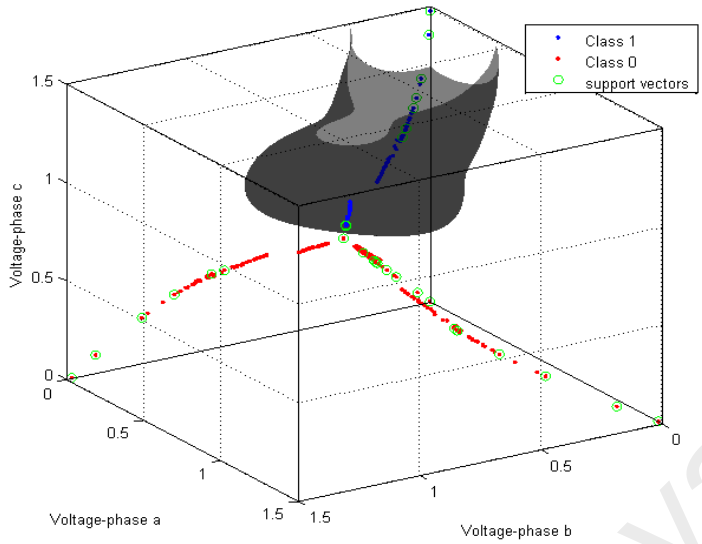

Figure 6.16 3D hyper plane for $DLGF_{ab}$– TNB network

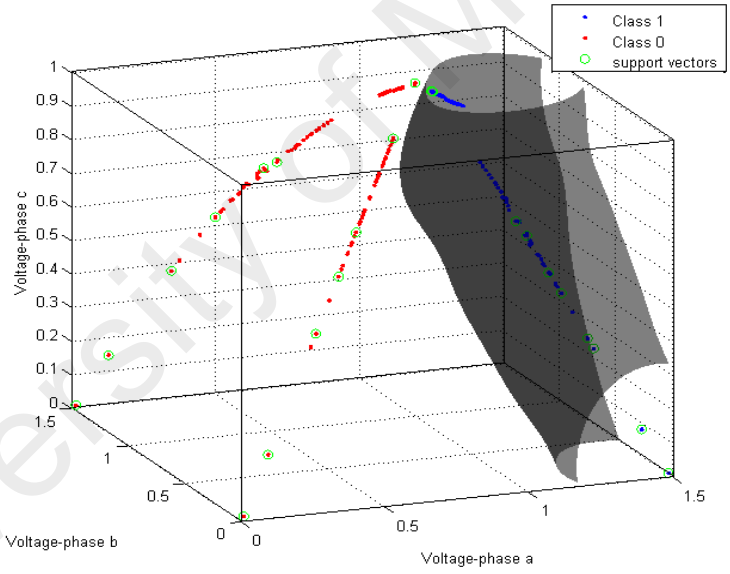

Figure 6.17 3D hyper plane for $DLGF_{bc}$– TNB network

If $DLGF_{bc}$ is not identified as the fault type, then the dataset of $DLGF_{ca}$ and $LLLGF_{abc}$ are considered for classification purpose. Figure 6.18 represents the voltage samples of $DLGF_{ca}$ and $LLLGF_{abc}$ with the separating hyper plane. A total of 50 support vectors are identified by mapping using kernel function.

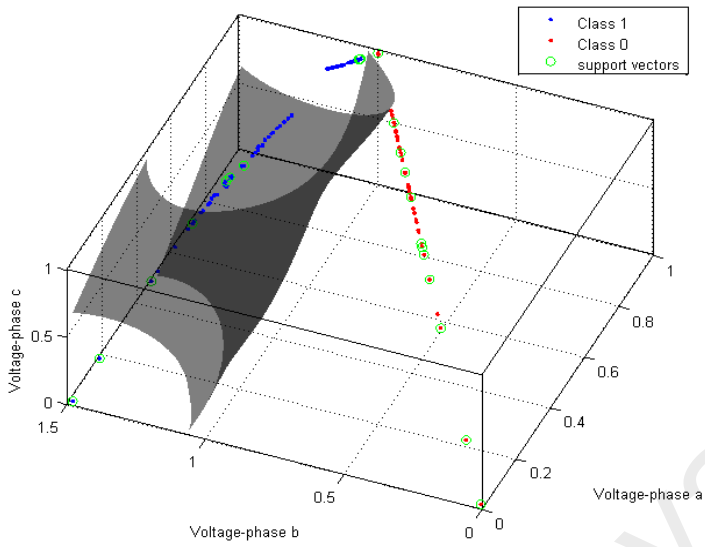

Figure 6.18 3D hyper plane for $DLGF_{ca}$ and $LLLGF_{abc}$– TNB network

Test cases were carried for fault at midpoint of all line section for fault resistances of 0Ω, 10Ω, 30Ω and 50Ω. The percentage accuracy of fault type using 3D analysis of SVC is tabulated in Table 6.4. This shows that the proposed method is 100% accurate for fault type classification. 3D analysis of SVC overcomes the limitation of 2D analysis using SVC since it considers the voltage sag at all three phases.

Table 6.4 Percentage accuracy of fault type in 3D analysis-TNB network

Type of fault	Percentage accuracy of fault type classification			
	0Ω	10Ω	30Ω	50Ω
$SLGF_a$, $SLGF_b$, $SLGF_c$	100%	100%	100%	100%
LLF_{ab}, LLF_{bc}, LLF_{ca}	100%	100%	100%	100%
$DLGF_{ab}$,$DLGF_{bc}$,$DLGF_{ca}$	100%	100%	100%	100%
$LLLGF_{abc}$	100%	100%	100%	100%

6.2.2.2 Fault Type in SaskPower Distribution Network

The proposed method was also tested using SaskPower distribution network for ten fault types ($SLGF_a$, $SLGF_b$, $SLGF_c$, LLF_{ab}, LLF_{bc}, LLF_{ca}, $DLGF_{ab}$, $DLGF_{bc}$, $DLGF_{ca}$ and $LLLGF_{abc}$). SVC was trained with 840 voltage samples using radial basis function

(RBF) for classification of 10 output. After training process, SVC identified a hyper plane for fault type classification, as shown in Figure 6.19 to Figure 6.27.

Figure 6.19 shows a total of 840 voltage sag data and 3D non-linear hyperplane identified for $SLGF_a$. The voltage sag data of $SLGF_a$ are marked with dark blue color. The x-axis represents the voltage at phase a, y-axis represents the voltage at phase b and z-axis represents the voltage at phase c. The training data of $SLGF_a$ are considered as class 1 and are marked with dark blue color. All remaining data ($SLGF_b$, $SLGF_c$, LLF_{ab}, LLF_{bc}, LLF_{ca}, $DLGF_{ab}$, $DLGF_{bc}$, $DLGF_{ca}$ and $LLLGF_{abc}$) are considered as class 0 and are marked with red color. A total of 144 support vectors are identified by mapping using kernel function for SLGF identification and are marked with green circles.

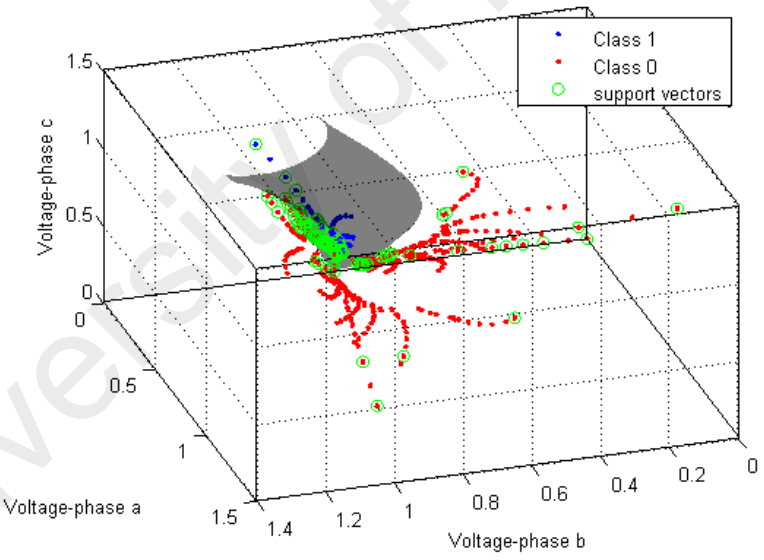

Figure 6.19 3D hyper plane for $SLGF_a$– SaskPower network

Figure 6.20 and Figure 6.21 represent the fault type classification for $SLGF_b$ and $SLGF_c$ respectively. A total of 137 support vectors are identified in $SLGF_b$ and 128 support vectors are identified in $SLGF_c$.

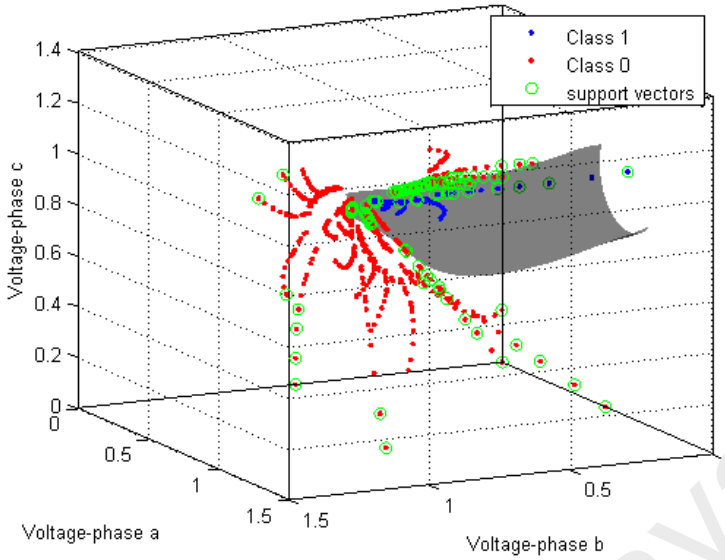

Figure 6.20 3D hyper plane for $SLGF_b$– SaskPower network

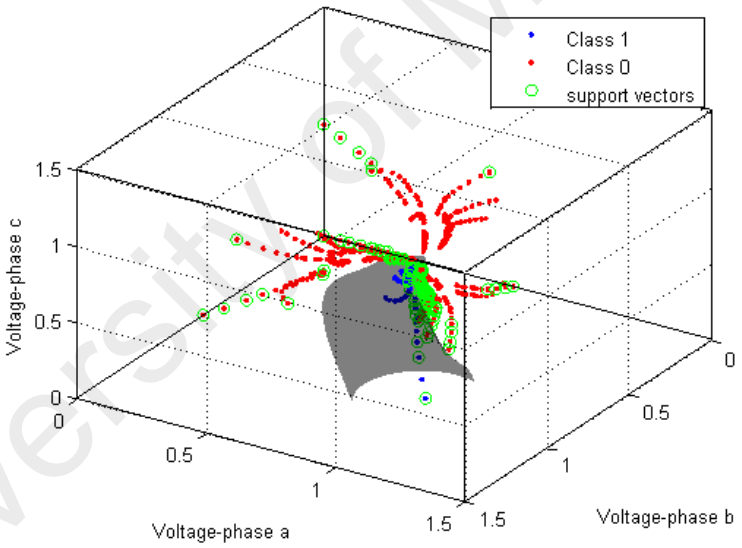

Figure 6.21 3D hyper plane for $SLGF_c$– SaskPower network

Figure 6.22, Figure 6.23 and Figure 6.24 show the 3D hyper plane identified for LLF_{ab}, LLF_{bc} and LLF_{ca} respectively. A total of 82 support vectors are identified by mapping using kernel function for classification of LLF_{ab}, 81 support vectors for LLF_{bc} and 80 support vectors for LLF_{ca}.

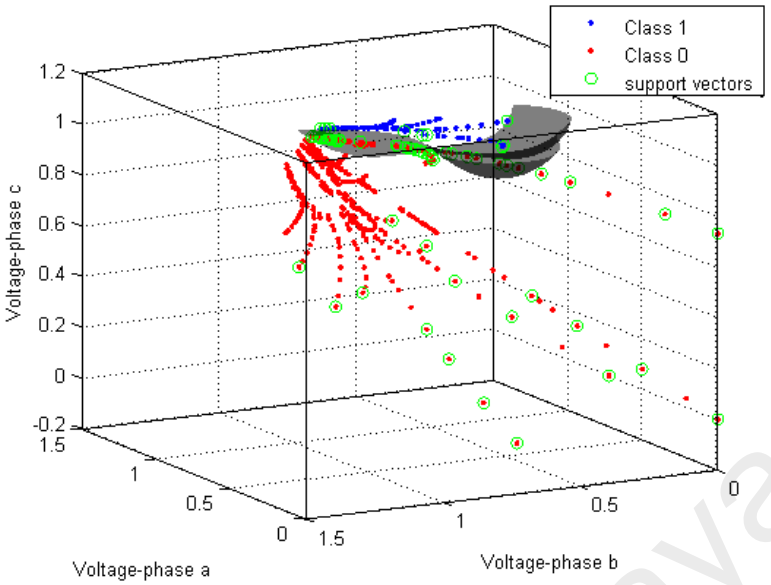

Figure 6.22 3D hyper plane for LLF_{ab}– SaskPower network

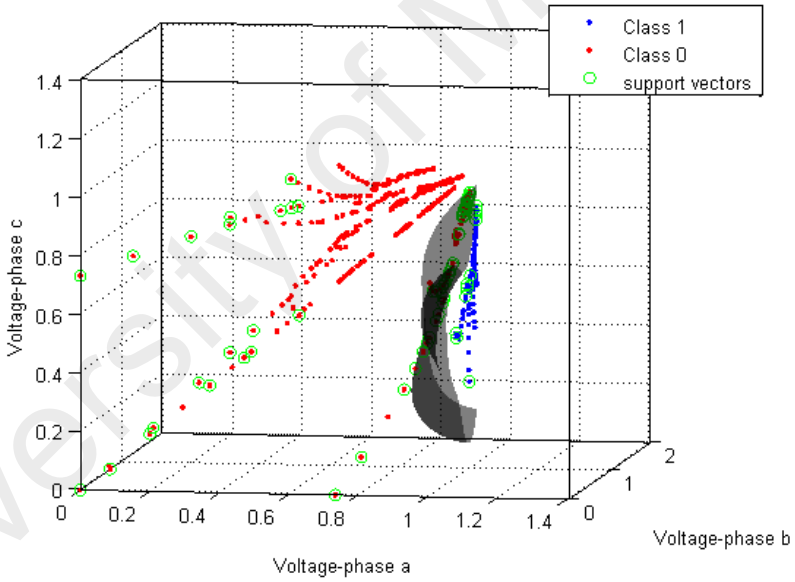

Figure 6.23 3D hyper plane for LLF_{bc}– SaskPower network

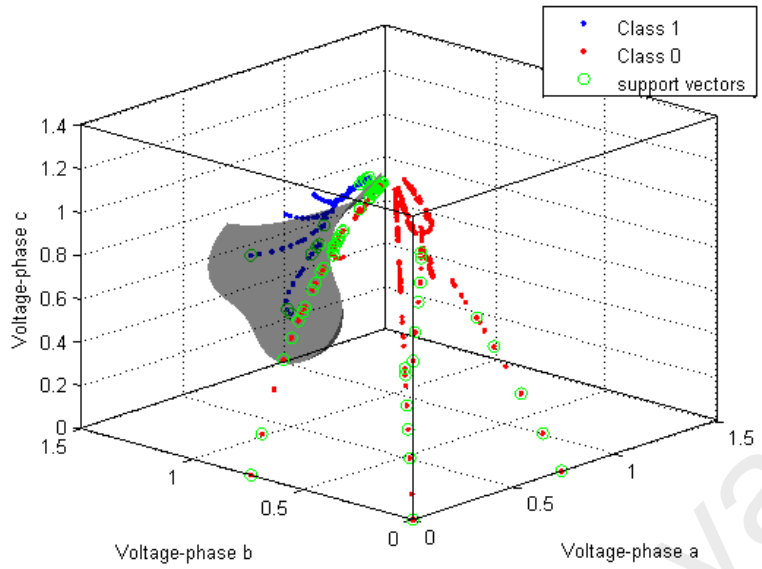

Figure 6.24 3D hyper plane for LLF_{ca}– SaskPower network

If the fault type is not identified under SLGF and LLF, the dataset of $DLGF_{ab}$, $DLGF_{bc}$, $DLGF_{ca}$ and $LLLGF_{abc}$ are considered for classification purpose. Figure 6.25 and Figure 6.26 represent the fault type of $DLGF_{ab}$ and $DLGF_{bc}$ and its separating hyper plane. A total of 56 support vectors are identified by mapping using kernel function for $DLGF_{ab}$ and 49 support vectors for $DLGF_{bc}$.

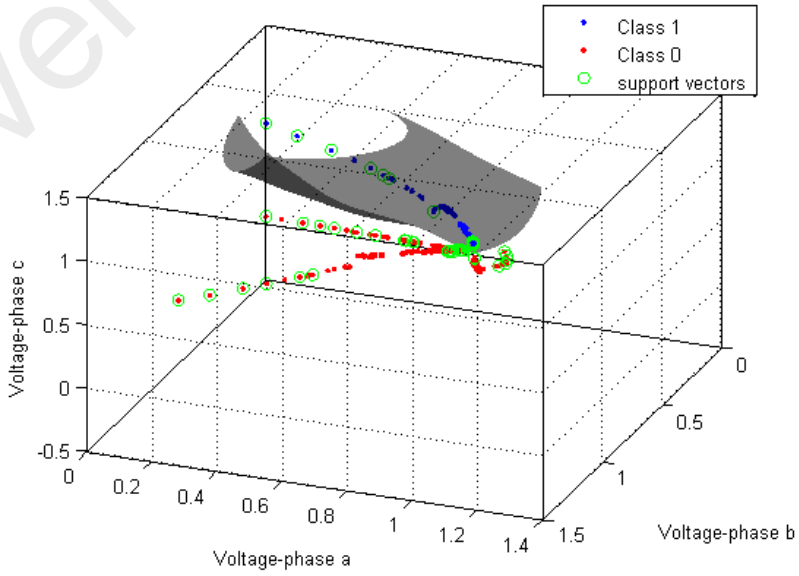

Figure 6.25 3D hyper plane for $DLGF_{ab}$– SaskPower network

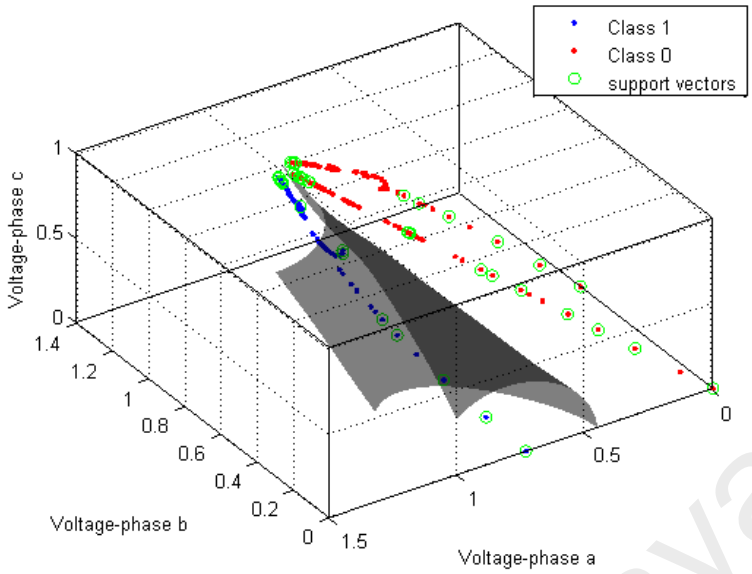

Figure 6.26 3D hyper plane for $DLGF_{bc}$– SaskPower network

If $DLGF_{bc}$ is not identified as the fault type, then the dataset of $DLGF_{ca}$ and $LLLGF_{abc}$ are considered for classification purpose. Figure 6.27 represents the voltage samples of $DLGF_{ca}$ and $LLLGF_{abc}$ with the separating hyper plane. A total of 43 support vectors are identified by mapping using kernel function.

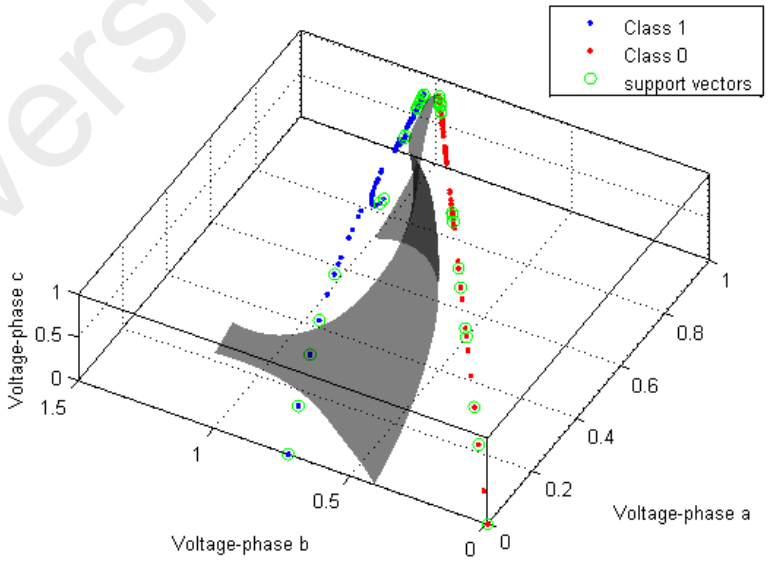

Figure 6.27 3D hyper plane for $DLGF_{ca}$ and $LLLGF_{abc}$– SaskPower network

Test cases were carried out for fault at midpoint of all line sections for fault resistances of 0Ω, 10Ω, 30Ω and 50Ω. The percentage accuracy of fault type using 3D SVC is tabulated in Table 6.5. 3D SVC is more accurate than 2D analysis of SVC since it considers the voltage sag at all three phases.

Table 6.5 Percentage accuracy of fault type in 3D analysis -SaskPower network

Type of fault	Percentage accuracy of fault type classification			
	0Ω	10Ω	30Ω	50Ω
$SLGF_a$, $SLGF_b$, $SLGF_c$	100%	100%	100%	100%
LLF_{ab}, LLF_{bc}, LLF_{ca}	100%	100%	100%	100%
$DLGF_{ab}$,$DLGF_{bc}$,$DLGF_{ca}$	100%	100%	100%	100%
$LLLGF_{abc}$	100%	100%	100%	100%

6.2.3 Comparison of Fault Type using SVC and Existing Method

A comparison of the fault type classification using SVC and voltage sag characteristic (Namrata B. Pawar, 2014; Suresh Kamble, 2014) is shown in Table 6.6. The method using voltage sag characteristic identifies the fault type by comparing the pattern of pre-fault voltage with the voltage during fault. However, for fault far from the measurement location, the different is not noticeable and may lead to wrong identification of fault type. Also, the existing method requires pre-fault voltage sag and voltage sag during fault but the proposed method requires only the voltage sag during fault.

For example, fault between nodes 9 and 10 in TNB Network are considered. The pre-fault voltage sag data for phase a is 0.992301 pu, phase b is 0.992292 pu and phase c is 0.992278 pu. The fault voltage at the measurement node for LLF_{ab} at phase c is 0.992279 (30Ω resistance). Here the fault voltage at phase c is not equal to the pre-fault voltage at phase c but greater than the pre-fault voltage. Hence the fault type is identified as $DLGF_{ab}$ in existing voltage sag characteristic method. The proposed classification using SVC identifies the hyperplane to classify fault types. Table 6.6

clearly shows that the proposed SVC classifies fault type accurately but in the existing method, due to a small decimal change in LLF_{ab} (30Ω and 50Ω) it may wrongly identify LLF_{ab} as $DLGF_{ab}$.

Table 6.6 Comparison of fault type using SVC and existing method

Type of fault	Fault Resistance (Ω)	Fault voltage at measurement node			Identified fault Type	
		Phase a (pu)	Phase b (pu)	Phase c (pu)	SVC	Voltage sag characteristic (Namrata B. Pawar, 2014; Suresh Kamble, 2014)
$SLGF_a$	10	0.754318	1.120263	1.136016	$SLGF_a$	$SLGF_a$
	30	0.883681	1.048522	1.052406	$SLGF_a$	$SLGF_a$
	50	0.922039	1.028349	1.030159	$SLGF_a$	$SLGF_a$
LLF_{ab}	10	0.911248	0.94568	0.992278	LLF_{ab}	LLF_{ab}
	30	0.940135	0.97699	0.992279	LLF_{ab}	$DLGF_{ab}$
	50	0.968171	0.983296	0.992280	LLF_{ab}	$DLGF_{ab}$
$DLGF_{ab}$	10	0.921326	0.904124	1.163444	$DLGF_{ab}$	$DLGF_{ab}$
	30	0.950386	0.946046	1.08438	$DLGF_{ab}$	$DLGF_{ab}$
	50	0.962766	0.960712	1.055358	$DLGF_{ab}$	$DLGF_{ab}$
$LLLGF_{abc}$	10	0.985267	0.985267	0.985266	$LLLGF_{abc}$	$LLLGF_{abc}$
	30	0.990586	0.990586	0.990586	$LLLGF_{abc}$	$LLLGF_{abc}$
	50	0.991479	0.991479	0.991479	$LLLGF_{abc}$	$LLLGF_{abc}$

6.3 Test on Fault Resistance Analysis

Test cases on fault resistance was performed for fault simulations on actual distribution networks from Malaysia and Canada. The performance results are given in section 6.3.1 and section 6.3.2.

6.3.1 Fault Resistance in 2D Analysis

Fault resistance was calculated by training the simulated voltage sag data using SVR. The test cases were carried out for all fault types (SLGF, LLF, DLGF and LLLGF) at 10Ω, 30Ω and 50Ω. For analysis using TNB network, line sections between nodes 1-2, 4-5, 9-10, 13-14, 15-16, 27-28 and 36-37 were considered. For analysis using SaskPower network, line sections between nodes 1-2, 7-8, 13-14 and 18-19 were

considered. The obtained results of fault resistance for TNB network are tabulated in Table 6.7 and for SaskPower network in Table 6.8. It can be seen from the results that the calculated fault resistance is close to the actual fault resistance in all cases.

Table 6.7 Calculated fault resistance in 2D analysis–TNB Network

Section Number	Test Section	Actual fault resistance	Calculated fault resistance (Ω)			
			SLGF	LLF	DLGF	LLLGF
1	1-2	10 Ω	8.080	11.914	10.214	9.929
		30 Ω	31.811	30.659	29.570	28.441
		50 Ω	48.232	49.328	49.688	49.105
4	4-5	10 Ω	11.804	11.368	10.714	9.269
		30 Ω	33.513	32.658	31.044	28.802
		50 Ω	49.227	49.788	48.673	49.332
9	9-10	10 Ω	10.066	8.466	9.134	12.583
		30 Ω	30.110	32.576	34.198	29.123
		50 Ω	50.161	50.203	48.501	49.526
13	13-14	10 Ω	10.192	9.637	11.023	12.499
		30 Ω	30.675	32.326	33.348	29.035
		50 Ω	49.906	50.090	48.005	49.473
18	15-16	10 Ω	13.379	7.841	11.048	12.526
		30 Ω	28.779	30.384	32.542	29.051
		50 Ω	49.966	50.115	48.116	49.480
27	27-28	10 Ω	10.650	11.852	13.752	13.562
		30 Ω	28.374	30.578	29.467	30.529
		50 Ω	52.264	51.848	51.785	50.590
36	36-37	10 Ω	11.718	12.385	9.419	13.137
		30 Ω	30.701	29.333	31.594	30.032
		50 Ω	51.244	51.229	50.045	50.255

Table 6.8 Calculated fault resistance in 2D analysis-SaskPower Network

Section Number	Test Section	Actual fault resistance	Calculated fault resistance (Ω)			
			SLGF	LLF	DLGF	LLLGF
1	1-2	10 Ω	11.543	12.899	13.922	11.044
		30 Ω	32.702	33.615	30.207	32.470
		50 Ω	46.257	51.867	51.237	48.336
7	7-8	10 Ω	13.281	13.832	12.816	10.466
		30 Ω	29.348	27.743	32.542	31.000
		50 Ω	46.863	48.958	51.275	47.962
13	13-14	10 Ω	11.402	12.070	11.306	9.5056
		30 Ω	30.655	29.835	27.671	28.306
		50 Ω	50.582	48.373	48.787	53.707
19	18-20	10 Ω	12.534	13.531	12.728	10.213
		30 Ω	28.270	27.846	28.340	29.001
		50 Ω	50.805	48.170	53.011	53.964

6.3.2 Fault Resistance in 3D Analysis

Similar analysis as in section 6.3.1 was carried out for fault resistance in 3D analysis using SVR. The test results using TNB network are given in Table 6.9 and test results of SaskPower network are given in Table 6.10. For testing, fault at mid-point of all line sections at actual fault resistances of 10Ω, 30Ω and 50Ω are considered. The analysis was carried out for all 10 fault types ($SLGF_a$, $SLGF_b$, $SLGF_c$, LLF_{ab}, LLF_{bc}, LLF_{ca}, $DLGF_{ab}$, $DLGF_{bc}$, $DLGF_{ca}$ and $LLLGF_{abc}$). It can be seen that the calculated fault resistance is close to the actual fault resistance in all cases.

Table 6.9 Calculated fault resistance in 3D analysis-TNB Network

Section Number	Test Section	Actual fault resistance	Calculated fault resistance (Ω)			
			$SLGF_a$, $SLGF_b$, $SLGF_c$	LLF_{ab}, LLF_{bc}, LLF_{ca}	$DLGF_{ab}$, $DLGF_{bc}$, $DLGF_{ca}$	$LLLGF_{abc}$
1	1-2	10 Ω	7.8983	8.0168	7.6562	8.400
		30 Ω	28.709	32.329	29.526	30.676
		50 Ω	48.234	47.971	48.512	50.484
4	4-5	10 Ω	11.140	10.2122	13.214	9.315
		30 Ω	30.657	32.498	29.435	30.675
		50 Ω	49.229	48.332	48.078	49.466
9	9-10	10 Ω	9.681	10.160	9.034	8.551
		30 Ω	28.295	26.771	29.052	28.444
		50 Ω	50.973	51.249	50.674	52.646
13	13-14	10 Ω	8.941	11.633	8.790	7.958
		30 Ω	28.263	29.404	28.991	28.107
		50 Ω	51.036	51.377	50.723	53.734
18	15-16	10 Ω	13.521	12.1986	12.830	11.275
		30 Ω	32.090	33.350	31.569	30.675
		50 Ω	49.963	48.589	49.230	50.457
27	27-28	10 Ω	12.089	13.244	11.991	9.142
		30 Ω	32.059	33.990	33.809	30.675
		50 Ω	52.217	49.959	52.306	49.432
36	36-37	10 Ω	11.322	9.2956	10.547	9.981
		30 Ω	33.205	32.552	34.254	30.675
		50 Ω	51.215	49.471	50.858	50.442

Table 6.10 Calculated fault resistance in 3D analysis –SaskPower Network

Section Number	Test Section	Actual fault resistance	Calculated fault resistance (Ω)			
			$SLGF_a$, $SLGF_b$, $SLGF_c$	LLF_{ab}, LLF_{bc}, LLF_{ca}	$DLGF_{ab}$, $DLGF_{bc}$, $DLGF_{ca}$	$LLLGF_{abc}$
1	1-2	10 Ω	10.487	13.399	9.152	10.983
		30 Ω	30.386	31.767	28.044	27.782
		50 Ω	51.875	52.799	50.802	47.828
7	7-8	10 Ω	11.629	9.0094	11.579	11.959
		30 Ω	29.362	32.011	28.277	28.040
		50 Ω	53.888	50.617	46.724	48.456
13	13-14	10 Ω	11.269	13.571	9.038	11.272
		30 Ω	29.683	30.791	32.550	33.701
		50 Ω	46.712	49.886	48.093	51.218
19	18-20	10 Ω	12.085	13.581	9.970	12.751
		30 Ω	30.073	27.074	29.684	28.390
		50 Ω	48.904	48.820	49.694	51.566

6.4 Test on Voltage Sag Data Analysis

The test results of estimating voltage sag data using SVR and its percentage reduction in terms of database size and time are discussed in this section.

6.4.1 Voltage Sag Estimation using SVR

For analysis of voltage sag estimation, line section between nodes 9 and 10 of TNB network is considered. The percentage error in estimating voltage sag data using SVR analysis is given in Table 6.11. The voltage sag magnitude is represented as V and angle as ϕ. It can be noticed that the percentage error is less than 1.933 for all fault resistance.

Table 6.11 Percentage error of voltage sag estimation

Node	Resistance (Ω)	Percentage error (%)							
		SLGF		LLF		DLGF		LLLGF	
		V	ϕ	V	ϕ	V	ϕ	V	ϕ
9	10	1.933	0.172	1.292	0.215	0.942	0.347	0.584	0.183
	30	1.247	0.090	0.729	0.151	0.303	0.192	0.357	0.063
	50	0.783	0.013	0.128	0.082	0.173	0.035	0.029	0.031
10	10	1.071	0.338	0.792	0.792	0.652	0.347	0.236	0.249
	30	0.606	0.086	0.101	0.101	0.143	0.057	0.065	0.130
	50	0.214	0.024	0.095	0.095	0.078	0.002	0.012	0.027

The overall performance in estimating the voltage sag data at all nodes is presented in Table 6.12 (TNB network) and Table 6.13 (SaskPower network). To validate the performance using voltage sag analysis, regression analysis was carried out. For analyzing the estimation of voltage sag data, training data were done with fault resistances of 0Ω, 20Ω, 40Ω and 60Ω. The test cases for estimating voltage sag data are for fault resistances of 10Ω, 30Ω and 50Ω for all types of fault. Table 6.12 shows the Regression (*R*), Root Mean Square Error (RMSE) and Mean Absolute Error (MAE) during voltage sag estimation.

Table 6.12 Test Results of database prediction - TNB Network

Fault type	Performance of SVR	Fault Resistance		
		10Ω	30Ω	50Ω
SLGF	*R*	0.9523	0.9759	0.9476
	RMSE	0.0191	0.1039	0.0542
	MAE	0.0154	0.1038	0.0541
LLF	*R*	0.8656	0.8500	0.8300
	RMSE	0.0796	0.0425	0.1028
	MAE	0.0794	0.0425	0.1028
DLGF	*R*	0.9046	0.9819	0.9703
	RMSE	0.0685	0.2786	0.0824
	MAE	0.0685	0.2786	0.0823
LLLGF	*R*	0.8553	0.8828	0.8931
	RMSE	0.3671	0.0930	0.0764
	MAE	0.3670	0.0930	0.0764

Regression values are calculated to identify the relationship of voltage sag estimated through simulation (target) and through SVR (output). The regression equation is a straight line equation $Y_{pred}=b_o+b_1(X)$ in which Y_{pred} stands for the predicted value of output Y, b_o is the intercept of regression line with the y-axis, b_1 is the slope of the regression line and X represents the input. A significant t-test is then used to identify the regression value which is in the range of 0 to 1. If regression is zero then the regression line will be a horizontal line. This means that there is no linear relationship between the variables. If the regression value is equal to 1 then it indicates that the output exactly

met the target. From Table 6.12, it can be seen that the regression values are greater than 0.83 for all the cases of TNB network, RMSE and MAE gives a maximum error of 0.36 (LLLGF at 10Ω). A comparison on the results of fault distance identified with and without voltage sag estimation is provided in section 6.6.5. The overall performance of voltage sag estimation for SaskPower network is given in Table 6.13.

Table 6.13 Test Results of database prediction - SaskPower Network

Fault type	Performance of SVR	Fault Resistance		
		10Ω	30Ω	50Ω
SLGF	*R*	0.9518	0.9287	0.9398
	RMSE	0.0112	0.0033	0.3079
	MAE	0.0073	0.0032	0.3077
LLF	*R*	0.9148	0.8936	0.8993
	RMSE	0.0841	0.2375	0.1095
	MAE	0.0839	0.2374	0.1093
DLGF	*R*	0.9129	0.9594	0.9538
	RMSE	0.0077	0.1480	0.1835
	MAE	0.0077	0.1480	0.1834
LLLGF	*R*	0.8936	0.8874	0.9221
	RMSE	0.2672	0.2207	0.1460
	MAE	0.2672	0.2206	0.1457

6.4.2 Reduction in Database Size

SVR estimates the voltage sag data which were not simulated. The estimation reduces reduces the space required to store huge information. Table 6.14 and

Table 6.15 shows the database size identified without voltage sag estimation and considering voltage sag estimation for TNB and SaskPower network. If the voltage sag is identified without estimation, the simulation has to be done for fault resistances of 0Ω, 10Ω, 20Ω, 30Ω, 40Ω, 50Ω and 60Ω. For fault at 40 nodes (TNB network) and for 9 different fault resistances, a total of 280x2 matrix data were created for each fault type. If the voltage sag is estimated using SVR, simulation is needed for fault resistances of 0Ω, 20Ω, 40Ω and 60Ω. A total of only 160x2 matrix data were created for each fault type. Thus, estimating the voltage sag saves the database size by 42.86%.

Table 6.14 Database size with and without voltage sag estimation - TNB Network

Types of fault	Without voltage sag estimation	With voltage sag estimation	Storage saving in percentage
SLGF	280x2 matrix	160x2 matrix	42.86%
LLF	280x2 matrix	160x2 matrix	42.86%
DLGF	280x2 matrix	160x2 matrix	42.86%
LLLGF	280x2 matrix	160x2 matrix	42.86%

Table 6.15 Database size with and without voltage sag estimation-SaskPower Network

Types of fault	Without voltage sag estimation	With voltage sag estimation	Storage saving in percentage
SLGF	147x2 matrix	84x2 matrix	42.86%
LLF	147x2 matrix	84x2 matrix	42.86%
DLGF	147x2 matrix	84x2 matrix	42.86%
LLLGF	147x2 matrix	84x2 matrix	42.86%

6.4.3 Reduction in Simulation Time

Estimation of voltage sag data using SVR also reduces the simulation time. Simulation of voltage sag data for fault at all nodes was done using PSCAD software. Voltage sag data which were not simulated using PSCAD were estimated using SVR. The time taken per node by PSCAD simulation and estimation using SVR is shown in Table 6.16 (TNB network) and Table 6.17 (SaskPower network). It can be noticed that SVR requires less computation time compared to PSCAD simulation. Furthermore, in PSCAD, fault condition has to be created at all nodes, which need manual effort, while SVR does not require any such manual effort.

Table 6.16 Time taken for PSCAD simulation and SVR estimation -TNB network

Type of fault	PSCAD simulation	SVR estimation	Percentage reduction in simulation time
	Time (sec)	Time(sec)	
SLGF	15	8.75	41.67 %
LLF	15	8.75	41.67 %
DLGF	15	8.75	41.67 %
LLLGF	15	8.75	41.67 %

Table 6.17 Time taken for PSCAD simulation and SVR estimation -SaskPower network

Type of fault	PSCAD simulation	SVR estimation	Percentage reduction in simulation time
	Time (sec)	Time(sec)	
SLGF	9.2	4.96	46.09 %
LLF	9.2	4.96	46.09 %
DLGF	9.2	4.96	46.09 %
LLLGF	9.2	4.96	46.09 %

6.5 Test on Ranking Process

Ranking performance was tested for faults at the midpoint of the line section. For training purpose, simulations were performed for fault at the nodes of the distribution system at 0Ω, 20Ω, 40Ω and 60Ω resistance. Ranking results using 2D analysis and 3D analysis are given in section 6.5.1 and section 6.5.2.

6.5.1 Ranking in 2D Analysis

The ranking in 2D analysis was performed for fault simulations on actual distribution networks from Malaysia and Canada. The performance results are given in section 6.5.1.1 and section 6.5.1.2.

6.5.1.1 Ranking in TNB Network

The total number of sections found correctly at various ranks at 0Ω is illustrated in Figure 6.28. For 0Ω fault resistance, almost 30 to 31 sections are identified in the first rank. A minimum of 1 section is identified in rank 3 for SLGF, DLGF and LLLGF. However, all faulty sections are successfully located and more than half of the sections are obtained at rank 1. Also, all possible faulty sections are identified in the first 3 ranking.

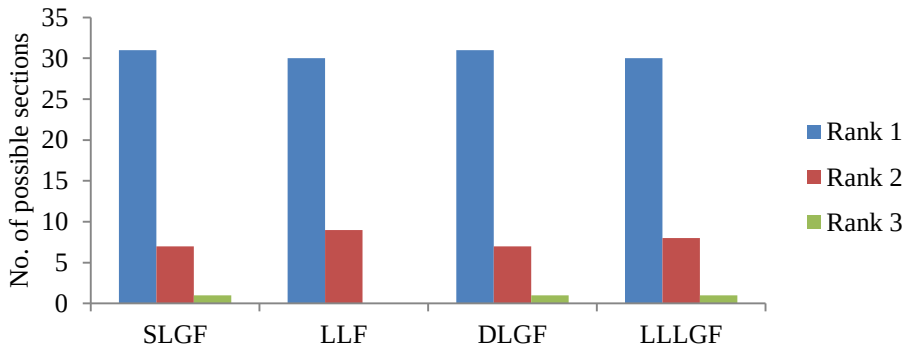

Figure 6.28 Ranking performance at 0Ω - TNB Network

Test cases were analyzed for other fault resistances of 5Ω, 25Ω and 45Ω. The result of test section 9-10 and section 15-16 for SLGF was analyzed in detail and the complete results are provided in Table 6.18.

Table 6.18 Possible fault location candidates for SLGF

Test Section	Fault Resistance	Possible faulty sections	Shortest distance	Rank Number
9-10	5	18	0.005372	1
		17	0.005983	2
		16	0.006418	3
		8	0.008223	4
		13	0.008369	5
		9 (9-10 node)	**0.009052**	**6**
9-10	25	8	0.000009	1
		15	0.00004	2
		13	0.000042	3
		19	0.000046	4
		9 (9-10 node)	**0.000071**	**5**
9-10	45	19	0.000002	1
		16	0.000007	2
		9 (9-10 node)	**0.000009**	**3**
15-16	5	1	0.00116	1
		20	0.002707	2
		19	0.006061	3
		16	0.00609	4
		15	0.006109	5
		18 (15-16 node)	**0.006111**	**6**
15-16	25	7	0.000024	1
		12	0.000039	2
		6	0.00005	3
		18 (15-16 node)	0.000062	4
15-16	45	**18 (15-16 node)**	**0.000008**	**1**

From the results above, the rank number of sections 9-10 and 15-16 at 5Ω is at the sixth position of the possible faulty sections. This rank corresponds to the mismatch value shown in shortest distance (column 4) which is the sixth lowest. Other possible sections were selected mainly due to the effect of fault resistance. These fault resistances cause the selection area of the possible sections to overlap with the selection area of sections 9-10 and 15-16.

The overall ranking performance of the proposed method for 45Ω resistance is shown in Figure 6.29. The x-axis represents the ranking and the y-axis represents the number of sections identified in the ranking. Ranking process was tested for all 39 sections by creating fault at the midpoint of the section. The results were analyzed for SLGF, LLF, DLGF and LLLGF. A maximum of 19 sections are identified using SLGF, 13 sections for LLF, 18 sections for DLGF and 4 sections for LLLGF. All of the sections are ranked within first seven ranking. Also it can be noticed that most of the sections are identified within first two rankings.

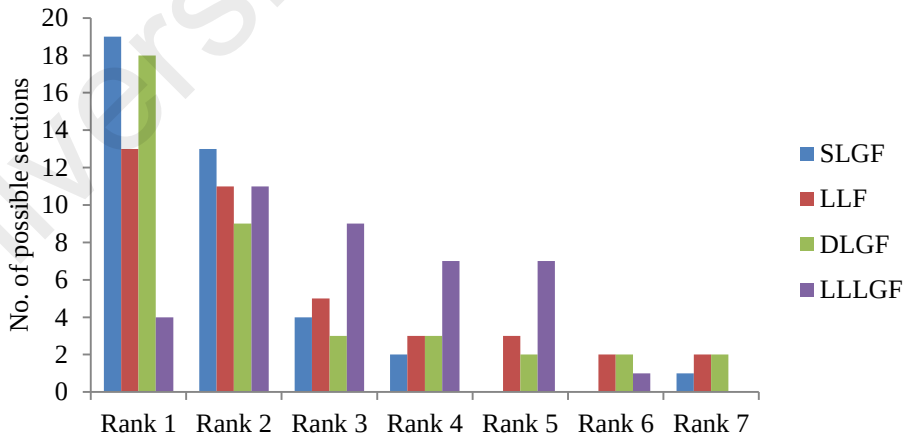

Figure 6.29 Ranking performance at 45Ω - TNB Network

6.5.1.2 Ranking in SaskPower Network

The overall ranking performance of the proposed method at 0Ω resistance is shown in Figure 6.30. Most of the faulty section performance can be detected in the first and

second ranks. The test sections found in the first rank is for SLGF (16 sections), followed by LLF, DLGF and LLLGF (13 sections). The test sections found in the second rank is for LLF (6 sections), followed by DLGF (5 sections) and then SLGF and LLLGF with 3 sections. The remaining faulty sections have rankings up to the fourth rank. Generally, the results show that all of the section can be determined.

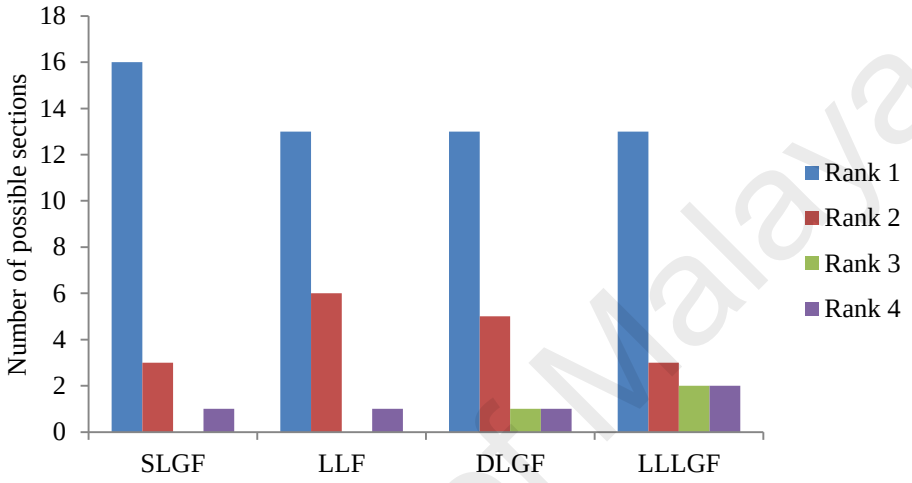

Figure 6.30 Ranking performance at 0Ω - SaskPower Network

Fault was simulated at 0.6035 km from node 1 of the test section 1-2 (SaskPower Network). The possible faulty sections and rank number of the section for various fault resistances of 0Ω, 5Ω, 25Ω and 45Ω are presented in Table 6.19. For sections 1-2, the method selected only one possible faulty section. In addition, the selected section for each tested resistance was also the correct faulty section. Only one section was selected because section 1-2 is not in parallel to any other section.

Table 6.19 Ranking for different fault resistances at midpoint of section1-2

		Rank Number			
Fault Resistance (Ω)	Possible faulty sections	SLGF	LLF	DLGF	LLLGF
0	1-2	1	1	1	1
5	1-2	1	1	1	1
25	1-2	1	1	1	1
45	1-2	1	1	1	1

The overall ranking performance is analyzed for fault at the midpoint of all the line sections and the test results of the proposed method are shown in Figure 6.31(a), (b), (c) and (d). The x-axis represents the fault resistance and the y-axis represents the number of sections identified in the ranking. Ranking process was tested for all 20 line sections by creating fault at the midpoint of the section. Generally, it can be shown that almost 6 to 11 of the sections are identified in the first rank for fault resistance of 5Ω. For other fault resistances of 25Ω and 45Ω, almost 6 to 8 sections are identified in the first rank for all fault types. When analyzed with 0Ω resistance, it can be noted that almost 13 to 16 sections are identified in Rank 1. This is due to for lower fault resistances, the voltage sag during fault deviates much from the pre-fault voltage while when the fault resistance increases, voltage sag is very close to the pre-fault voltage. Hence, the possibility of identifying the faulty section at rank 1 is higher for 0Ω resistance.

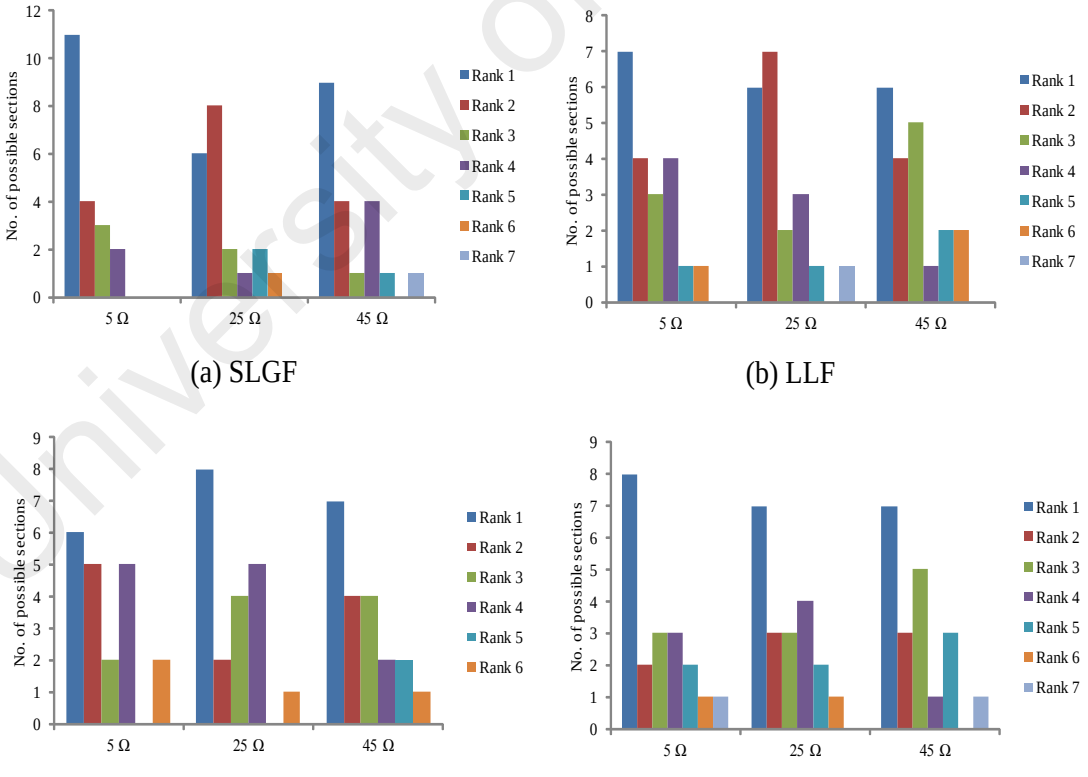

(a) SLGF (b) LLF

(c) DLGF (d) LLLGF

Figure 6.31 Ranking Performance on SaskPower Network in 2D analysis (a) SLGF, (b) LLF, (c) DLGF and (d) LLLGF

From the results, the rank number of section 11 for nodes between 6 to 12 is at the sixth position of the possible faulty sections for SLGF at 25Ω resistance. The possible faulty sections identified for this case are between nodes 6-7, 6-12, 15-16, 15-17, 18-19 and 18-20. The other possible sections were selected mainly due to the effect of fault resistance. These fault resistances cause the selection area of the possible sections to overlap with the selection area of sections. Thus, the actual section was ranked along with other possible sections.

From the result in Figure 6.31, most of the test sections found in the first rank are for SLGF with fault resistance 5 ohm (11 sections), followed by DLGF at 25Ω and LLLGF at 5Ω (8 sections). The faulty section performances of SLGF, LLF, DLGF and LLLGF have various rankings up to the seventh rank. Generally, the result shows that all of the section can be determined.

6.5.2 Ranking in 3D Analysis

The ranking in 3D analysis was performed for fault simulations on Malaysian (TNB) and Canadian (SaskPower) distribution networks. The performance results are given in section 6.5.2.1 and section 6.5.2.2.

6.5.2.1 Ranking in TNB Network

The ranking was also carried out for fault at mid-point of selected line sections; 1-2, 4-5, 9-10 nodes (Main at feeder1), 13-14 nodes (Branch at feeder1), 15-16 nodes (Sub branch at feeder1), 27-28 nodes (Branch at feeder2) and 36-37 nodes (Main at feeder2). Table 6.20 shows the calculated ranking results of selected faulty sections at 10Ω resistance.

Table 6.20 Ranking performance at 10 Ω resistance-3D analysis

Section Number	Test Section	Rank Number of the Actual Faulty Section			
		$SLGF_a$, $SLGF_b$, $SLGF_c$	LLF_{ab}, LLF_{bc}, LLF_{ca}	$DLGF_{ab}$, $DLGF_{bc}$, $DLGF_{ca}$	$LLLGF_{abc}$
1	1-2	1	1	1	1
4	4-5	4	6	2	2
9	9-10	4	6	2	2
13	13-14	5	1	7	2
18	15-16	1	1	1	1
27	27-28	2	3	6	6
36	36-37	6	1	6	7

The overall ranking performance is shown in Figure 6.32 to Figure 6.35. The x-axis represents the fault resistance and y-axis represents the number of sections identified. Figure 6.32 shows the ranking performance of $SLGF_a$, $SLGF_b$ and $SLGF_c$. The first rank is achieved in 9 sections at 10Ω resistance, 11 sections at 30Ω resistance and 8 sections at 50Ω resistance. All the sections are identified within seven ranking.

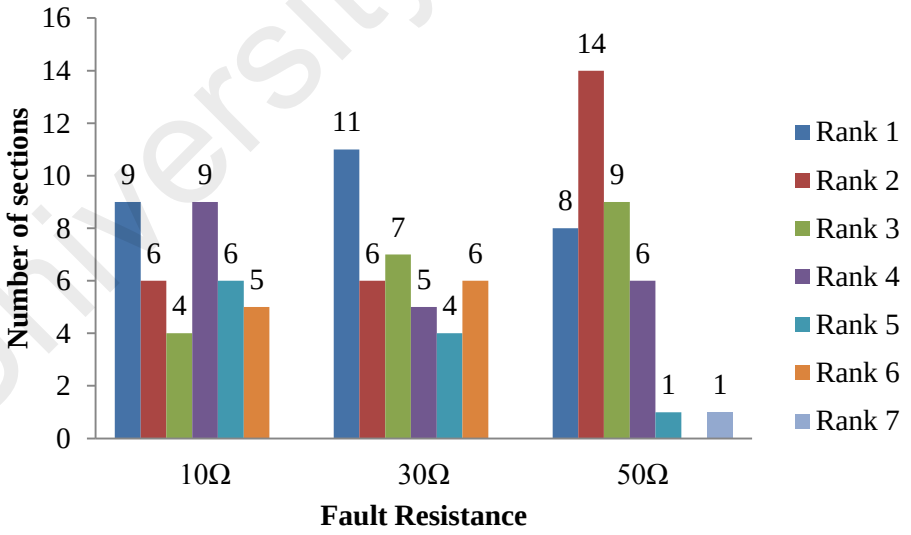

Figure 6.32 Ranking performance of $SLGF_a$, $SLGF_b$, $SLGF_c$-TNB network

Figure 6.33 shows the ranking performance of LLF_{ab}, LLF_{bc} and LLF_{ca}. The first rank is achieved in 13 sections at 10Ω resistance, 12 sections at 30Ω resistance and 7 sections at 50Ω resistance.

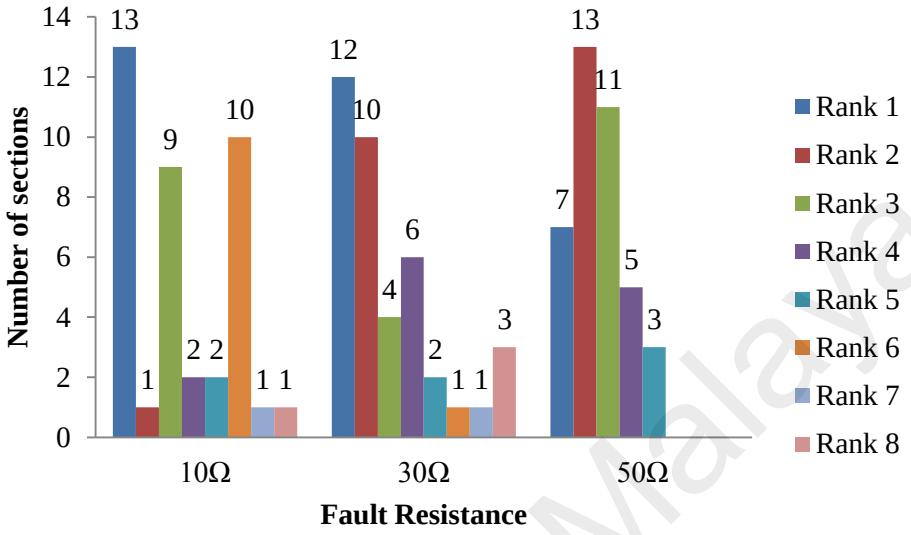

Figure 6.33 Ranking performance of LLF_{ab}, LLF_{bc}, LLF_{ca}-TNB network

Figure 6.34 shows the ranking performance of $DLGF_{ab}$, $DLGF_{bc}$ and $DLGF_{ca}$. A maximum of 16 sections are identified in first ranking at 50Ω resistance.

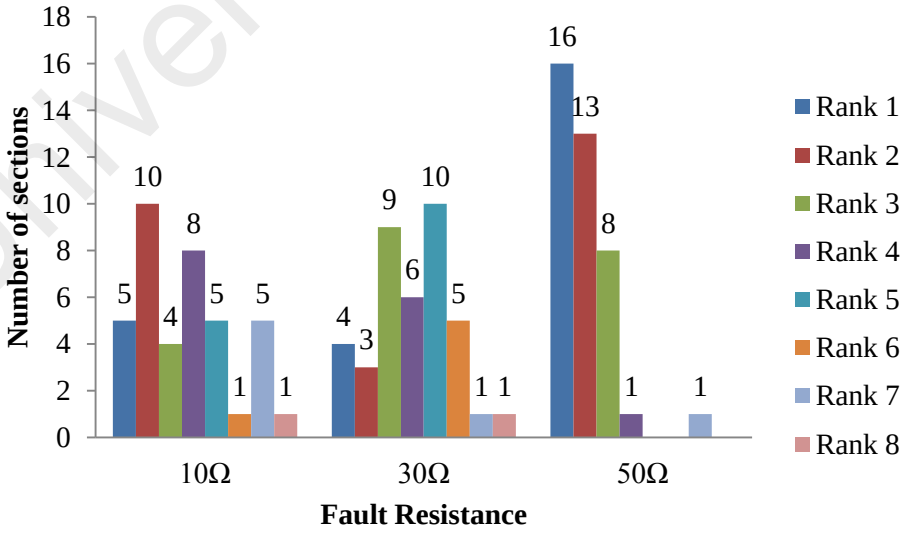

Figure 6.34 Ranking performance of $DLGF_{ab}$, $DLGF_{bc}$, $DLGF_{ca}$-TNB network

The ranking performance of $LLLGF_{abc}$ is given in Figure 6.35. A maximum of 13 sections are identified in second ranking (10Ω resistance), 10 sections in second ranking (30Ω resistance) and 11 sections in first ranking (50Ω resistance).

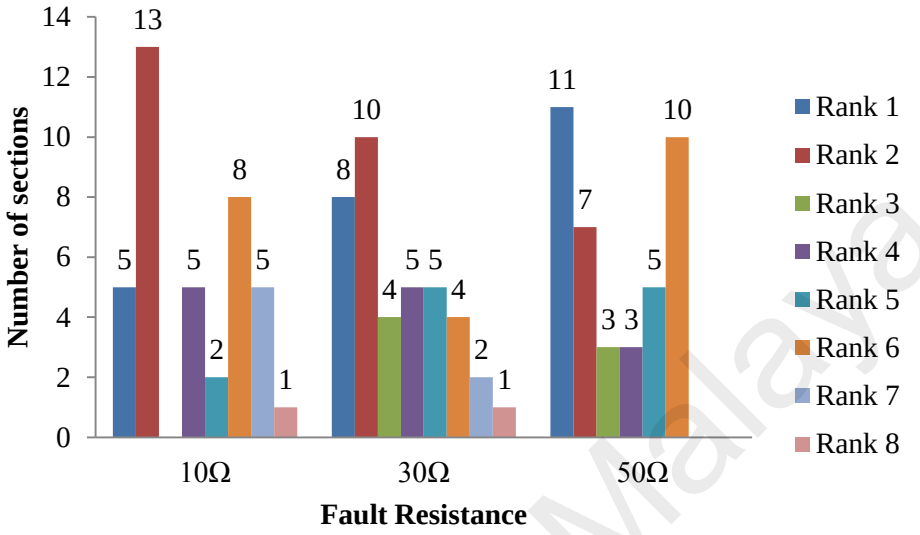

Figure 6.35 Ranking performance of $LLLGF_{abc}$-TNB network

It can be seen that most of the sections are ranked within the first six ranking and the maximum of rank 8 is obtained in some of the possible sections. The reason is the faulty section identification depends on the voltage sag database and is created with an interval of 20Ω resistance. In actual practice, the fault location has to be pin-pointed and the proposed method yields the possible sections in pin-pointing the exact fault location with a maximum of 8 possible faulty sections.

6.5.2.2 Ranking in SaskPower Network

The ranking was also carried out for fault at mid-point of selected line sections; 1-2, 7-8 nodes (Main at feeder), 13-14 nodes (Branch at feeder) and 18-20 nodes (Sub branch at feeder). Table 6.25 shows the calculated ranking results of selected faulty sections at 10Ω resistance. The test section 1-2 is completely radial line and does not overlap with any other line section. Hence, it can be identified in rank 1.

Table 6.21 Ranking performance at 10 Ω resistance-3D analysis

Section Number	Test Section	Rank Number of the Actual Faulty Section			
		$SLGF_a$, $SLGF_b$, $SLGF_c$	LLF_{ab}, LLF_{bc}, LLF_{ca}	$DLGF_{ab}$, $DLGF_{bc}$, $DLGF_{ca}$	$LLLGF_{abc}$
1	1-2	1	1	1	1
7	7-8	2	1	2	1
13	13-14	1	2	1	3
19	18-20	1	2	4	2

Overall, tests on SLGF at 10Ω, 30Ω and 50Ω resistance are shown in Figure 6.36. From the results, most of the test sections found in the first rank is for SLGF with fault resistance 10Ω (10 sections), 30Ω (10 sections) and 50Ω (9 sections). The faulty section performances of the remaining sections can be identified from rank 2 to rank 5. It can be noted that most of the faulty section performance can be detected in the first and second ranks for fault resistances of 10Ω, 30Ω, and 50Ω.

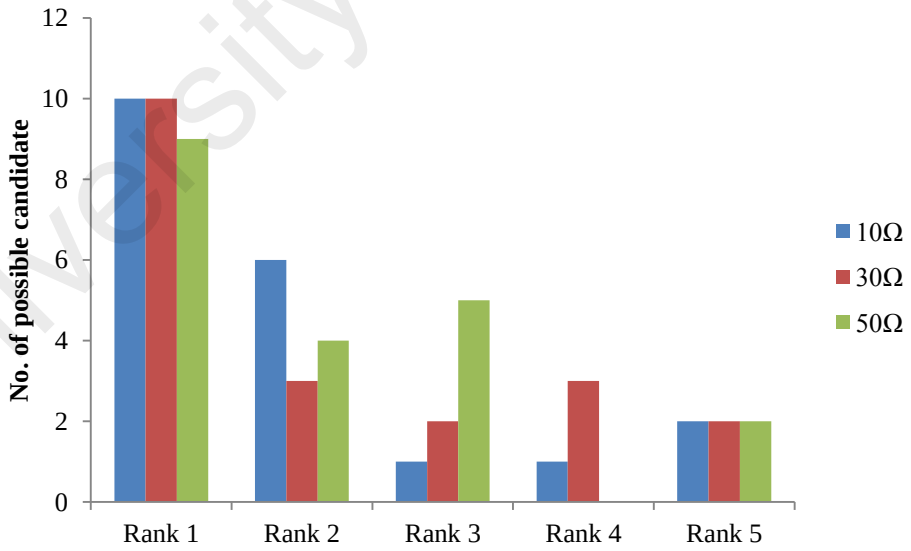

Figure 6.36 Ranking performance of $SLGF_a$, $SLGF_b$, $SLGF_c$-SaskPower network

The overall performance of LLF at 10Ω, 30Ω and 50Ω are shown in Figure 6.37. It shows that the maximum sections of 7 sections (10Ω), 11 sections (30Ω) and 11

sections (50Ω) are identified in first ranking. The remaining sections can be identified within six rankings.

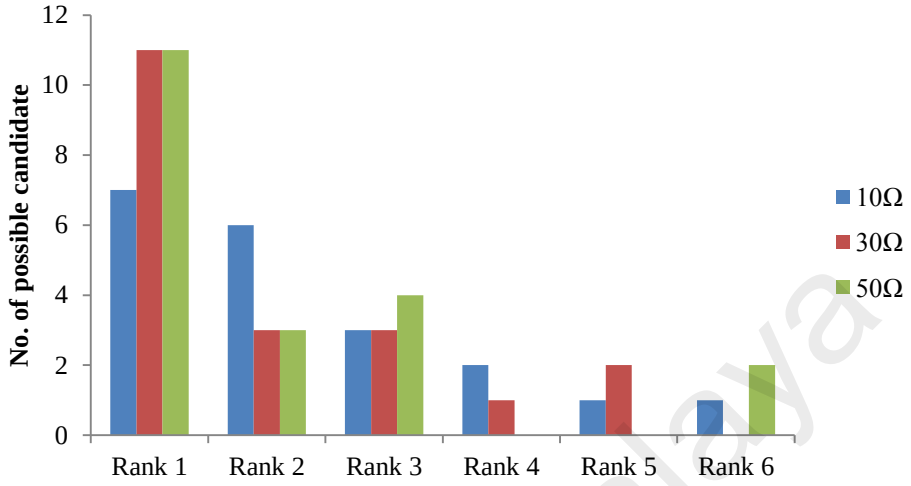

Figure 6.37 Ranking performance of LLF_{ab}, LLF_{bc}, LLF_{ca}- SaskPower network

The overall performance of DLGF is shown in Figure 6.38, which shows that a maximum of 16 sections are identified in rank 1 for DLGF at 50Ω resistance. At other resistances of 10Ω, 10 sections and at 30Ω, 8 sections are identified. All of the sections are ranked within six rankings.

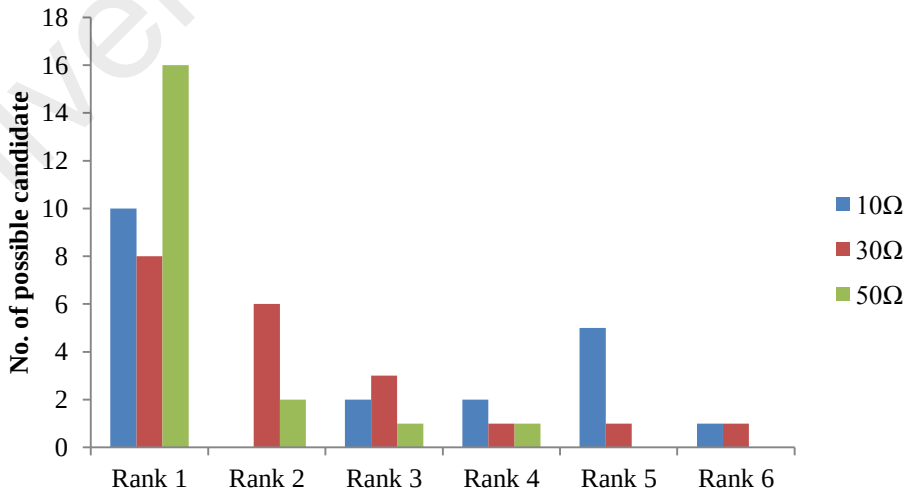

Figure 6.38 Ranking performance of $DLGF_{ab}$, $DLGF_{bc}$, $DLGF_{ca}$- SaskPower network

The ranking of LLLGF at 10, 30 and 50Ω resistances are shown in Figure 6.39. It can be noticed that most of the faulty sections are identified in Rank 1 (9 sections for 10Ω, 16 sections for 30Ω and 19 sections for 50Ω) A maximum of 5 sections are identified in rank 2 and rank 3 for SLGF.

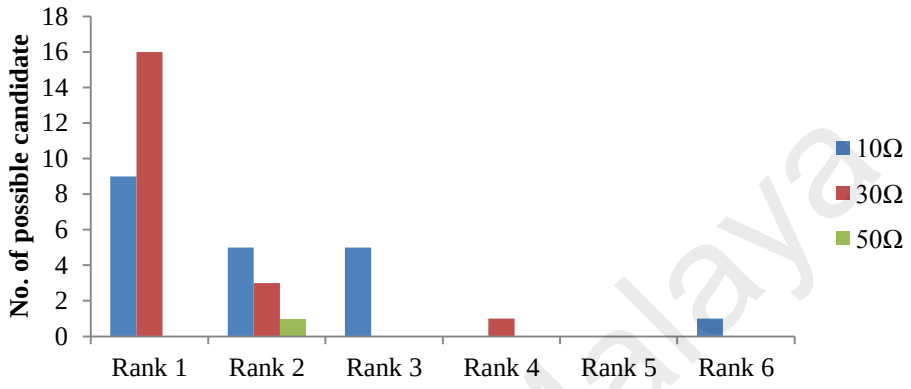

Figure 6.39 Ranking performance of $LLLGF_{abc}$ SaskPower network

The faulty section performances of SLGF, LLF, DLGF and LLLGF have various rankings up to the sixth rank. Most of the faulty section performance can be detected in the first ranks for fault resistances of 0Ω, 10Ω, 30Ω, and 50Ω. Other faulty sections can be determined in the second to sixth ranking. Generally, the result shows that all of the section can be determined within six ranking.

6.5.3 Comparison on Ranking Performance using 2D and 3D Analysis

A comparison using 2D and 3D analysis on the ranking performance is illustrated in this section. For analysis, ranking at the midpoint of section 9 (TNB Network) between nodes 9 and 10 is identified and tabulated in Table 6.22. Test results were also analyzed for various fault resistances of 0Ω, 10Ω, 30Ω and 50Ω respectively. The ranking at 0Ω resistance is almost the same when calculated using 2D and 3D analysis. For other fault resistance, it can be noticed that 3D analysis perform well in ranking the possible sections.

Table 6.22 Comparison on ranking using 2D and 3D analysis-TNB network

Fault type	Fault resistance (Ω)	Identified ranking using 2D analysis	Identified ranking using 3D analysis
SLGF	0	1	1
	10	6	4
	30	5	1
	50	3	3
LLF	0	1	1
	10	6	6
	30	6	5
	50	7	4
DLGF	0	1	1
	10	3	2
	30	6	5
	50	1	1
LLLGF	0	1	1
	10	4	2
	30	5	3
	50	4	1

A similar comparison of ranking using SaskPower distribution network for section 7-8 is calculated. The comparison table is given in Table 6.23.

Table 6.23 Comparison on ranking using 2D and 3D analysis -SaskPower network

Fault type	Fault resistance (Ω)	Identified ranking using 2D analysis	Identified ranking using 3D analysis
SLGF	0	1	1
	10	4	2
	30	4	1
	50	4	3
LLF	0	1	1
	10	4	1
	30	4	2
	50	7	3
DLGF	0	1	1
	10	2	2
	30	3	5
	50	3	1
LLLGF	0	1	1
	10	1	1
	30	3	1
	50	3	1

From the comparison results of SaskPower network, it can be noticed that 2D and 3D analysis perform well in ranking the possible sections. In the analyzed test case for section 7-8, the ranking using 3D analysis gives better ranking except DLGF at 30Ω. However, the advantage of ranking using 2D analysis use very minimal data compared to 3D analysis, where very few measurements are sufficient for ranking process.

6.6 Test on Fault Distance Calculation

The effect of fault resistance on the accuracy of the fault distance was also studied for all types of fault. The obtained results are based on two different methods; (a) Euclidean distance method, and (b) SVR. The percentage accuracy of fault distance estimation for SLGF, LLF, DLGF and LLLGF tests were discussed. The percentage error of fault distance can be estimated using

$$\%\ Error = \left| \frac{f_d^{(actual)} - f_d}{f_d} \right| \times 100 \tag{6.1}$$

where $f_d^{(actual)}$ is the actual fault distance and f_d is the calculated fault distance using proposed method.

6.6.1 Fault Distance using Euclidean Distance Approach

The fault distance calculation using Euclidean distance were performed for fault simulations on Malaysian and Canadian distribution networks. The fault distance was analyzed for resistances of 5Ω, 25Ω and 45Ω. The fault resistance values are chosen since the database is available for 0Ω, 10Ω, 20Ω, 30Ω, 40Ω, 50Ω and 60Ω. Here the voltage sag database for 0Ω, 20Ω, 40Ω and 60Ω are obtained through PSCAD simulation and the voltage sag database for 10Ω, 30Ω and 50Ω are estimated using SVM. The test results of voltage sag data analysis is given in section 6.4.

6.6.1.1 TNB Distribution Network

The calculated fault distance using Euclidean distance is shown in Figure 6.40 to Figure 6.42. The x-axis represents the faulty section and y-axis represents the percentage error of the calculated fault distance. Figure 6.40 shows the calculated fault distance for a fault resistance of 5Ω. A maximum percentage error of 33.2 is obtained for SLGF between nodes 38-39. The calculated fault distance is 0.1km whereas the actual distance is 0.15km. The absolute error is 0.05km/50 meter, which is a small length when compared with the distribution system of length 25.533km.

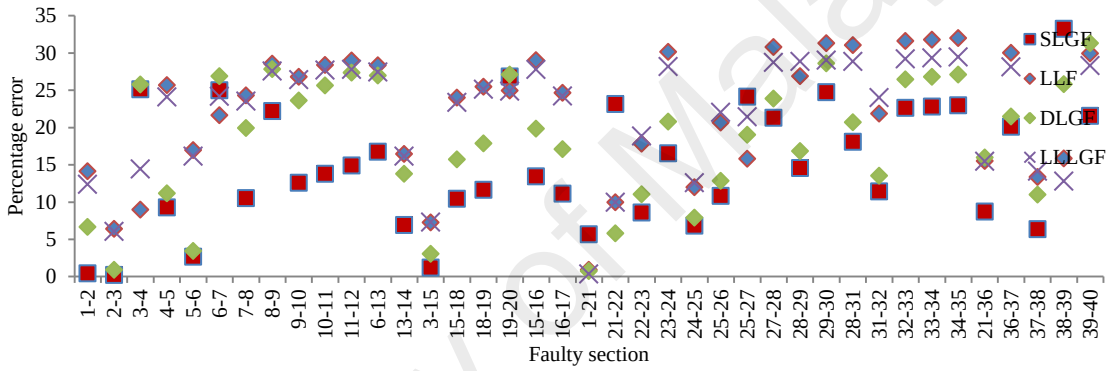

Figure 6.40 Calculated fault distance at 5Ω

The percentage error of fault distance calculated for a fault resistance of 25Ω is given in Figure 6.41. The calculated fault distance for DLGF has a higher percentage error of 30.37% between nodes 6-7. The remaining fault types have even lesser percentage error of fault distance.

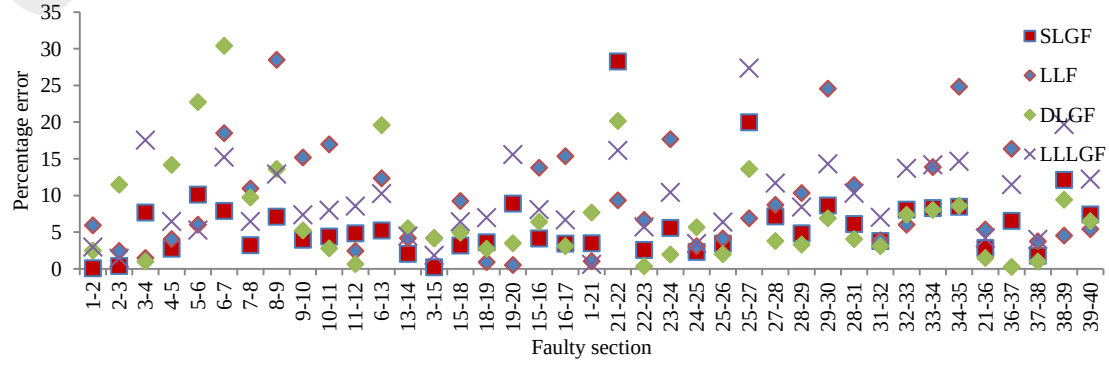

Figure 6.41 Calculated fault distance at 25Ω

The percentage error of fault distance calculated for a fault resistance of 45Ω is shown in Figure 6.42. The percentage error is higher between nodes 21-22 (30.5%) for LLF and lesser than 30.5% for other fault types.

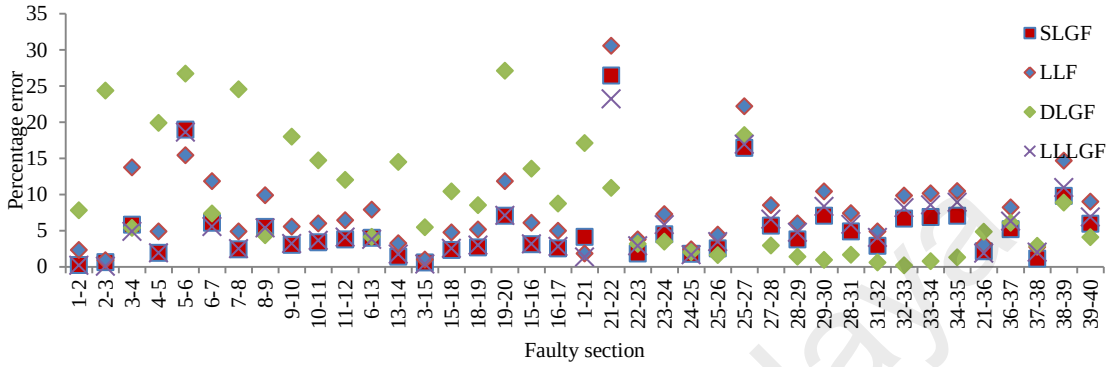

Figure 6.42 Calculated fault distance at 45Ω

Overall, it can be identified that the proposed method gives a maximum percentage error of 33.2% in the analyzed test cases. The test results are less deviating, when compared to the actual fault distance and thus the proposed method is proved to be accurate.

6.6.1.2 SaskPower Distribution Network

The fault distance test results for some of the test section (1-2, 7-8, 13-14 and 18-20) of SaskPower network were analyzed using Euclidean distance approach. The test cases are repeated for fault resistance of 5Ω, 25Ω and 45Ω respectively. Table 6.24 gives the actual and calculated fault distance for SLGF, LLF, DLGF and LLLGF. It can be noticed that the calculated fault distance is closer to the actual fault distance in all the test cases. A maximum absolute error of 0.25km is obtained in DLGF (section 19) at 45Ω resistance. Hence the percentage error within section 19 is 16.12%. All other faulty sections have even lesser percentage error.

Table 6.24 Fault distance using Euclidean distance approach

Fault Type	Section Number	Test Section	Actual fault distance (km)	Calculated fault distance (km)		
				5 Ω	25 Ω	45 Ω
SLGF	1	1–2	1.207	1.056	1.198	1.093
	7	7–8	2.575	2.698	2.731	2.433
	13	13–14	1.207	1.003	1.138	1.267
	19	18–20	1.6095	1.463	1.563	1.735
LLF	1	1–2	1.207	1.126	1.198	1.321
	7	7–8	2.575	2.479	2.383	2.611
	13	13–14	1.207	1.329	1.407	1.193
	19	18–20	1.6095	1.518	1.729	1.416
DLGF	1	1–2	1.207	1.362	1.177	1.004
	7	7–8	2.575	2.655	2.587	2.621
	13	13–14	1.207	1.182	1.256	1.238
	19	18–20	1.6095	1.806	1.854	1.869
LLLGF	1	1–2	1.207	1.275	1.001	1.068
	7	7–8	2.575	2.559	2.497	2.638
	13	13–14	1.207	1.267	1.282	1.367
	19	18–20	1.6095	1.625	1.773	1.698

6.6.2 Fault Distance using SVR in 2D Analysis

The fault distance calculation using 2D analysis of SVR were performed for fault simulations on Malaysian and Canadian distribution networks. The performance results are given in section 6.6.2.1 and section 6.6.2.2.

6.6.2.1 TNB Distribution Network

From Appendix C.1, it can be seen that when a zero ohm fault resistance was applied, the smallest fault distance error was achieved for all types of fault. The test results of fault distance for other fault resistance of 5Ω, 25Ω and 45Ω by using SVR are given in Table 6.25. For analysis sections 1-2, 4-5, 9-10, 13-14, 15-16, 27-28 and 36-37 are considered. Generally, it can be seen that the highest fault distance estimation error by using SVR occurs on test section 1-2 on all fault types. Section 1-2 has a maximum error percentage of 17.4% for SLGF in 2D analysis. It can be noted that the actual fault distance is 0.25km while the calculated fault distance is 0.2935km. The difference

between the actual and the calculated fault distance is 43.5 meters, which is a small distance compared to the whole distribution system. All other calculated fault distances have lower percentage error than section 1-2 of SLGF at 5Ω resistance.

Table 6.25 Fault distance of SLGF -TNB Network

Section number	Test section	Actual fault distance (km)	Calculated fault distance (km)		
			5 Ω	25 Ω	45 Ω
1	1-2	0.25	0.2935	0.2500	0.25001
4	4-5	0.2	0.2147	0.2000	0.200001
9	9-10	0.25	0.2579	0.2500	0.250001
13	13-14	0.375	0.3965	0.3751	0.375001
18	15-16	0.1975	0.2053	0.1975	0.197501
27	27-28	0.25	0.2538	0.2500	0.250001
36	36-37	0.2365	0.2429	0.2365	0.236501

6.6.2.2 SaskPower Distribution Network

For fault distance calculation, the test results were analyzed using various kernel functions such as polyhomog, multiquadric and RBF functions. Table 6.26 shows the results of fault at the midpoint of line section 7-8 at a distance of 2.575km for various fault type and resistances. From the test results, it can be noted that the RBF kernel yields more accurate results compared to other kernel functions.

Table 6.26 Fault distance calculation at line section 7-8

Fault type	Fault resistance (Ω)	Calculated fault distance (km)		
		Polyhomog kernel	Multiquadric kernel	RBF kernel
SLGF	5	2.014	2.851	2.576
	25	1.743	3.025	2.568
	45	2.799	3.168	2.545
LLF	5	2.209	2.396	2.575
	25	2.347	2.796	2.575
	45	3.095	3.142	2.575
DLGF	5	1.673	3.100	2.577
	25	2.579	3.142	2.604
	45	2.987	2.122	2.570
LLLGF	5	1.960	2.836	2.575
	25	3.524	2.800	2.575
	45	2.631	2.769	2.575

The test results of fault distance for some of the test section (1-2, 7-8, 13-14 and 18-20) were analyzed using SVR and are given in Table 6.27. It can be noticed that the calculated fault distance is closer to the actual distance in the analyzed test cases.

Table 6.27 Fault distance of SLGF -SaskPower Network

Section number	Test section	Actual fault distance (km)	Calculated fault distance (km)		
			5 Ω	25 Ω	45 Ω
1	1–2	1.207	1.158	1.363	1.2070
7	7–8	2.575	2.575	2.578	2.516
13	13–14	1.207	1.207	1.206	1.207
19	18–20	1.6095	1.6095	1.609501	1.612568

6.6.3 Fault Distance using SVR in 3D Analysis

The fault distance in 3D analysis was performed for fault simulations on Malaysian and Canadian distribution networks. The performance results are given in section 6.6.3.1 and section 6.6.3.2.

6.6.3.1 TNB Distribution Network

The fault distance was calculated using SVR analysis. The test cases were performed for fault at the midpoint of line section of TNB Network. Figure 6.43 shows the percentage error of fault distance for $SLGF_a$, $SLGF_b$ and $SLGF_c$ at resistances of 10Ω, 30Ω and 50Ω. The test results of fault distance for $SLGF_a$, $SLGF_b$ and $SLGF_c$ are the same because the voltage sag at phase a, phase b and phase c are just interchanged. A maximum percentage error of 35% is obtained for SLGF in section 3-15 for a fault resistance of 10Ω. The calculated fault distance is 0.419 km while the actual distance is 0.645 km. The absolute error is 0.226 km, which is small length compared to the whole distribution system. At 30 ohm resistance, SLGF has a maximum percentage error of 19% (section 3-15) and 6% at 50 Ω resistance (section 3-15).

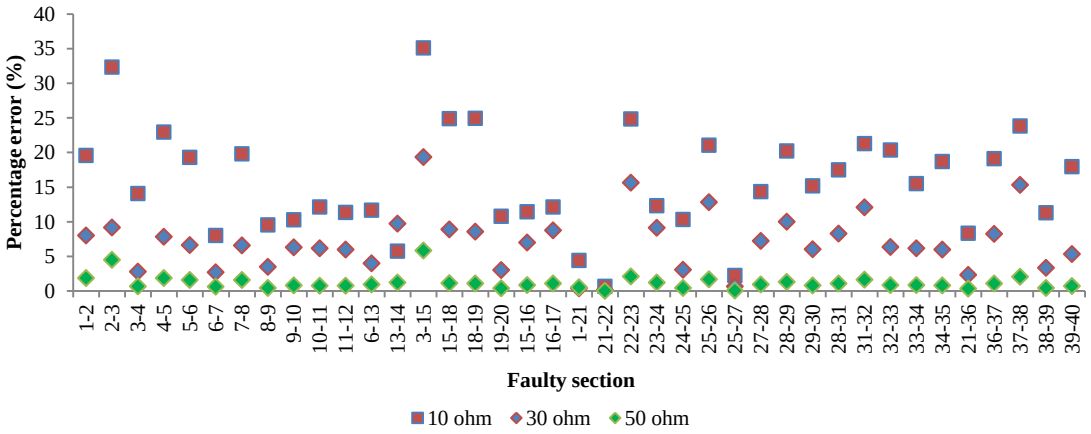

Figure 6.43 Calculated fault distance for $SLGF_a$/ $SLGF_b$/ $SLGF_c$-TNB Network

The percentage error of the calculated fault distance at LLF is shown in Figure 6.44. The maximum percentage error in LLF is obtained at section 1-21 for 10Ω, 30Ω and 50Ω fault resistance. 10Ω resistance has a maximum percentage error of 1.1%, 30Ω resistance has 0.85% and 50Ω resistance has a maximum of 0.13% percentage error.

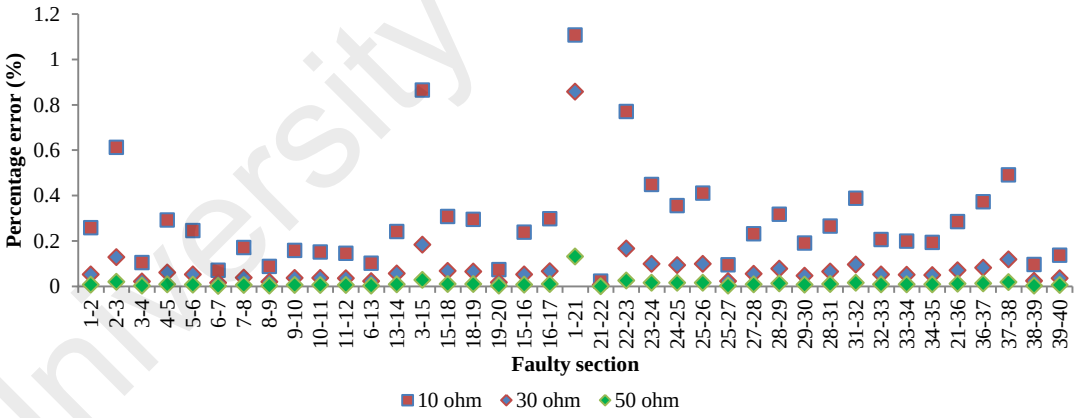

Figure 6.44 Calculated fault distance for LLF_{ab}/ LLF_{bc}/ LLF_{ca}-TNB Network

Figure 6.45 shows the percentage error of calculated fault distance for DLGF. The maximum percentage error of 10 Ω resistance is 30% (at section 2-3 and section 3-15), 30Ω resistance is 17.7% (section 3-15) and 50Ω resistance is 5% (section 3-15).

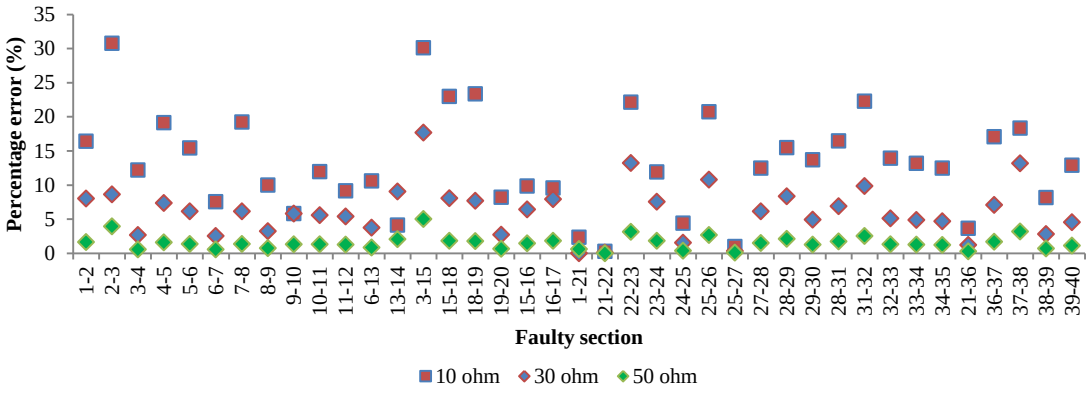

Figure 6.45 Calculated fault distance for $DLGF_{ab}$/ $DLGF_{bc}$/ $DLGF_{ca}$-TNB Network

Figure 6.46 shows the percentage error of calculated fault distance for LLLGF. The maximum percentage error is 0.095% at 10 Ω resistance (at section 1-21), 0.015% at 30Ω resistance (section 1-21) and 0.002% at 50Ω resistance (section 1-21). The percentage error of 50Ω resistance is less compared to 10Ω and 30Ω resistance. All other calculated fault distances have lower error percentage. Therefore, the proposed method has managed to identify the fault distance with greater accuracy.

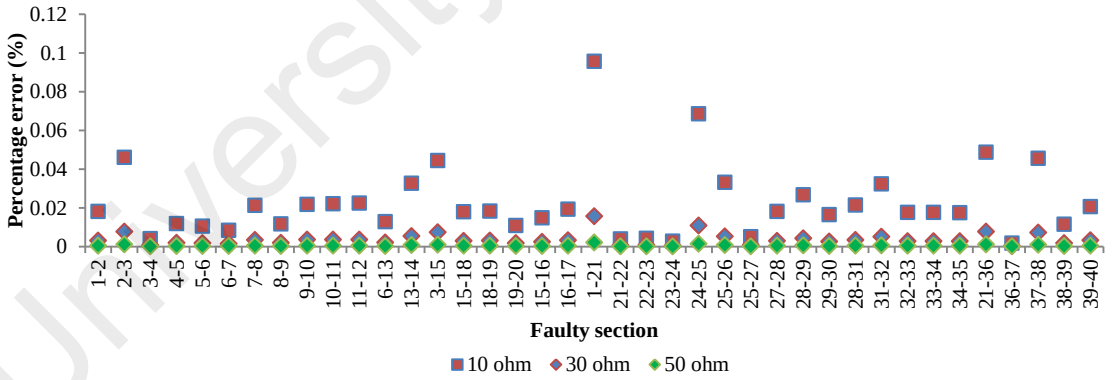

Figure 6.46 Calculated fault distance for $LLLGF_{abc}$-TNB Network

6.6.3.2 SaskPower Distribution Network

The fault distance was also analyzed using SaskPower distribution network for fault at the midpoint of line section. Figure 6.47 shows the percentage error of fault distance for $SLGF_a$, $SLGF_b$ and $SLGF_c$ at resistances of 10Ω, 30Ω and 50Ω. The test results of fault distance for $SLGF_a$, $SLGF_b$ and $SLGF_c$ are the same because the voltage sag at

phase a, phase b and phase c are just interchanged. A maximum percentage error of 24.7% is obtained in section 1-2 for a fault resistance of 10Ω. At 30 ohm resistance, SLGF has a maximum error of 7.32% (section 8-13) and 2.79% at 50 Ω resistance (section 8-13). The percentage error is also calculated for LLF_{ab}, LLF_{bc} and LLF_{ca} and is shown in Figure 6.48 and the percentage error for $DLGF_{ab}$, $DLGF_{bc}$ and $DLGF_{ca}$ is shown in Figure 6.49.

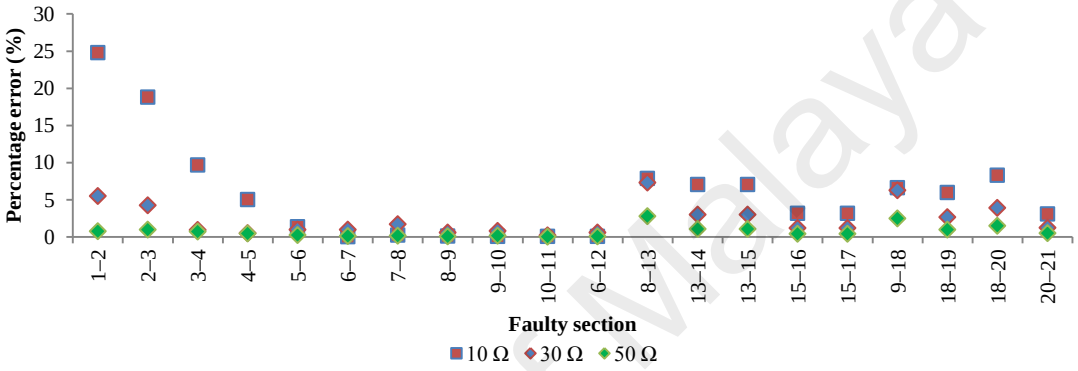

Figure 6.47 Calculated fault distance for $SLGF_a$/ $SLGF_b$/ $SLGF_c$-SaskPower network

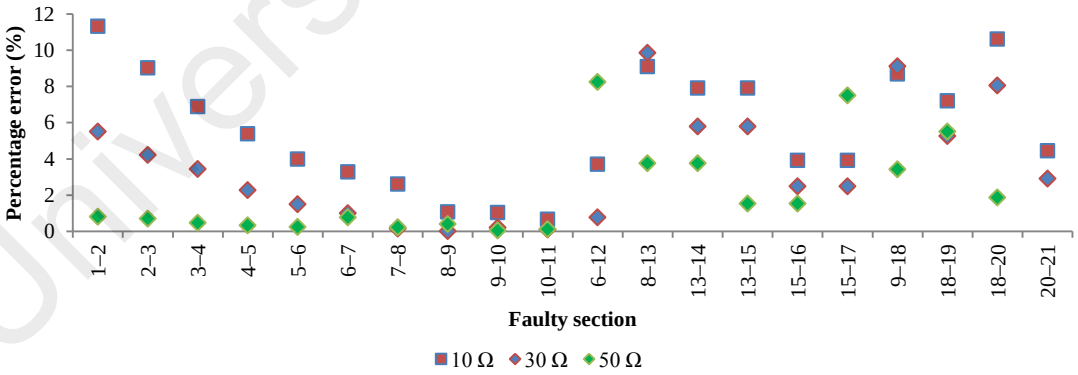

Figure 6.48 Calculated fault distance for LLF_{ab}/ LLF_{bc}/ LLF_{ca}-SaskPower network

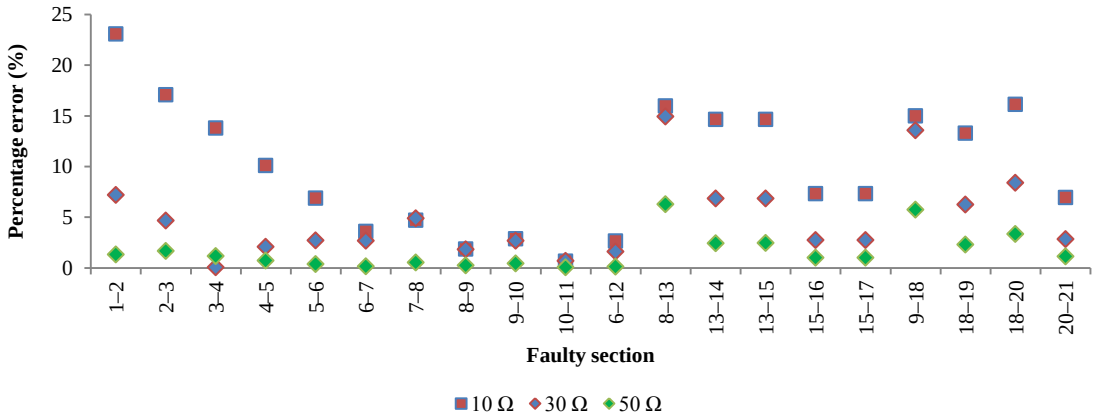

Figure 6.49 Calculated fault distance for $DLGF_{ab}$/ $DLGF_{bc}$/ $DLGF_{ca}$-SaskPower network

The percentage error for $LLLGF_{abc}$ is given in Figure 6.50. The maximum percentage error is 30% at 10 Ω resistance (at section 1-2). The reason is section 1-2 has higher voltage sag deviation compared to other sections.

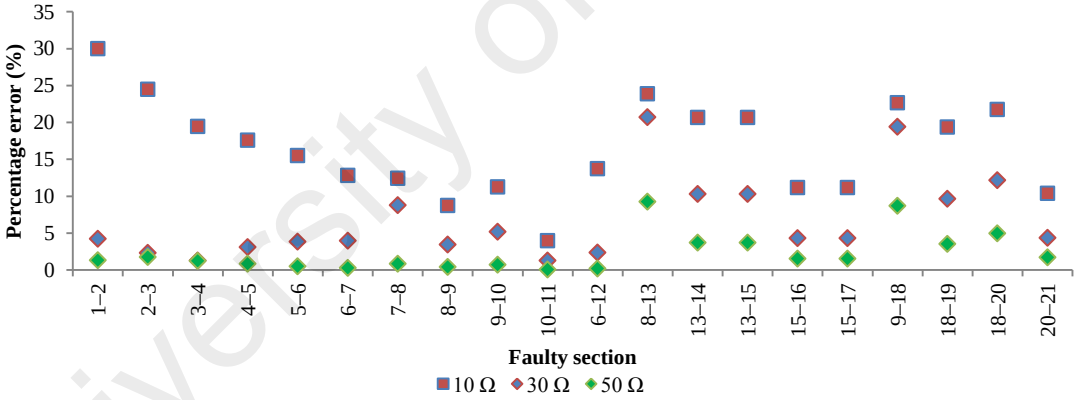

Figure 6.50 Calculated fault distance for $LLLGF_{abc}$-SaskPower network

The percentage error of fault distance at 50Ω resistance is less compared to 10Ω and 30Ω resistances. The reason is 50Ω resistance has lower voltage sag deviation compared to other fault resistance. Therefore, the proposed method has managed to identify the fault distance with greater accuracy.

6.6.4 Comparison of Fault Distance using Euclidean Distance and Trigonometric Approach

A comparison was made with the existing trigonometric method (Lilik Jamilatul Awalin et al., 2013) of fault location and the results are tabulated in Table 6.28. Test results were analyzed for fault distance of 0.25 km between nodes 9 and 10 for fault resistance of 21, 23, 25, 27 and 29 Ω (TNB network).

Table 6.28 Comparison of fault distance with (Lilik Jamilatul Awalin et al., 2013)

Fault type	Fault resistance (Ω)	Existing Trigonometric method fault location (km)	Euclidean distance calculation (km)
SLGF	21	0.06180	0.22371
	23	0.18998	0.21928
	25	0.28992	0.26210
	27	0.37788	0.24051
	29	0.45677	0.23534
LLF	21	0.07369	0.22432
	23	0.17294	0.25847
	25	0.27351	0.21271
	27	0.37313	0.26863
	29	0.46289	0.23496
DLGF	21	0.05787	0.28338
	23	0.17584	0.23294
	25	0.27644	0.26340
	27	0.36719	0.21789
	29	0.44894	0.23176
LLLGF	21	0.09770	0.25563
	23	0.18814	0.23572
	25	0.26105	0.23160
	27	0.32543	0.26584
	29	0.43233	0.23418

For fault resistance of 25Ω, the fault distance calculation using the existing method is closer to the actual distance but for other fault resistances, the calculated distance is deviating much from the actual distance. This is because the existing method considers a linear line joining the minimum and maximum voltage sag data of a section (Figure 4.5). However, the proposed fault location considers the minimum and maximum

voltage sag data of each node in a section (Figure 4.17). Hence, the proposed method identified the fault distance closer to actual fault distance irrespective of fault resistances.

6.6.5 Comparison of Fault Distance between SVR estimation and PSCAD Simulation of Voltage Sag Data

A comparison was made with the fault distance identified considering voltage sag estimation using SVR and using PSCAD simulation in TNB Network. Test results were analyzed for fault at midpoint of line section (0.25 km) between nodes 9 and 10 for fault resistance of 25Ω. The results are tabulated in Table 6.29. The fault distance was identified using Euclidean distance approach. It can be noticed that the fault distance using 'SVR estimation of voltage sag data' is less deviated from the distance calculated using 'PSCAD simulation of voltage sag data'.

Table 6.29 Comparison of fault distance with voltage sag using SVR and PSCAD

Type of fault	Calculated fault distance (km) using Euclidean distance	
	SVR estimation of voltage sag data	PSCAD simulation of voltage sag data
SLGF	0.2721	0.2612
LLF	0.2196	0.2249
DLGF	0.2732	0.2891
LLLGF	0.2125	0.2346

6.6.6 Comparison of Fault Distance using 2D and 3D Analysis

A comparison using 2D and 3D analysis of SVR for fault distance calculation was carried out and the results are tabulated in Table 6.30. For analysis, fault at the midpoint of section 9 (TNB Network), a fault distance of 0.25 km between nodes 9 and 10 is identified and tabulated. Test results were also analyzed for various fault resistances of 10Ω, 30Ω and 50Ω respectively. It can be noticed that the calculated fault distance is closer to the actual fault distance in all cases. A maximum of 3.18% error is obtained

with 2D analysis of SVR for SLGF(10Ω resistance) and 10.3% error for 3D analysis of SVR. With 10.3% error, the calculated fault distance is 0.224229 and the absolute error is 25.8 meters. The 3D analysis of SVR for LLF and LLLGF gives lesser percentage error than 2D analysis of SVR. For SLGF and DLGF, 2D analysis of SVR gives lesser percentage error than 3D analysis. Hence both the methods (2D and 3D analysis) perform equally well in identifying the fault distance.

Table 6.30 Comparison of fault distance using 2D and 3D analysis of SVR - TNB network

Fault type	Fault resistance (Ω)	Calculated fault distance using 2D SVR (km)	Calculated fault distance using 3D SVR (km)
SLGF	0	0.252754	0.253031
	10	0.257944	0.224229
	30	0.250048	0.234162
	50	0.250001	0.247995
LLF	0	0.255131	0.252707
	10	0.251159	0.249605
	30	0.250182	0.249906
	50	0.250011	0.249985
DLGF	0	0.255654	0.254042
	10	0.251150	0.235474
	30	0.250283	0.235446
	50	0.250046	0.246659
LLLGF	0	0.256331	0.255340
	10	0.251875	0.250054
	30	0.250030	0.250008
	50	0.250002	0.250001

A similar comparison using SaskPower distribution network for section 7-8 at an actual fault distance of 2.575 km is calculated. The comparison table is given in Table 6.31. The maximum error of 17.4% is obtained with 3D analysis at LLLGF (10Ω). Also, from the comparison results, it can be noticed that 2D and 3D analysis perform equally well in identifying the fault distance. However, the fault distance using 2D analysis uses very minimal data and is sufficient for fault location.

Table 6.31 Comparison of fault distance with 2D and 3D analysis of SVR-SaskPower network

Fault type	Fault resistance (Ω)	Calculated fault distance using 2D SVR (km)	Calculated fault distance using 3D SVR (km)
SLGF	0	2.598596	2.59918
	10	2.585004	2.581913
	30	2.578924	2.618793
	50	2.575101	2.579557
LLF	0	2.60419	2.585018
	10	2.58605	2.507678
	30	2.58075	2.578915
	50	2.57505	2.594842
DLGF	0	2.604729	2.610853
	10	2.52849	2.69662
	30	2.641388	2.701517
	50	2.57500	2.588994
LLLGF	0	2.599408	2.628671
	10	2.57699	3.023883
	30	2.57559	2.801106
	50	2.57500	2.596798

6.6.7 Comparison of Fault Distance with ANN, Deep Neural Network (DNN) and kriging methods

Comparison of the proposed fault distance with ANN, DNN and Kriging was carried out to show the performance of proposed method in TNB network (3D analysis). For the analysis of the results, a line section between nodes 9-10 is considered. A fault was created at the mid-point of line section at a distance of 0.25km. The test results are analyzed for 3D data at various resistances of 10Ω, 30Ω and 50Ω. The structure of ANN and DNN uses sigmoid as the activation function with two hidden layers, 30 hidden nodes in first layer and 12 hidden nodes in second layer. ANN was trained for a maximum iteration (epoch) of 100 and mean square error (mse) of $1x10^{-12}$. The training performance for single line to ground fault at 30Ω resistance is shown in Figure 6.51. It

can be seen that the best training performance is obtained with mse of $3.07x10^{-15}$ at epoch 28.

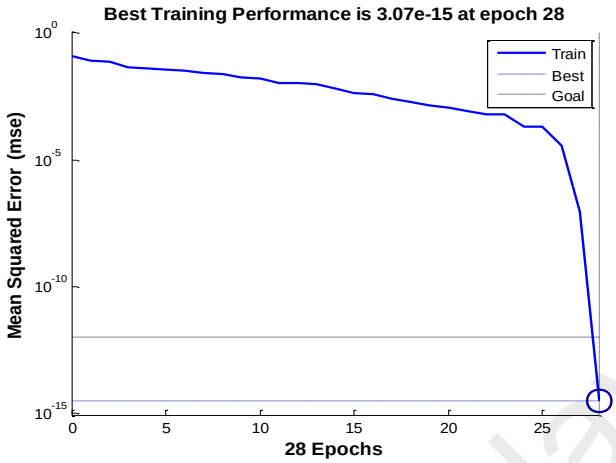

Figure 6.51 Training performance using ANN

Comparison results of fault distance using SVR, ANN, DNN and Kriging are shown in Table 6.32. SVR and DNN have the maximum absolute error of 2.5% and 2.9% ($SLGF_a$, $SLGF_b$, $SLGF_c$) at 10Ω resistance. A maximum percentage error of 4.6% and 3.9% is obtained using ANN and Kriging ($DLGF_{ab}$, $DLGF_{bc}$ and $DLGF_{ca}$) at 50Ω resistance. Thus it can be noticed that the absolute error using SVR gives better accuracy than ANN, DNN and kriging methods.

Table 6.32 Comparison of proposed fault distance with ANN, DNN and Kriging

Type of fault	Fault Resistance (Ω)	Fault Distance (Absolute Error %)			
		SVR	ANN	DNN	Kriging
$SLGF_a$, $SLGF_b$, $SLGF_c$	10	2.5771	3.2926	2.913	2.5362
	30	1.1481	1.5838	1.409	1.1524
	50	0.2005	4.7177	0.685	1.8541
LLF_{ab}, LLF_{bc}, LLF_{ca}	10	0.0395	3.9634	1.812	0.5183
	30	0.0093	3.1169	1.044	2.4235
	50	0.0015	0.8389	0.278	1.5241
$DLGF_{ab}$, $DLGF_{bc}$, $DLGF_{ca}$	10	1.4526	1.7379	1.646	1.8514
	30	1.0554	2.7527	1.08	1.9752
	50	0.3341	4.6895	0.581	3.9352
$LLLGF_{abc}$	10	0.0055	0.1599	0.0049	0.241
	30	0.0009	2.5427	1.5868	0.1103
	50	0.0001	4.6406	2.8238	0.1039

6.7 Summary

This chapter has presented the test results for various fault conditions such as considering fault resistance, fault type and various fault locations. The test results are summarized as follows:

- The first test is the identification of fault type. It can be noticed that fault type using 2D analysis is less accurate than 3D analysis of SVC. Also, 3D analysis gives 100% accurate results of all 10 fault types, which include the faulty phase while with 2D analysis, the faulty phase was not considered.
- The second test is fault resistance estimation using SVR. Calculations were done for all fault types using 2D and 3D analysis. Test results were analyzed for actual fault resistances of 10Ω, 30Ω and 50Ω. The calculated fault resistance is close to the actual fault resistance and the results are promising.
- The third test is on the process of estimating voltage sag data using SVR. Calculations were done for all types of fault and the performance was evaluated using Regression, Root Mean Square Error and Mean Absolute Error. Fault distance was also calculated using the estimated voltage sag data and the results were found to be successful.
- The fourth set of test was done for selecting the faulty section and also ranking using matching approach. If the test section is in parallel with other sections, the number of possible sections will also increase. Higher fault resistance values also cause the voltage seen at the monitored node to be a nominal voltage. This narrowed the selection intervals of the section; hence the method identifies the correct possible faulty section within eight ranking.
- The fifth test is on fault location identification. Test results shows that the method is able to locate faults at any location along a line section. A comparison was also made with the existing method, which shows that the proposed method gives

reasonable accuracy than the previous method (Lilik Jamilatul Awalin et al., 2013). Also, comparison results were performed for fault distance identified using voltage sag estimation and PSCAD simulation; 2D and 3D analysis of SVR; and SVR with other regression methods such as ANN, DNN and Kriging.

From the observation of each test result, it can be concluded that all of the tested conditions influenced the performance of the proposed method. The accuracy of 3D analysis using SVC for fault type is higher than the 2D analysis. 2D and 3D analysis perform equally well for faulty section and fault distance calculation. However 2D analysis is more advantageous since it requires less input data compared to 3D analysis.

CHAPTER 7: CONCLUSION AND FUTURE WORK

7.1 Conclusion

To minimize the impact of faults and to improve service reliability in a distribution system, the faults need to be quickly and accurately identified. In this work, fault analysis was successfully performed on 40-bus test system of TNB, Malaysia and 21-bus test system of SaskPower, Canada. Although there are various methods for locating fault, estimation of database was not considered in the past. The database was created by simulation, which is time consuming. Therefore, in this work, a fault location method by using limited simulation of voltage sag data has been proposed for distribution systems. Also, none of research work focuses on finding the faulty phase, fault type, faulty section and fault distance of distribution system using SVM. The proposed method locates fault considering the faulty phase, fault type, faulty section and fault distance. The four main objectives of this research, outlined in chapter 1 have been fulfilled. The outcome of each objective is as follows.

The first objective is to establish a method to identify the fault type in distribution system using support vector classification analysis considering the faulty phase. The fault type can be identified using classification principle of SVM. The proposed method identifies fault type using 2D and 3D analysis of SVC. 2D analysis of SVC considers only the voltage sag phase and angle while 3D SVC considers the voltage sag magnitude at all three phases a, b and c. The 2D analysis identifies fault type of SLGF/LLF/DLGF/LLLGF and the details of SVC are given in section 4.6.1 and 3D analysis ($SLGF_a$, $SLGF_b$, $SLGF_c$, LLF_{ab}, LLF_{bc}, LLF_{ca}, $DLGF_{ab}$, $DLGF_{bc}$, $DLGF_{ca}$ and $LLLGF_{abc}$) is discussed in section 4.6.2. The test results were analyzed for two different networks (TNB and SaskPower) and presented in section 6.2.1 and section 6.2.2. It can be noticed that fault type using 2D analysis is less accurate than 3D analysis of SVC.

3D analysis gives 100% accurate results of all 10 fault types, which include the faulty phase. Whereas using 2D analysis, the faulty phase was not considered.

The second objective is to propose a method to estimate voltage sag data using support vector regression based on limited simulated data. Existing methods identify the possible faulty section and fault distance by matching the measured data with the simulated data in the database (Hazlie Mokhlis & Li, 2011). Also, artificial intelligent methods such as Fuzzy logic, ANN and SVM require database for training process. The methods depend on the stored database for locating fault. Hence, in this work, a method using limited simulation of voltage sag data is proposed for locating fault. The proposed method uses voltage sag data measured at primary substation. The establishment of voltage sag data is explained in chapter 5, section 5.2.1. Test results using voltage sag estimation are discussed in section 6.4. SVR was used for estimating the voltage sag database by training the voltage sag data at the nodes. Estimating the voltage sag data has managed to reduce the simulation time (41.67 % in TNB and 46.09 % in SaskPower network) and also helps in saving the database size by 42.86%.

The third objective is to estimate the fault distance using Euclidean approach and support vector regression analysis. a) A fault distance equation is formulated using Euclidean distance of voltage sag profile. The fault distance formulation produces a more accurate distance compared to the previous equation, especially for fault at different location and resistances, as explained in Chapter 4, section 4.8.1. The proposed algorithm works by identifying the possible faulty sections and its corresponding fault distances. A linear model of voltage sag profile between two adjacent nodes was considered. The voltage sag data at each node of a section were considered to find the fault distance. The test results are shown in section 6.6.1, in which a maximum percentage error of 33.2% for SLGF between nodes 38-39. The calculated fault distance

is 0.1km whereas the actual distance is 0.15km. The absolute error is 0.05km/50 meter, which is a small length when compared with the whole distribution system. Also the proposed method has shown improvement over the previous methods in locating different types of faults. Test result has been discussed in Chapter 6, section 6.6.6 for various fault resistance of 21, 23, 25, 27 and 29 Ω. In SLGF, the existing trigonometric method gives percentage error of 15.9% for 25Ω resistance whereas for other fault resistances the percentage error varies from 24% to 82%. The proposed method identifies fault distance with a percentage error varying from 3.8% to 12.3%. Thus the proposed method finds more accurate fault distance for all values of fault resistance. b) To estimate the fault distance using 2D and 3D analysis of SVR. The method identifies the possible faulty sections and its respective distance from the sending node. In 2D analysis, voltage sag magnitude and phase angle have been adopted to identify the faulty section. The matching approach has been used to select the possible faulty section. Although this method has been applied in the existing method (H Mokhlis et al., 2011), the proposed method formulates a new equation in ranking the faulty section. By doing this, all possible faulty sections can be checked according to the priority of the faulty section. The ranking process is explained in chapter 4, section 4.7.1 and the test results using 2D analysis are explained in section 6.5.1. The fault distance is identified for the possible faulty sections as per ranking. The test results of calculated fault distance are given in section 6.6.2. In 3D analysis of faulty section identification, the proposed formulation is discussed in section 4.7.2. The results at section 5.5.2 and section 5.6.2 show that most of the faulty sections were identified correctly in the first attempt for 0Ω resistance. Also, test cases for various other fault resistances of 10Ω, 30Ω and 50Ω resistance are explained in section 6.5.2. The results show that most of the faulty sections were identified correctly within the first eight ranking. The fault distance for the possible faulty sections is discussed in section 6.6.2 and section 6.6.3.

It can be concluded that based on the obtained results, the proposed method using 3D analysis can serve as an alternative technique for estimating faulty phase, fault type, faulty section and fault distance in distribution networks. This is due to its ability to detect faults by using single end measurements at the primary substation. Also the accuracy of 3D analysis using SVC for fault type is higher than the 2D analysis. For faulty section and fault distance calculation 2D and 3D analysis perform equally well, but the limitation is that the method does not consider the faulty phase in distribution systems.

7.2 Future Work

Future work can be conducted in the following areas to improve the proposed method:

1. Consideration of FACTS devices

   With increasing number of FACTS devices, such as Static Var Compensator, TCSC (Thyristor-Controlled Series Capacitor), STATCOM (Static Synchronous Compensator) and SSSC (Static Synchronous Series Compensator) in distribution systems, it will be necessary to include its model in the proposed fault location method.

2. Consideration of DG, measurement error and loading variations

   To consider multiple sources in the test system by including DG. The voltage sag data for fault identification are recorded at the monitoring nodes using measurement devices. There is a possibility of minor error due to change in measurement devices. Thus, the measurement error can be considered when locating a fault. Also, the proposed method does not consider dynamic loads modelling with load profile variations and its effect on distribution systems.

Loading variations can be considered in the future work and its impact on locating fault can be analyzed.

3. Further evaluation

Further evaluation using a large-scale network can be proposed to study the performance of the method. Actual voltage sag from real measurements due to faults from a genuine distribution network is suggested. It will be interesting to see the performance of the method when actual data is used.

4. On-line Implementation

For on-line implementation, the proposed method should be developed into PC-based fault location system with Graphical User Interface (GUI). The GUI should have user-friendly features and informative displays using a Windows-based programming development environment.

REFERENCES

A. A. Bhole, A. M. P. (2014). An overview on different methods of fault location in underground cable system *International Journal of Electrical Engineering and Technology (IJEET), Vol 5*(3), 27-33.

Adly A. Girgis, C. M. F., David L. Lubkeman. (1993). A Fault Location Technique for Rural Distribution Feeders. *IEEE Transactions on Industry Applications, Vol 29*.

Akerlund, J. (2004). Utveckling Elkvalitet Slutrapport (in Swedish) *Elforsk report 04:46*.

Ali, M. S., Abu Bakar, A. H., Mokhlis, H., Arof, H., & Azil Illias, H. (2014). High-impedance fault location using matching technique and wavelet transform for underground cable distribution network. *IEEJ Transactions on Electrical and Electronic Engineering*, *9*(2), 176-182. doi: 10.1002/tee.21953

Ancell, G. B., & Pahalawaththa, N. C. (1994). Maximum likelihood estimation of fault location on transmission lines using travelling waves. *IEEE Transactions on Power Delivery*, *9*(2), 680-689. doi: 10.1109/61.296245

Anderson, P. M. (1995). Analysis of Faulted Power Systems. *The Institute of Electrical and Electronics Engineers, Inc.*

Aslan, Y. (2012). An alternative approach to fault location on power distribution feeders with embedded remote-end power generation using artificial neural networks. *Electrical Engineering*, *94*(3), 125-134. doi: 10.1007/s00202-011-0218-2

Awalin, L. J., & Mokhlis, H. (2012). Improved Fault Location on Distribution Network Based on Multiple Measurements of Voltage Sags Pattern. *IEEE International Conference on Power and Energy (PECon)*.

Awalin, L. J., Mokhlis, H., Abu Bakar, A., Mohamad, H., & Illias, H. A. (2013). A generalized fault location method based on voltage sags for distribution network. *IEEJ Transactions on Electrical and Electronic Engineering*, *8*(S1), S38-S46. doi: 10.1002/tee.21916

B., R., Thukaram, D., & Khincha, H. P. (2008). Knowledge-Based Approach Using Support Vector Machine for Transmission Line Distance Relay Co-ordination. *Journal of Electrical Engineering & Technology*, *3*, 363-372.

Bao, J. Z., & Mao, Z. T. Y. (2011). A Fault Location and Realization Method for Overhead High Voltage Power Transmission. *Procedia Engineering*, *15*, 964-968. doi: http://dx.doi.org/10.1016/j.proeng.2011.08.178

Bastard, P., Garcia-Santander, L., Pivert, X. L., Gal, I., & Parra, E. L. (2002, 17-19 April 2002). *A voltage-based fault location method for radial distribution networks.* Paper presented at the Fifth International Conference on Power System Management and Control.

Bedekar, P. P., Bhide, S. R., & Kale, V. S. (2011). Fault section estimation in power system using Hebb's rule and continuous genetic algorithm. *International Journal of Electrical Power & Energy Systems, 33*(3), 457-465. doi: http://dx.doi.org/10.1016/j.ijepes.2010.10.008

Billinton, R., & Jonnavithula, S. (1996). Optimal switching device placement in radial distribution systems. *IEEE Transactions on Power Delivery, 11*(3), 1646-1651. doi: 10.1109/61.517529

Bollen, M. H. (2000). *Understanding power quality problems* (Vol. 3): IEEE press New York.

Bollen, M. H. J. (1996). Fast assessment methods for voltage sags in distribution systems. *IEEE Transactions on Industry Applications, 32*(6), 1414-1423. doi: 10.1109/28.556647

Bollen, M. H. J. (2000). *Understanding Power Quality Problems: Voltage Sags and Interruptions*. Piscataway, NJ: IEEE Inc.

Bouboulis, P., Theodoridis, S., Mavroforakis, C., & Evaggelatou-Dalla, L. (2015). Complex Support Vector Machines for Regression and Quaternary Classification. *IEEE Transactions on Neural Networks and Learning Systems, 26*(6), 1260-1274. doi: 10.1109/TNNLS.2014.2336679

Bretas, A. D. F. M. R. R. H. S. A. S. (2011). Distribution systems fault analysis considering fault resistance estimation. *International Journal of Electrical Power & Energy Systems, Vol 33*, 1326–1335.

Cao, L. J., & Tay, F. E. H. (2003). Support vector machine with adaptive parameters in financial time series forecasting. *IEEE Transactions on Neural Networks, 14*(6), 1506-1518. doi: 10.1109/TNN.2003.820556

Choi, M.-S., Lee, S.-J., Lee, D.-S., & Bo-Gun Jin. (2004). A new fault location algorithm using direct circuit analysis for distribution systems. *IEEE Transactions on Power Delivery, Vol:19* 35 - 41

Chunju, F., Li, K. K., Chan, W. L., Weiyong, Y., & Zhaoning, Z. (2007). Application of wavelet fuzzy neural network in locating single line to ground fault (SLG) in distribution lines. *International Journal of Electrical Power & Energy Systems, 29*(6), 497-503. doi: http://dx.doi.org/10.1016/j.ijepes.2006.11.009

Cortes, C., & Vapnik, V. (1995). Support-Vector Networks. *Machine Learning, 20*(3), 273-297. doi: 10.1023/A:1022627411411

D. Novosel, D. H., and Myllymaki, J. (1998). System for locating faults and estimating fault resistance in distribution networks with tapped loads. *US Patent number 5,839,093*.

Das, B. (2006). Fuzzy logic-based fault-type identification in unbalanced radial power distribution system. *IEEE Transactions on Power Delivery, 21*(1), 278-285. doi: 10.1109/TPWRD.2005.852273

Das, B., & Reddy, J. V. (2005). Fuzzy-logic-based fault classification scheme for digital distance protection. *IEEE Transactions on Power Delivery, 20*(2), 609-616. doi: 10.1109/TPWRD.2004.834294

Das, R. (1998). *Determining the locations of faults in distribution systems.* (Doctoral thesis), University of Saskatchewan, Saskatoon, Canada,.

Das, R., Sachdev, M. S., & Sidhu, T. S. (1997, 25-27 Mar 1997). *Determining locations of faults in distribution systems.* Paper presented at the Sixth International Conference on Developments in Power System Protection.

Dash, P. K., Samantaray, S. R., & Panda, G. (2007). Fault Classification and Section Identification of an Advanced Series-Compensated Transmission Line Using Support Vector Machine. *IEEE Transactions on Power Delivery, 22*(1), 67-73. doi: 10.1109/TPWRD.2006.876695

Deng, X., Yuan, R., Xiao, Z., Li, T., & Wang, K. L. L. (2015). Fault location in loop distribution network using SVM technology. *International Journal of Electrical Power & Energy Systems, 65*(0), 254-261. doi: http://dx.doi.org/10.1016/j.ijepes.2014.10.010

Ekici, S. (2012). Support Vector Machines for classification and locating faults on transmission lines. *Applied Soft Computing, 12*(6), 1650-1658. doi: http://dx.doi.org/10.1016/j.asoc.2012.02.011

Ferrero, A., Sangiovanni, S., & Zappitelli, E. (1995). A fuzzy-set approach to fault-type identification in digital relaying. *IEEE Transactions on Power Delivery, 10*(1), 169-175. doi: 10.1109/61.368401

Filomena, A. D. F. U. o. R. G. d. S., Porto Alegre ; Salim, R.H. ; Resener, M. ; Bretas, A.S. (2008). Ground Distance Relaying With Fault-Resistance Compensation for Unbalanced Systems. *IEEE Transactions on Power Delivery, Vol 23*, 1319 - 1326.

Force, U.-C. P. S. O. T., Abraham, S., et al. . (2004). US-Canada Power System Outage Task Force. *Final Report on the August 14, 2003 Blackout in the United States and Canada: Causes and Recommendations*.

Gonen, T. (2009). *Electric Power Transmission System Engineering, Analysis and Design*: Crc Press Taylor and Francis Group.

Guo, G., Li, S. Z., & Chan, K. L. (2001). Support vector machines for face recognition. *Image and Vision Computing, 19*(9–10), 631-638. doi: http://dx.doi.org/10.1016/S0262-8856(01)00046-4

H. K. K. Abolfazl Jalilvand, H. F. (2010). High Impedance Fault Detection Using Duffing Oscillator and FIR Filter. *International Review of Electrical Engineering, 5*, 10.

H. Mokhlis, H. M., A. H. A. Bakar and H. Y.Li. (2011). Evaluation of fault location based on voltage sags profiles: a study on the influence of voltage sags patterns. *International Review of Electrical Engineering, 6*(2).

Hagh, M. T., Razi, K., & Taghizadeh, H. (2007, 3-6 Dec. 2007). *Fault classification and location of power transmission lines using artificial neural network.* Paper presented at the Power Engineering Conference, 2007. IPEC 2007. International.

Han, F., Yu, X., Al-Dabbagh, M., & Wang, Y. (2007). Locating Phase-to-Ground Short-Circuit Faults on Radial Distribution Lines. *IEEE Transactions on Industrial Electronics, 54*(3), 1581-1590. doi: 10.1109/TIE.2007.894722

IEEE Guide for Determining Fault Location on AC Transmission and Distribution Lines. (2005). *IEEE Std C37.114-2004*, 1-44. doi: 10.1109/IEEESTD.2005.96207

IEEE Guide for Fault Locating Techniques on Shielded Power Cable Systems. (2007). *IEEE Std 1234-2007*, 1-37. doi: 10.1109/IEEESTD.2007.4385340

IEEE Recommended Practice for Evaluating Electric Power System Compatibility With Electronic Process Equipment. (1998). *IEEE Std 1346-1998*, 0_1. doi: 10.1109/IEEESTD.1998.87816

IEEE Recommended Practice for Monitoring Electric Power Quality. (1995). *IEEE Std 1159-1995*, i. doi: 10.1109/IEEESTD.1995.79050

IEEE Recommended Practice for the Design of Reliable Industrial and Commercial Power Systems - Redline. (2007). *IEEE Std 493-2007 (Revision of IEEE Std 493-1997) - Redline*, 1-426.

Janik, P., & Lobos, T. (2006). Automated classification of power-quality disturbances using SVM and RBF networks. *IEEE Transactions on Power Delivery, 21*(3), 1663-1669. doi: 10.1109/TPWRD.2006.874114

Jarventausta, P., Verho, P., & Partanen, J. (1994). Using fuzzy sets to model the uncertainty in the fault location process of distribution networks. *IEEE Transactions on Power Delivery, 9*(2), 954-960.

Javadian, S. A. M., Nasrabadi, A. M., Haghifam, M. R., & Rezvantalab, J. (2009, 9-11 June 2009). *Determining fault's type and accurate location in distribution systems with DG using MLP Neural networks.* Paper presented at the International Conference on Clean Electrical Power.

Jin, Q., & Ju, R. (2012, 27-30 May 2012). *Fault Location for Distribution Network Based on Genetic Algorithm and Stage Treatment.* Paper presented at the Spring Congress on Engineering and Technology (S-CET).

Johns, A. T., & Agrawal, P. (1990). New approach to power line protection based upon the detection of fault induced high frequency signals. *IEE Proceedings Generation, Transmission and Distribution, 137*(4), 307-313.

Jun, Z., Lubkeman, D. L., & Girgis, A. A. (1997). Automated fault location and diagnosis on electric power distribution feeders. *IEEE Transactions on Power Delivery, 12*(2), 801-809.

Khorashadi-Zadeh, H. (2004, 8-8 Sept. 2004). *A novel approach to detection high impedance faults using artificial neural network.* Paper presented at the 39th International Universities Power Engineering Conference.

Kui, W., & Kim-Hui, Y. (2006). Fuzzy SVM for content-based image retrieval: a pseudo-label support vector machine framework. *IEEE Computational Intelligence Magazine, 1*(2), 10-16. doi: 10.1109/MCI.2006.1626490

Lamoree, J., Mueller, D., Vinett, P., Jones, W., & Samotyj, M. (1994). Voltage sag analysis case studies. *IEEE Transactions on Industry Applications, 30*(4), 1083-1089. doi: 10.1109/28.297926

Lee, H., & Mousa, A. M. (1996). GPS travelling wave fault locator systems: investigation into the anomalous measurements related to lightning strikes. *IEEE Transactions on Power Delivery, 11*(3), 1214-1223.

Leora, L., Michael, J. S., Kent Van, L., Aaron, K., & Joseph, H. E. (2003). A Framework and Review of Customer Outage Costs: Integration and Analysis of Electric Utility Outage Cost Surveys. Berkeley: Lawrence Berkeley National Laboratory.

Li, Y., Zhang, S., Li, H., Zhai, Y., Zhang, W., & Nie, Y. (2012). A fault location method based on genetic algorithm for high-voltage direct current transmission line. *European Transactions on Electrical Power, 22*(6), 866-878. doi: 10.1002/etep.1659

Lin, S., He, Z. Y., Li, X. P., & Qian, Q. Q. (2012). Travelling wave time-frequency characteristic-based fault location method for transmission lines. *IET Generation, Transmission & Distribution, 6*(8), 764-772. doi: 10.1049/iet-gtd.2011.0703

Lopes, F. V., Silva, K. M., Costa, F. B., Neves, W. L. A., & Fernandes, D. (2015). Real-Time Traveling-Wave-Based Fault Location Using Two-Terminal Unsynchronized Data. *IEEE Transactions on Power Delivery, 30*(3), 1067-1076. doi: 10.1109/TPWRD.2014.2380774

M. Saha, E. R. (2002). Method and device of fault location for distribution networks. *US Patent number 6,483,435*.

Melhorn, C. J., Davis, T. D., & Beam, G. E. (1998). Voltage sags: their impact on the utility and industrial customers. *IEEE Transactions on Industry Applications, 34*(3), 549-558. doi: 10.1109/28.673725

Mokhlis, H., Bakar, A., Talib, D., & Mohamad, H. (2010). The improvement of voltage sags pattern approach to locate a fault in distribution network. *International Review of Electrical Engineering, 5(3).*

Mokhlis H, L. H., Khalid AR. (2010). The application of voltage sags pattern to locate a faulted section in distribution network. *IEEE International Review of Electrical Engineering, Vol 5*, 173–179.

Mokhlis, H., & Li, H. (2011). Non-linear representation of voltage sag profiles for fault location in distribution networks. *Electrical Power and Energy Systems, 33*, 124–130.

Mokhlis, H., & Li, H. Y. (2007, 4-6 Sept. 2007). *Fault location estimation for distribution system using simulated voltage sags data.* Paper presented at the 42nd International Universities Power Engineering Conference, UPEC 2007. .

Mokhlis, H., Mohamad, H., Bakarl, A., & Li, H. (2011). Evaluation of Fault Location based on Voltage Sags Profiles: a Study on the Influence of Voltage Sags Patterns. *International Review of Electrical Engineering, 6*(2).

Mora-Flòrez, J., Meléndez, J., & Carrillo-Caicedo, G. (2008). Comparison of impedance based fault location methods for power distribution systems. *Electric Power Systems Research, 78*(4), 657-666. doi: http://dx.doi.org/10.1016/j.epsr.2007.05.010

Mora-Florez, J., Morales-Espana, G., & Perez-Londono, S. (2009). Learning-based strategy for reducing the multiple estimation problem of fault zone location in radial power systems. *IET Generation, Transmission & Distribution, 3*(4), 346-356. doi: 10.1049/iet-gtd.2008.0164

Mosavi, M. R., & Tabatabaei, A. (2014). Wavelet and Neural Network-Based Fault Location in Power Systems Using Statistical Analysis of Traveling Wave. *Arabian Journal for Science and Engineering, 39*(8), 6207-6214. doi: 10.1007/s13369-014-1158-8

Moshtagh, P. J. J. (2009). High Impedance Fault Location for Aged Power Distribution Cables Using Combined Neural Networks & Wavelet Analysis. *International Review of Electrical Engineering, 4*, 8.

Namrata B. Pawar, D. M. K. (2014). Generation of Different Types of Voltage Sag Using Matlab/Simulink. *International Journal of Engineering and Innovative Technology, 3*(9).

Novosel, D., Hart, D. G., Udren, E., & Garitty, J. (1996). Unsynchronized two-terminal fault location estimation. *IEEE Transactions on Power Delivery, 11*(1), 130-138. doi: 10.1109/61.484009

Ohrstrom, M., & Soder, L. (2003, 23-26 June 2003). *A comparison of two methods used for voltage dip characterization.* Paper presented at the Power Tech Conference Proceedings, 2003 IEEE Bologna.

Parikh, U. B., Das, B., & Maheshwari, R. (2010). Fault classification technique for series compensated transmission line using support vector machine. *International Journal of Electrical Power & Energy Systems, 32*(6), 629-636. doi: http://dx.doi.org/10.1016/j.ijepes.2009.11.020

Parsaei, H., & Stashuk, D. W. (2012). SVM-Based Validation of Motor Unit Potential Trains Extracted by EMG Signal Decomposition. *IEEE Transactions on Biomedical Engineering, 59*(1), 183-191. doi: 10.1109/TBME.2011.2169412

Pereira, R. A., Kezunovic, M., & Mantovani, J. R. (2009). Fault location algorithm for primary distribution feeders based on voltage sags. *INTERNATIONAL JOURNAL OF INNOVATIONS IN ENERGY SYSTEMS AND POWER,(ISSN 1913-133X), 4*, 1-8.

Pereira, R. A. F., da Silva, L. G. W., Kezunovic, M., & Mantovani, J. R. S. (2009). Improved Fault Location on Distribution Feeders Based on Matching During-Fault Voltage Sags. *IEEE Transactions on Power Delivery, 24*(2), 852-862. doi: 10.1109/tpwrd.2009.2014480

Pradhan, A., Routray, A., & Madhan Gudipalli, S. (2007). Fault direction estimation in radial distribution system using phase change in sequence current. *IEEE Transactions on Power Delivery, 22*(4), 2065-2071.

Pradhan, A. K., Routray, A., & Biswal, B. (2004). Higher order statistics-fuzzy integrated scheme for fault classification of a series-compensated transmission line. *IEEE Transactions on Power Delivery, 19*(2), 891-893. doi: 10.1109/TPWRD.2003.820413

Prarthana Warlyani, A. J., A.S.Thoke, and R.N.Patel. (2011). Fault Classification and Faulty Section Identification in Teed Transmission Circuits Using ANN. *International Journal of Computer and Electrical Engineering, 3*, 807-811.

Purushothama, G. K., Narendranath, A. U., Thukaram, D., & Parthasarathy, K. (2001). ANN applications in fault locators. *International Journal of Electrical Power & Energy Systems, 23*(6), 491-506. doi: http://dx.doi.org/10.1016/S0142-0615(00)00068-5

Ravikumar, B., Thukaram, D., & Khincha, H. P. (2008). Application of support vector machines for fault diagnosis in power transmission system. *IET Generation, Transmission & Distribution, 2*(1), 119-130. doi: 10.1049/iet-gtd:20070071

Ray, P., Panigrahi, B. K., & Senroy, N. (2013). Hybrid methodology for fault distance estimation in series compensated transmission line. *IET Generation, Transmission & Distribution, 7*(5), 431-439. doi: 10.1049/iet-gtd.2012.0243

Rojo-Álvarez, J. L., Camps-Valls, G., Martínez-Ramón, M., Soria-Olivas, E., Navia-Vázquez, A., & Figueiras-Vidal, A. R. (2005). Support vector machines framework for linear signal processing. *Signal Processing, 85*(12), 2316-2326. doi: http://dx.doi.org/10.1016/j.sigpro.2004.12.015

Saadat, H. *Power System Analysis*: Milwaukee Scholl of Engineering, WBC McGraw-Hill.

Sachdev, M. S., & Agarwal, R. (1988). A technique for estimating transmission line fault locations from digital impedance relay measurements. *IEEE Transactions on Power Delivery, 3*(1), 121-129. doi: 10.1109/61.4237

Sadinezhad, M. J. I. (Oct 2008). An Adaptive Precise One End Fault Location in Transmission Lines Based on Hybrid Complex Least Error Squares Algorithm and Adaptive Artificial Neural Networks. *International Review of Electrical Engineering, 3 No. 5*, 803-810.

Salat, R., & Osowski, S. (2004). Accurate fault location in the power transmission line using support vector machine approach. *IEEE Transactions on Power Systems, 19*(2), 979-986. doi: 10.1109/TPWRS.2004.825883

Salim, R. H., de Oliveira, K., Filomena, A. D., Resener, M., & Bretas, A. S. (2008). Hybrid Fault Diagnosis Scheme Implementation for Power Distribution Systems Automation. *IEEE Transactions on Power Delivery, 23*(4), 1846-1856. doi: 10.1109/tpwrd.2008.917919

Salim, R. H., Resener, M., Filomena, A. D., Rezende Caino de Oliveira, K., & Bretas, A. S. (2009). Extended Fault-Location Formulation for Power Distribution Systems. *IEEE Transactions on Power Delivery, 24*(2), 508-516. doi: 10.1109/TPWRD.2008.2002977

Sant, M. T., & Paithankar, Y. G. (1979). Online digital fault locator for overhead transmission line. *Proceedings of the Institution of Electrical Engineers, 126*(11), 1181-1185. doi: 10.1049/piee.1979.0201

Sant, M. T., & Paithankar, Y. G. (1983). Fault locator for long EHV transmission lines. *Electric Power Systems Research, 6*(4), 305-310. doi: http://dx.doi.org/10.1016/0378-7796(83)90042-1

Sapankevych, N. I., & Sankar, R. (2009). Time Series Prediction Using Support Vector Machines: A Survey. *IEEE Computational Intelligence Magazine, 4*(2), 24-38. doi: 10.1109/MCI.2009.932254

Seung-Jae, L., Myeon-Song, C., Sang-Hee, K., Bo-Gun, J., Duck-Su, L., Bok-Shin, A., . . . Sang-Bong, W. (2004). An intelligent and efficient fault location and diagnosis scheme for radial distribution systems. *IEEE Transactions on Power Delivery, 19*(2), 524-532. doi: 10.1109/TPWRD.2003.820431

Seyed, A. M. J., & Maryam, M. (2011). A fault location method in distribution networks including DG. *Indian Journal of Science and Technology, Vol.4*.

Shutao, L., Kwok, J. T. Y., Tsang, I. W., & Yaonan, W. (2004). Fusing images with different focuses using support vector machines. *IEEE Transactions on Neural Networks, 15*(6), 1555-1561. doi: 10.1109/TNN.2004.837780

Springs, L. Y. a. C. (1998). One terminal fault location system that corrects for fault resistance effects. *US Patent number 5,773,980*.

Srinivasan, K., & St-Jacques, A. (1989). A New Fault Location Algorithm for Radial Transmission Lines with Loads. *IEEE Power Engineering Review, 9*(7), 52-52. doi: 10.1109/MPER.1989.4310803

Suresh Kamble, C. T. (2012). Characteristics Analysis of Voltage Sag in Distribution System using RMS Voltage Method. *ACEEE International Journal on Electrical and Power Engineering, 3*(1), 6. doi: 01.IJEPE.3.1.3

Suresh Kamble, C. T. (2014). Voltage Sag Characterization in a Distribution Systems: A Case Study. *Journal of Power and Energy Engineering, 2*, 546-553. doi: dx.doi.org/10.4236/jpee.2014.24074

Takagi, T., Yamakoshi, Y., Yamaura, M., Kondow, R., & Matsushima, T. (1982). Development of a New Type Fault Locator Using the One-Terminal Voltage and Current Data. *IEEE Transactions on Power Apparatus and Systems, PAS-101*(8), 2892-2898.

Thukaram, D., Khincha, H. P., & Vijaynarasimha, H. P. (2005). Artificial neural network and support vector Machine approach for locating faults in radial distribution systems. *IEEE Transactions on Power Delivery, 20*(2), 710-721. doi: 10.1109/tpwrd.2005.844307

Vapnik, V. (1982). *Estimation of Dependences Based on Empirical Data*. New York: Springer-Verlag.

Vapnik, V. (1995). *The Nature of Statistical Learning Theory*. New York: Springer-Verlag.

Wang, Z. Q., & Zhu, S. Z. (2002). *Comparative study on power quality disturbance magnitude characterization.* Paper presented at the International Conference on Power System Technology.

Warrington, A. (1968). *Protective relays, their theory and practice*

Wen-Hui, C., Chih-Wen, L., & Men-Shen, T. (2000). On-line fault diagnosis of distribution substations using hybrid cause-effect network and fuzzy rule-based method. *IEEE Transactions on Power Delivery, 15*(2), 710-717.

Yang;, M.-S. C. S.-J. L. S.-I. L. D.-S. L. X. (2007). A Direct Three-Phase Circuit Analysis-Based Fault Location for Line-to-Line Fault. *IEEE Transactions on Power Delivery, Vol:22*(4), 2541- 2547

Yanhun, Z., & Chongqing, L. (2003). Face recognition based on support vector machine and nearest neighbor classifier. *Journal of Systems Engineering and Electronics, 14*(3), 73-76.

Ying-Hong, L., Chih-Wen, L., & Chi-Shan, Y. (2002). A new fault locator for three-terminal transmission lines using two-terminal synchronized voltage and current phasors. *IEEE Transactions on Power Delivery, 17*(2), 452-459. doi: 10.1109/61.997917

LIST OF PUBLICATIONS AND PAPERS PRESENTED

List of Publication

This research has been reported in the following publications:

1) Gururajapathy, S. S., Mokhlis H. & Illias H. A. B. (2017). Fault location and detection techniques in power distribution systems with distributed generation: A review. *Renewable & Sustainable Energy Reviews*, *74*, 949-958.
2) Gururajapathy, S. S., Mokhlis, H., Illias, H. A. B. & Awalin, L. J. (2017). Support vector classification and regression for fault location in distribution system using voltage sag profile. *IEEJ Transactions on Electrical and Electronic Engineering*, doi:10.1002/tee.22407.
3) Gururajapathy, S. S., Mokhlis, H., Illias, H. A. B., Bakar H. A. & Awalin, L. J. (2016). Fault Identification in an Unbalanced Distribution System Using Support Vector Machine. *Journal of Electrical Systems*, *12*(4), 786-800.
4) Gururajapathy, S. S., Mokhlis, H., Illias, H. A. B., Bakar H. A. & Awalin, L. J., Fault Location in an Unbalanced Distribution System using Support Vector Classification and Regression Analysis. *IEEJ Transactions on Electrical and Electronic Engineering*. (Accepted on 15 March 2017)
5) Gururajapathy, S. S., Mokhlis H. & Illias H. A. B., Classification and Regression Analysis using Support Vector Machine for Classifying and Locating Faults in Distribution System. *Applied Soft Computing*. (Under Review after 1st correction)

List of Conferences

1) Gururajapathy, S. S., Mokhlis. H. & Illias, H. A. B (2014). *Fault Location using Direct Circuit Analysis considering Measurement error*. Paper presented at the AUN/SEED-net international conference on EEE, Malaysia.
2) Gururajapathy, S. S., Mokhlis, H., Illias, H. A. B. & Awalin, L. J. (2015). Fault Distance Calculation in Radial Distribution System using Second Order Polynomial Analysis of Voltage Sag Profile. *Applied Mechanics and Materials*, 785, 460-464.